NTNU – Trondheim
Norwegian University of
Science and Technology

Design and analysis of a large wind floater

A reinforced concrete pontoon-type
semi-submersible supporting the DTU 10MW
reference turbine

Marius Deac

Wind Energy
Submission date: June 2014
Supervisor: Torgeir Moan, IMT
Co-supervisor: Max Hendriks, TU Delft

Norwegian University of Science and Technology
Department of Marine Technology

Master Thesis of Science

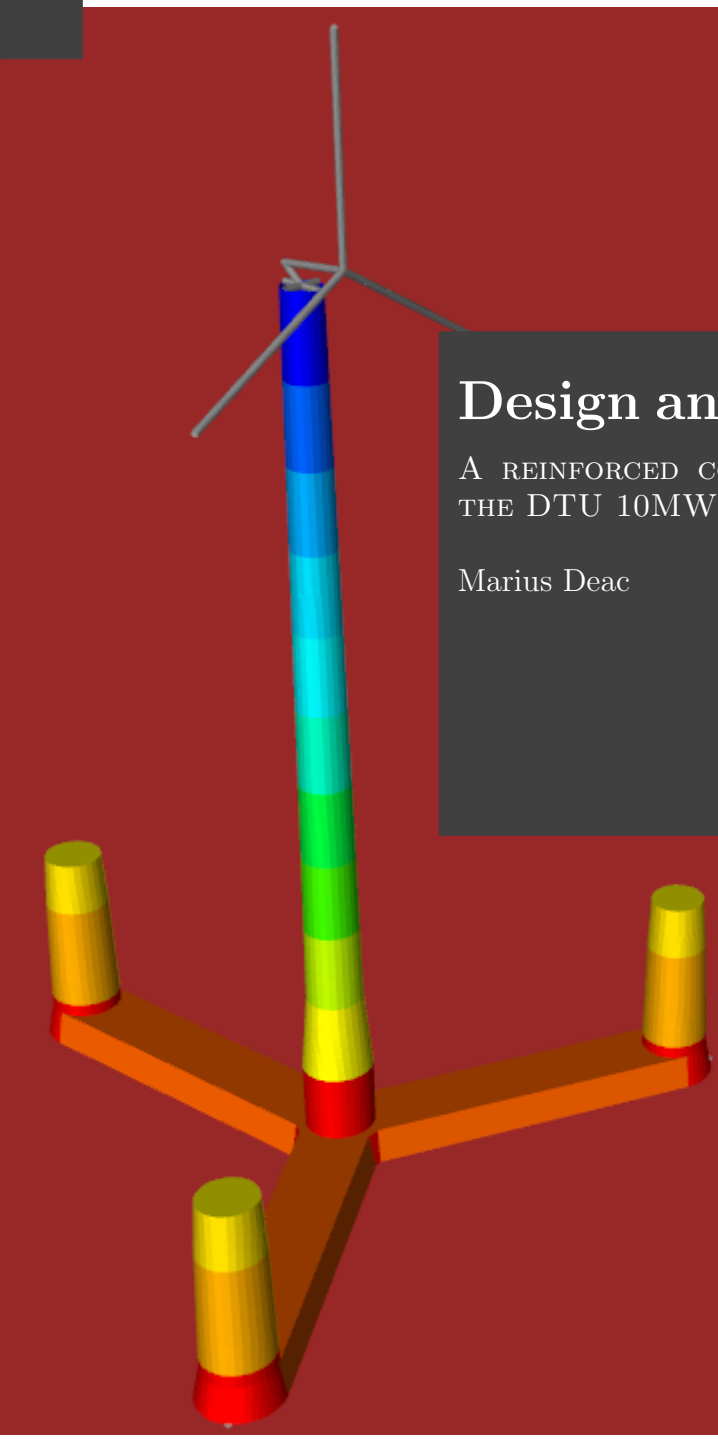

Design and analysis of a large wind floater

A reinforced concrete pontoon-type semi-submersible supporting the DTU 10MW reference turbine

Marius Deac

June 20, 2014

European Wind Energy Master - EWEM- Offshore Engineering Track

Design and analysis of a large wind floater

A reinforced concrete pontoon-type semi-submersible supporting the DTU 10MW reference turbine

Master of Science Thesis

For obtaining the degree of Master of Science in Offshore Engineering at Delft University of Technology and in Technology-Wind Energy at Norwegian University of Science and Technology.

Marius Deac

June 20, 2014

European Wind Energy Master - EWEM
NTNU - Norwegian University of Science and Technology
TU Delft - Delft University of Technology

European Wind Energy Master - EWEM
Of
Offshore Engineering Track

The undersigned hereby certify that they have read and recommend to the European Wind Energy Master - EWEM for acceptance a thesis entitled **"Design and analysis of a large wind floater"** by **Marius Deac** in partial fulfillment of the requirements for the degree of **Master of Science**.

Dated: June 20, 2014

Supervisor: _____
Prof. Torgeir Moan of NTNU

Supervisor: _____
Prof. J.G. Rots of TU Delft

Reader: _____
Dr. Ir. Zhen Gao of NTNU

Reader: _____
Dr.ir. M.A.N. Hendriks of TU Delft

Reader: _____
Ir. Hoving, J.S of TU Delft

Summary

Wind industry is developing fast, moving from onshore to offshore and from shallow water to greater depths. At the same time, it is facing significant cost challenges. There are certain advantages to placing wind turbines offshore: better wind resources, economies of scale and increased public acceptance. The cost of traditional substructure solutions for shallow waters, such as monopiles, is greatly increasing with the depth. At the same time, reports show that considerable wind resources could be accessed in deep water, if alternatives to bottom fixed substructures are developed, such as floating wind turbines. Traditionally, their support hulls are manufactured of welded steel plates and represent a major contributor to the final cost of energy. Meanwhile, reinforced concrete is the most utilized material on our planet, in multiple industries, especially in large scale applications. However, the idea of possible cost reductions boosted by the use of alternative construction materials, has received very little attention in the offshore wind industry, with no full scale attempt and only one prototype, to the present date. Two reinforced concrete floaters have ever been built in the offshore oil and gas. Another option for reducing the total cost of floating wind energy could be utilizing large scale turbines which harness more wind. Furthermore, these suggested cost cut alternatives could be coupled into a large scale reinforced concrete floating wind turbine.

The present work considers the design and analysis towards an optimizable baseline, of a braceless reinforced concrete semi-submersible supporting a DTU 10MW reference wind turbine. Initially, an extensive literature review is conducted and a design basis is established, given limited previous experience exists. Following, simple analytic formulas are applied to determine the main characteristics of the floater, in terms of its stability and motions, relevant for ensuring an adequate operation. Next, numerical analysis tools are used to confirm these findings. With the determined hydrodynamic and static loads, a quasi-static linear structural analysis with constant material properties, is conducted. The floater is modeled as shell elements. The resulting stresses are post-processed based on the actual non-linear material behavior, for the ULS. A corresponding bill of quantities and materials cost estimate are developed, together with an assessment of the CO_2 impact. Consequently, the main conclusions and advice for suitable future research are formulated.

Acknowledgements

First of all, I would like to express my gratitude towards the main organizers of the EWEM program. Your team has done a wonderful job in providing us, the first graduating cohort, with an enriching learning and social experience. Also, thank you for awarding me with an Erasmus Mundus scholarship, without which this life changing journey would not have been possible.

Furthermore, I would like to state my very great appreciation for Professor Torgeir Moan, who has always found the time and patience to provide me with great advice and inspiration regarding my work. The quality of his supervision was more than one could have expected. I would also like to thank his assistant Dr. Zhen Gao and to Chenyu Luan, for the useful discussions held during our often progress meetings. Moreover, I am grateful towards Professor Jan Rots, Dr. Max Hendriks and Ir. Jeroen Hoving, for their supervision, constructive feedback and great flexibility shown during this project.

Bente Skovseth Nyhus, Rikke Ellingsen and Anders Myhr of Dr. Techn. Olav Olsen AS, all deserve my appreciation for providing me with a free software license for ShellDesign and with the required support in the post-processing work.

My special thanks go to my family, colleagues and friends, for adding a fun touch to this otherwise very educational experience!

Contents

Summary **v**

Acknowledgements **vii**

List of Figures **xiv**

List of Tables **xvi**

Nomenclature **xvii**

1 Introduction **1**
1.1 Background 1
1.2 Concept selection 2
1.3 Previous work 4
1.4 Thesis goals, objectives and tasks 6
1.5 Design procedure and tools 7

2 History of offshore concrete structures **13**

3 Theories for modeling membrane and shell reinforced concrete elements **17**
3.1 Lower bound theory of plasticity for membrane elements 17
3.2 Lower bound theory of plasticity for shell elements 21
3.3 Modified compression field theory and its relation to ShellDesign 21

4 Design basis **25**
4.1 Loads and materials safety factors 25
4.2 Functional requirements 26
4.2.1 Determined by the wind turbine 26

4.2.2 Stability and motion . . . 28
4.3 Environmental data for ULS . . . 30
4.3.1 Design wave load . . . 30
4.3.2 Wind load . . . 32
4.4 Materials . . . 33
4.5 Construction methods . . . 37
4.6 Durability . . . 40
4.7 Environmental aspects . . . 40

5 Updated floater concept **43**
5.1 Floating bodies main theory and approach . . . 43
5.2 Updated model dimensions and characteristics . . . 44

6 Finite element and panel models generation **47**
6.1 Brief software overview: Pre-processor DNV Sesam GeniE V6.5 . . . 47
6.2 Global structural model . . . 48
6.3 Meshing and resulting models . . . 52
6.3.1 Structural model (Mass model) . . . 52
6.3.2 Panel models . . . 53
6.3.3 Morison model . . . 55

7 Environmental analysis **57**
7.1 Software overview: DNV Sesam HydroD . . . 57
7.2 Hydrostatic analysis and results . . . 60
7.3 Hydrodynamic motion analysis and results . . . 62
7.4 Hydrodynamic loads analysis . . . 66

8 Structural analysis and results **67**
8.1 Brief software overview: DNV Sesam Sestra . . . 67
8.2 Free vibration dynamic analysis and results . . . 69
8.3 Static analysis . . . 71
8.3.1 Stress results discussion . . . 72

9 Post-processing and results **73**
9.1 Limit states and design calculations . . . 74
9.2 Design sections . . . 74
9.3 Load cases and design combinations . . . 75
9.4 Materials . . . 76
9.5 ULS Results . . . 77
9.5.1 BS_1 . . . 78
9.5.2 TS_1 . . . 79
9.5.3 AW_{12} and AW_{11} . . . 80
9.5.4 CC . . . 81
9.5.5 OC_1 . . . 82
9.5.6 Bill of quantities and cost estimate . . . 83
9.6 Additional features: Non-linear structural response . . . 83

10 Conclusions and recommendations for future work **85**
10.1 Conclusions 85
10.2 Recommendations for future work 87

References **89**

A DTU 10MW reference wind turbine **93**

B Basic load cases **97**

C Post-processing. Design sections and local axis system definition **105**

D Structural drawings **121**

List of Figures

1.1 DOFs of a floating wind turbine [10] 2
1.2 Classification of floaters [10] 3
1.3 Top view of the pre-project concept 5
1.4 Increase in computing power in recent years [19] 8
1.5 Overall design procedure 10
1.6 Overview of the Sesam system [31] 11

2.1 Gravity base structure (Gullfiks, North Sea, [17]) 13
2.2 Existing offshore concrete structures for oil and gas production [12] 14
2.3 Floaters with concrete hulls [17] 15
2.4 VolturnUS in scale 1:8 [5] 16

3.1 Equilibrium of an infinitesimal element in a thin walled section under M and V 18
3.2 Box girder under M and V 18
3.3 H cross sectional distribution due to V 19
3.4 Thin walled cross section subjected to torsional load T 20
3.5 Orthogonal reinforced concrete disk 20
3.6 Structures composed of membrane/ shell elements [13] 22
3.7 Deteriorated compression response in cracked reinforced concrete elements [14] 22
3.8 Sectional forces in an infinitesimal shell section [32] 23

4.1 1P and 3P rotational frequencies of the DTU 10MW reference wind turbine 27
4.2 Righting moment and wind heeling moment curves [10] 28
4.3 Applicability ranges of various wave theories [25] 31

4.4 Vertical wind profile 32
4.5 $\triangle$ C_D Drag coefficient for smooth circular cylinder [15] 33
4.6 Concrete raw materials 34
4.7 Examples of applications of mass concrete 34
4.8 Concrete batching plant 35
4.9 Reinforcement couplers[4] 36
4.10 Reinforcement arrangement of a deep slab, with T-bars [33] 37
4.11 GBS under construction in Belgium, Thornton Bank Project [1] 38
4.12 Spencer dock bridge Dublin [2] 39
4.13 Reinforcement production setup prototype [3] 39

5.1 Top view of the updated concept 45

6.1 Guiding geometry for the global model 49
6.2 Global structural model 50
6.3 Reinforced concrete bulkheads 50
6.4 Supports location 51
6.5 Structural and mass model mesh 52
6.6 Mesh quality inspection 53
6.7 Dummy hydro pressure along the wet surface 54
6.8 Panel models 54
6.9 Morison model 55

7.1 Classification of wave forces [15] 59
7.2 Righting moment against heeling moment 60
7.3 Heave RAO with/ out viscous effects 63
7.4 Heave RAO 64
7.5 Pitch RAO for different wave headings (composed model) 64
7.6 Roll RAO for different wave headings (composed model) 65
7.7 1P and 3P vs. Motions frequencies 65

8.1 Schematic illustration of the capabilities of Sestra [31] 67
8.2 Sestra input and output [31] 69
8.3 The quadrilateral shell element SCQS with stress points [31] 69
8.4 Structural mode shapes 70
8.5 1P and 3P vs. eigen frequencies 71

9.1 Input to design calculations [32] 73
9.2 Reinforcement directions [32] 77
9.3 Interaction scheme of Sestra and ShellDesign in the iterative mode [32] . . 84

List of Tables

1.1 DOFs of a floating wind turbine 2
1.2 Main characteristics of the pre-project concept 4

2.1 General properties and design conditions of the VolturnUS [5] 16

4.1 Load factors γ_f 26
4.2 Material factors 26
4.3 10MW DTU Reference wind turbine data 27
4.4 Centers of mass 28
4.5 General site information and statistics 30
4.6 CO_2-equivalent for some building materials [12] 41

5.1 Main characteristics of the updated concept 45

6.1 Material properties 48
6.2 Thickness of structural elements 48
6.3 Support characteristics 52

7.1 Main steps of the stability analysis 60
7.2 Main results of the stability analysis 61
7.3 List of considered wave periods 62
7.4 Lift and drag coefficients [7] 62
7.5 Heave, roll and pitch natural periods 63

8.1 Eigenvalues and eigen frequencies 70

9.1 Design sections 75
9.2 Factored load combinations 76
9.3 Utilization ratios for BS_1 78

9.4 Utilization ratios for TS_1 79
9.5 Utilization ratios for AW_{12} 80
9.6 Utilization ratios for CC 81
9.7 Utilization ratios for OC_1 82
9.8 Bill of quantities for the baseline concept 83
9.9 Baseline materials cost and estimated equivalent CO_2 impact 83

B.1 Original load cases transferred from HydroD to Sestra 103

Nomenclature

Latin Symbols

A	Area	$[m^2]$
C_D	Drag coefficient	[-]
f_y	Yield tension	$[MPa]$
$H_{S,50}$	Significant wave height with a 50 year return period	$[MPa]$
M	Moment around y axis	$[kNm]$
s	Length on y axis	$[m]$
T	Torsional moment	$[kNm]$
t	Thickness	$[m]$
t	Time	$[s]$
V	Shear force	$[kN]$

Greek Symbols

γ_f	Load factors	$[m]$
λ	Wave length	$[m]$
σ_c	Uniaxial concrete compression stress	$[\frac{kN}{m^2}]$
σ_{xx}	Normal stress along x axis	$[\frac{kN}{m^2}]$
σ_{yy}	Normal stress along y axis	$[\frac{kN}{m^2}]$
τ_{xy}	Shear stress	$[\frac{kN}{m^2}]$

Abbreviations

$1P$	Once Per revolution
$3P$	Three Per revolution
CoB	Center of Buoyancy
CoG	Center of Gravity
DNV	Det Norske Veritas
DOF	Degree of Freedom
DTU	Technical University of Denmark
FE	Finite Element
FEM	Finite Element Method
FLS	Fatigue Limit State
FS	Shell section along 1 axis
GBS	Gravity Base Structure
HS	Shell section along 2 axis
ID	Identity
$MCFT$	Modified Compression Field Theory
MW	Mega Watt
$NEDO$	New Energy and Industrial Technology Development Organization
$NREL$	National Renewable Energy Laboratory
OLC	Original Load Case
RAO	Response Amplitude Operator
SLS	Serviceability Limit State
TLP	Tension Leg Platform
ULS	Ultimate Limit State
UR	Utilization Ratio

Chapter 1

Introduction

1.1 Background

Wind industry develops very fast in recent years, moving from onshore to offshore and from shallow water to greater depths. The economics of offshore wind turbines are presently less favorable than for onshore wind energy. The major challenge this industry is facing is cutting the cost of energy, while moving to deeper water sites, which brings along other technical and environmental issues. The support structures are particularly expensive to fabricate, install and maintain.

There are certain advantages to having wind farms placed offshore. The wind resources are far superior, due to less turbulence intensity and greater wind speeds achieved at similar hub heights. The public acceptance is also increased, predominantly for aesthetic reasons. Moreover, economies of scale could be achieved faster than with on land developments. Larger wind farms could be built as the size limitations are less stringent. Currently, the record holder in terms of size is the London Array offshore wind farm developed by Dong Energy, E.On UK Renewables and Masdar , with a total capacity of 630 MW. It is roughly the equivalent of half a nuclear power plant, proving that wind farms could realistically replace traditional ways of generating energy. However, this wind park is rather classic in terms of utilized technology, consisting of 341 wind turbine generators supported by monopiles. Unfortunately, in other countries worldwide, this solution of supporting wind turbine generators for electrical power is not technically feasible, as they lack shallow waters. Moreover, the costs of bottom founded substructures to support wind turbines increases drastically with the water depth.

NREL shows that 61% of the United States offshore wind resources are in water depths of more than 100 m. Nearly all of Japan's offshore wind resources are in deep water (NEDO) together with various European locations, such as the coast of Norway and the Mediterranean, as shown in [21]. This is where floating substructures come into attention. Many concepts have been proposed for water depth larger than 100-200 m and some of them have been developed into prototypes that are now undergoing testing at sea, such

as Hywind and WindFloat. Nevertheless, they are manufactured in a traditional manner, of thick welded steel plates, which makes them rather pricey.

In this context, utilizing a different material for constructing the floater, such as reinforced concrete, might prove to be more economically feasible. Another method to reduce the cost of floating wind energy could be using a larger wind turbine, absorbing more power. DTU has developed a 10MW reference wind turbine, which was scaled-up based on the 5MW NREL solution. Furthermore, the cost cutting advantages of these two suggestions could be brought together, resulting into a reinforced concrete large scale wind floater.

1.2 Concept selection

In order to analyze and design a full floating wind turbine, a reference system is considered as in figure 1.1, with the origin in the still water level and one axis directed against the direction of the mean wind speed.

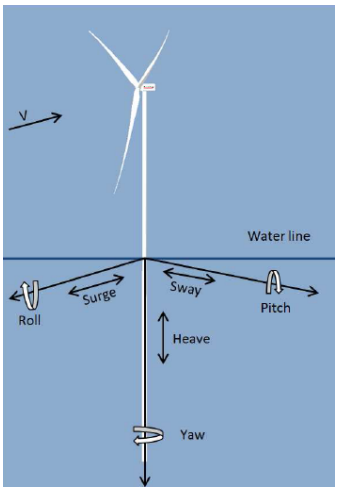

Figure 1.1: *DOFs of a floating wind turbine [10]*

Six degrees of freedom, corresponding to the six rigid-body modes of motions, are defined as in table 1.1.

DOF	Value
Surge	Translation along the longitudinal axis (main wind direction)
Sway	Translation along the lateral axis (transverse to the main wind direction)
Heave	Translation along the vertical axis
Roll	Rotation about the longitudinal axis
Pitch	Rotation about the lateral axis
Yaw	Rotation about the vertical axis

Table 1.1: *DOFs of a floating wind turbine*

Floaters are classified in three basic types, based on the way they achieve their stability in pitch/ roll, as illustrated in figure 1.2.

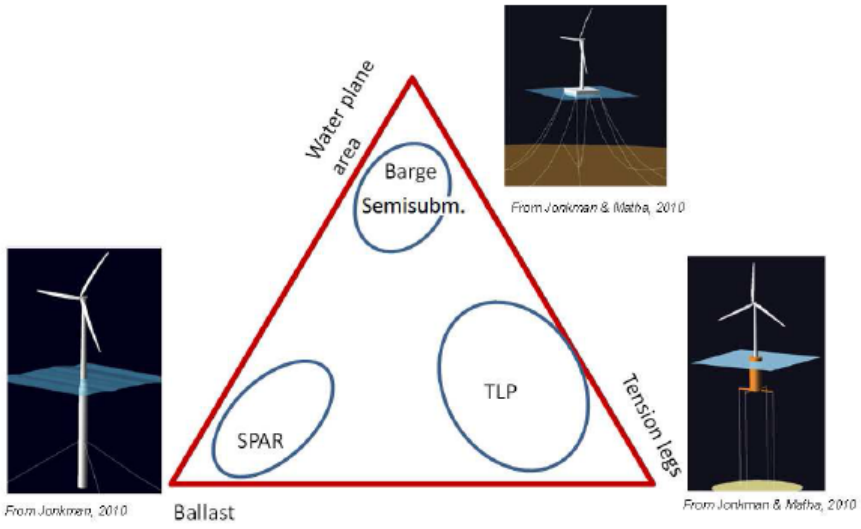

Figure 1.2: *Classification of floaters [10]*

In the present thesis a semi-submersible is selected for investigation, which in general obtains its pitch restoring from a combination of buoyancy and ballasting. Semi-submersibles developed in the oil and gas industry are usually column stabilized units with relatively small water plane areas. The major part of the buoyancy is provided by submerged pontoons which extend beyond the deck. Semi-submersibles may experience motions of significant magnitude, both wave frequent and low frequent. The motions in the horizontal plane are susceptible to higher order excitation, whereas the ones in the vertical plane to first order waves. This concept is singled out as the concept of choice for several reasons, among which the intention to reach a technically feasible solution, applicable in intermediate water depths as well. Furthermore, it is meant to support a DTU 10MW reference wind turbine, in order to maximize the economies of scale. This is not an optimized solution, relatively heavy, generating a large average thrust force at a high hub level. These functional requirements disqualify a spar type floater, which would require a very deep draft for ensuring stability. TLP solutions in intermediate water depths also bring along numerous uncertainties with their complex mooring system, such as possible slack tethers, ringing or springing. For such practical motifs, it is reasoned that a semi-submersible floater is a simpler and hence could be a more robust and stable design.

Such a solution could be built in different construction materials, e.g. steel, reinforced concrete. The latter is selected for a number of reasons. First of all, it is an environmentally friendly material boosting a huge potential for achieving low production costs through mass production and industrialization, worldwide. According to [12], it has local content to as much as 50 - 90% and can be fabricated virtually anywhere, also not requiring that specialized skills and equipment, as with steel constructions. This also implies that the competition could be improved due to the high number of potential fabricators, eventually leading to the establishment of an efficient and effective supply chain. Furthermore, it has technical advantages, offering an increased dynamic performance, with high fatigue resistance, in flexible designs. Last but certainly not least, it has an established history as a marine construction material. Judging by examples from the industry of offshore concrete structures which have been built for different purposes along time, it is observed

that when designed and constructed properly, a long design life (70 years) involving low structural maintenance can be achieved [34]. [12] mentions a planned underwater parking facility in Oslo, with a target design life of 300 years.

1.3 Previous work

In the pre-project work, an initial design of a braceless star shaped concrete semi-submersible to support the DTU 10MW reference wind turbine, was developed. In particular, the focus was on designing the pontoons and columns, including considerations on the arrangement and dimensioning of reinforcement steel bars and concrete material over the cross-sections. The overall shape was inspired by work submitted by [16], which focuses on the design procedure of large wind semi-submersibles manufactured of steel.

With assumed dimensions and structural cross sectional characteristics, the pre-project work investigated the floaters stability and motions behavior. The concept was firstly established in an Excel tool, based on simple theory of floating bodies; its accuracy was consequently verified against commercial numerical tools, with good agreement. Initially, the desired operational draft was fixed to 15 m. This value was chosen in order to provide a relatively shallow draft, while also ensuring that in extreme environmental conditions the rectangular box shaped pontoons remain fully submerged, in order to avoid possible water exit and slamming loads. The free board height was fixed to 20 m, in order to ensure the circular hollow columns are not submerged under the extreme operational heeling angle (wind gust). Moreover, the diameter of the central column was fixed to 10 m, at the turbine tower connection. High density reinforced concrete was selected as the construction material, with ρ=2500$\frac{kg}{m^3}$. In terms of the wall thickness, based on previous design experience, the constant value of 0.6 m was adopted overall.

The resulting semi-submersible had one central column supporting the wind turbine and three side columns, connected at the bottom by submerged pontoons which provided most of the buoyancy. The floater achieved stability through its columns, without ballast. The heeling angle under the average wind thrust force was below 7 deg. The resulting dimensions, are summarized in table 1.2, as confirmed with numerical tools.

	Unit	Value
Central column diameter	[m]	10
Offset column diameter	[m]	12.5
Pontoon height	[m]	5
Pontoon width	[m]	12.5
Column height	[m]	35
Free board	[m]	20
Overall length on x	[m]	75.5
Overall length on y	[m]	85.25
Cross sectional thickness	[m]	0.6
Displacement	[T]	13243
Total mass of reinforced concrete	[T]	11750

Table 1.2: *Main characteristics of the pre-project concept*

A top view of the pre-project floater is presented in figure 1.3.

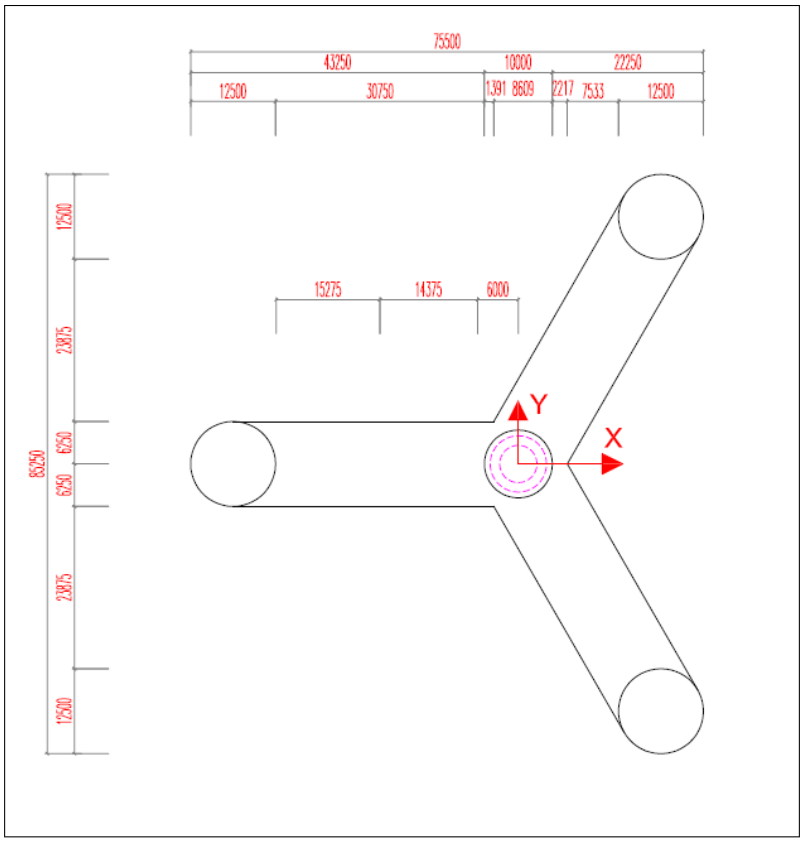

Figure 1.3: *Top view of the pre-project concept*

Two frequency domain hydrodynamic analysis have also been conducted. The main findings related to motions characteristics and loads are summarized next:

- Heave natural period of the floater is 17.5 s.
- 13 wave directions have been investigated and it was seen that the floater is not highly sensitive to this parameter. The directions of interest ranged between 0-180 deg and were considered to be representative for the entire floater, due to the geometrical symmetry established by the horizontal axis.
- A composed model analysis is required for properly capturing the response of the floater at resonance. A panel model analysis, fully based on potential theory (only includes potential damping), does not suffice. A composed model which includes both panel and Morison models, accounting for the linearised viscous effects is required. This is consistent with the theory [15], considering that near the resonance the radiation damping is small in the inviscid solution, because of the long wave regime.
- Sectional forces have been determined along one of the pontoons, at three representative cross sections. A simple design check based on the membrane theory has been performed. This has confirmed that the assumed wall thickness was reasonable in the critical section. No out of plane shear was considered.

With these remarks, the floater design was considered acceptable at the pre-project stage, to be further improved and completed in the present work.

1.4 Thesis goals, objectives and tasks

The task of analyzing and designing an offshore concrete floater to support a large wind turbine is challenging. Typical phases in the life of a wind floater are the following:

- Construction in a dry dock/ afloat.
- Mating of the wind turbine assembly (steel tower, nacelle, hub, blades).
- Tow to field.
- Installation at the offshore location.
- Operation.
- Decommissioning/ Removal.

The structure has to be hydrodynamically stable under many different conditions. Its dynamic response is also relevant in all stages. Ideally, the loads it undergoes during these phases should be identified and the final design should satisfy the different governing load combinations and code checks. However, such an attempt could not be made during such a short time frame.

Consequently, in the present work it is intended to develop the pre-project design into an optimizable baseline design. This is desired to meet or exceed the outlined functional needs, in terms of compatibility with the wind turbine, operational stability under the maximum average wind thrust and motions in the vertical plane. Furthermore, for investigating the structural response, finite element analysis is conducted. With the resulting stresses, a ULS sectional design is performed. The objectives also include developing structural drawings, a corresponding bill of quantities and a rough cost estimate. The equivalent CO_2 emission for producing the required materials is also assessed. These elements represent the basis for potential optimization studies and more detailed design work, potentially leading towards the fulfillment of the overall goal of reducing the cost of offshore floating wind energy.

The focus is on the floater during operation and also the ULS global loads acting on the pontoons and the columns are addressed. Consequently, a linear structural analysis and ULS sectional design checks are carried out. The analysis and design work is achieved in close cooperation with Olav Olsen AS, whose engineers are experienced in offshore oil and gas concrete platforms.

The following main tasks are addressed in the thesis:

1. Literature study on the design of semi-submersible floaters and offshore concrete structures. Establish a design basis, to outline the main functional requirements determined by the wind turbine characteristics, motions and stability. Select a suitable installation site. Investigate the ULS load effects due to wind and wave actions on the braceless semi-submersible.

2. Improve the numerical global model that was established in the project work, for analysis of cross-sectional loads due to environmental actions. Investigate the floater motions susceptible to first order wave excitation (in the vertical plane). Increase the heave natural period outside of the waves range and possibly reduce the number of the investigated wave directions. For the central column that supports the wind turbine, wind loads need to be considered when assessing the cross-sectional loads in that column.
3. Cooperate with Olav Olsen AS on design of concrete floating wind turbines. Study the sectional design criteria and procedure, and the methods and software for structural analysis of concrete platform. Investigate the design challenge for concrete hulls (pontoons and columns in this case).
4. Establish a shell structural model for stress analysis under the obtained global loads. DNV Sesam software package is used in the analysis.
5. Perform ULS sectional design checks for the entire floater, based on the structural analysis results, in order to ensure acceptable reinforcement and concrete ratios, in the critical areas. Prepare a preliminary bill of quantities, a cost estimate and evaluate the impact on the environment, of the required construction materials.
6. Conclude the work and give recommendations for future work.
7. Write the MSc thesis report.

In the thesis, the personal contribution to the resolution of the problem within the scope of the thesis work is presented. Theories and conclusions are based on mathematical derivations and/or logic reasoning, identifying the various steps in the deduction. The thesis is organized in a rational manner to give a clear exposition of results, assessments, and conclusions. The text is intended to be brief while to the point, with a clear language.

1.5 Design procedure and tools

First of all, the functional requirements due to the wind turbine are identified. These have to be ensured, next to a proper motions and stability behavior while in operation. The key steps in the structural analysis and design are to identify the ULS loads, to calculate the internal load effects on the structure when subjected to different governing combinations of these loads and finally to perform a code check to verify that the design criteria is fulfilled.

In order to have a solid starting point, the external geometry as well as weights and rigidity (and hence cross sectional thickness) need to be reasonably approximated in the preliminary design stage. This is achieved based on basic understanding of structural mechanics and shell theory, together with previous design experience gathered during the pre-project work and through specialized literature. Simplified analytic methods are key design tools.

The global analysis provides an accurate and detailed knowledge of the design load effects over the entire structure. According to [17], it is carried out almost exclusively by linear analysis. Nevertheless, they are usually supplemented by non linear models for some

of the local designs at the intersection of the shell elements where irregularities might be introduced. Also according to [19], linear models are widely used and accepted in the global design. To the present date, the global structural analysis of offshore concrete floaters in the oil and gas industry, have mainly been based on a linear theory of elasticity. Structural analysis and design based on linear theory allows for redistribution of internal stresses, having a greater safety margin than the combined design load and material factors imply.

Like most complex structures, the design of offshore concrete platforms utilizes Finite Element Method (FEM) computer programs. Beginning with the mid-seventies the use of large finite element programs has increased, sometimes with over one million degrees of freedom, which required supercomputers. As seen in [6], the computer FEM analysis procedures for reinforced concrete structures have seen important advancement over the last half of century. At the same time, and no less significant, an accelerated development of computing technology and hardware was witnessed. Figure 1.4 illustrates graphically the tremendous exponential growth in computing power over the recent years. It is seen that the computing speed has increased by five orders of magnitude in 25 years.

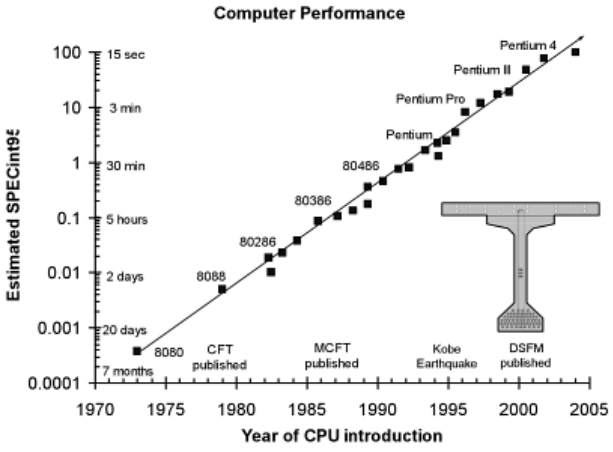

Figure 1.4: *Increase in computing power in recent years [19]*

Linear elastic based stress analysis using FEM is an important tool. Some of its advantages are:

- Well established method which is relatively easy to apply.
- It can easily accommodate for multiple load cases with a minimal change in the input data.

On the other hand, its main drawbacks are:

- It does not provide information on the collapse load of the structure (lower bound to the strength limit design load).
- It is not intuitively obvious how to interpret output of such an analysis and how to detail the reinforcement.

The output of a linear elastic FE analysis is expressed in terms of stresses and strains in a Cartesian coordinate system, with its axis chosen parallel to the envisaged reinforcement directions. For practical reasons, it is preferable to detail the reinforcement along axis orthogonal to the axis of the structure or structural element being designed, even though the elastic load path is given by the principal stresses. The principal stresses and their respective directions are calculated by plotting Mohr's circle. It is shown in [12], that for panels which require reinforcement in only one direction, the solution of providing reinforcement steel along one axis of the structure is less efficient than when reinforcing in the major principal stress direction. Nevertheless, it is more practical. In the present work, the floater in reinforced along a local system of coordinates defined relative to the global system of coordinates.

The concrete floater is subjected to a large number of loading conditions during its different phases, of which the survival under extreme weather is of interest in the present report. Furthermore, it presents a rather complex geometry, with both straight and curved tapered shells, subjected to a large number of design checks. Hence, the floater analysis and design involve a large amount of data manipulation. To make the assessment more straightforward, a tailor made post-processor is used. The basic idea behind it is that the reinforced concrete strength is checked point wise, by comparing the stress resultants with the strength in the same point, considering a non-linear material response.

A schematic representation of the design and analysis procedure is illustrated in figure 1.5. It represents the backbone, the structure of this document. During the pre-project, steps 1 to 4 were investigated in general. Part of the present work, the design basis is updated. In this context, it is decided to increase the heave natural period of the floater, in order to avoid resonant behavior. For these reasons and in order to provide the reader of this document with a clear overview of the entire procedure, it is decided to pursue a fresh iteration, while relating to the pre-project main findings.

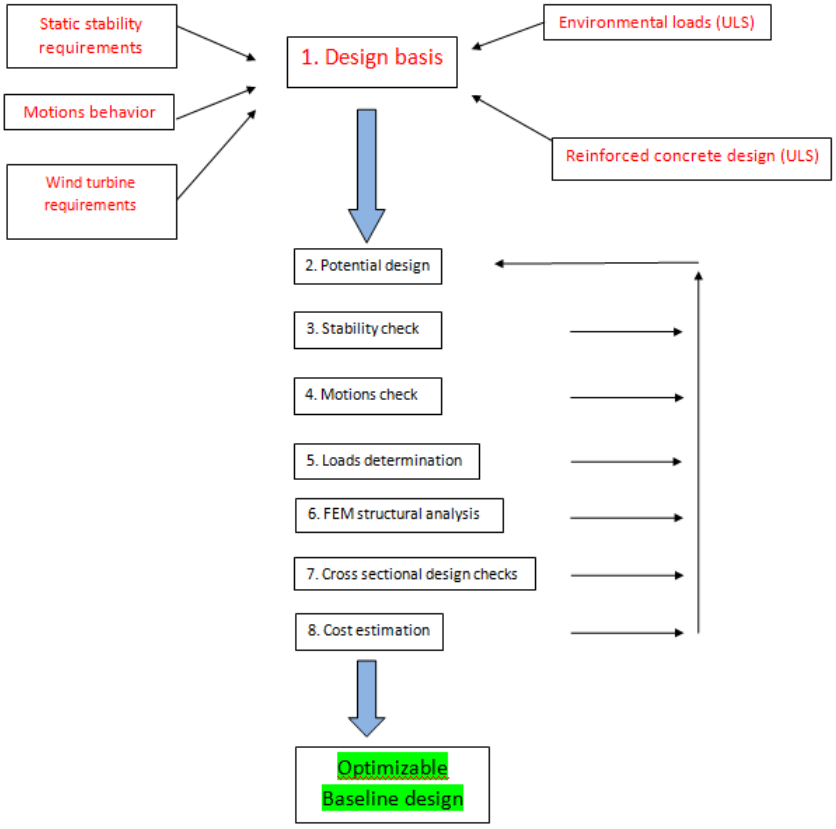

Figure 1.5: *Overall design procedure*

Chapters 2 and 3 provide the reader with a brief history of the offshore concrete structures and with an overview of the theories available for modeling reinforced concrete elements, respectively.

Following, the design and analysis process starts with updating the design basis. This is achieved in chapter 4, which reflects the main requirements in accordance with the structure's function and the concerned standards and practices acknowledged by the offshore concrete industry.

Based on the pre-project work and considering the updated design basis, in chapter 5, an updated floater outer shape with cross sectional properties is proposed, based on a simple analytic tool.

The analysis and design of a reinforced concrete semi-sub concept involves extensive numerical investigations, both in terms of hydrodynamics and structural strength. Converging towards an acceptable design which would represent a baseline for further detailed design and optimization requires several iterations, to be ideally performed by an entire team of designers. Nevertheless, for achieving this target the DNV Sesam software package is made use of. An overview of this system of tools is presented in figure 1.6.

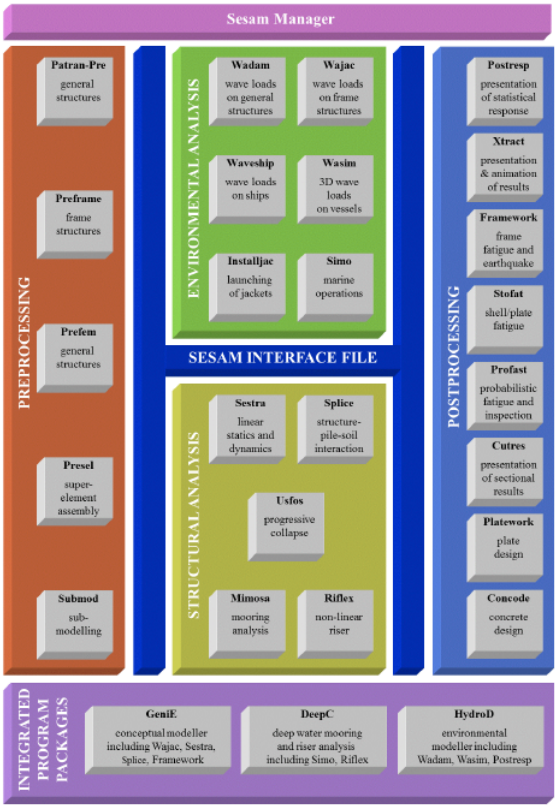

Figure 1.6: *Overview of the Sesam system [31]*

Chapter 6 describes the pre-processing work, required in order to attempt the different computational analysis, which eventually lead to post-processing the stress results. This initial step is achieved in GeniE.

After the static stability is ensured, a hydrodynamic analysis is carried out in the waves frequency domain for determining the floater's motions behavior and the associated structural loads. These steps are illustrated in chapter 7. The analysis tool is HydroD, whereas the results are post-processed in Postresp and Matlab. With the wave loads determined, a free vibration analysis followed by a quasi-static structural analysis are carried out, as shown in chapter 8, based on Sestra tool from Sesam package.

With the resulting stresses, ULS cross sectional design checks are performed, for ensuring acceptable utilization ratios for the reinforcement and concrete grade, in the critical areas. This is achieved by using ShellDesign, a specialized tool developed and provided by Dr.techn. Olav Olsen AS. The post-processing work and results are further presented in 9.

The paper is concluded and recommendations for future work are given in chapter 10.

Chapter 2

History of offshore concrete structures

Major activity in the construction of offshore concrete platforms has started around 1970 to a large extent in the North Sea, with players such as Norway and the UK, thus is a relatively young industry. Offshore concrete platforms are currently mostly encountered in the oil and gas production.

Multiple concepts have been developed along time. These structures come in various shapes and sizes, adapted to the particular site conditions in terms of water depth, environmental loads and functional requirements. The most common type is that of a GBS, which is bottom fixed to the sea floor and acquires stability under its own weight. Furthermore, it is capable of supporting heavy topsides and it also has oil storage capacity in its large base caissons. A typical GBS substructure is illustrated in figure 2.1.

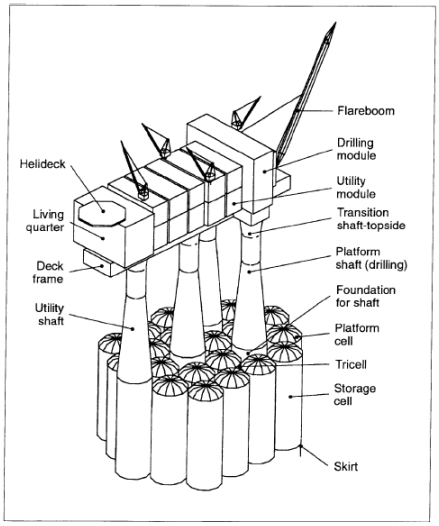

Figure 2.1: *Gravity base structure (Gullfiks, North Sea, [17])*

It generally consists of a shell/ plate caisson structure connected to a number of tapered/ straight shafts which support the topside and at the same time house the drilling and production equipment. The caisson is provided with skirts which during the installation procedures penetrate through the seafloor, requiring little to no site preparation, while ensuring the foundation stability. Thus, the caisson provides the required buoyancy during tow out operations, while when installed it works as a foundation with storage capacity.

As the exploitation of hydrocarbons moved into deeper waters, buoyant structures increased their competitiveness. As such, we have other examples of concrete in marine applications like floating concrete hulls for semi-submersible and tension leg platforms, together with concrete barges, concrete islands and LNG terminals. The table presented in figure 2.2 summarizes the main characteristics of the major existing concrete structures for oil and gas production.

Nr	Year Install.	Original Operator	Field/ Unit	Platform Type	Water Depth	Concrete vol. m³	Location
1	1973	Phillips	Ekofisk	Caisson, Jarlan Wall	71 m	80 000	North Sea (N)
2	1974	Atlantic Richfield	Ardjuna Field	LPG Barge	43 m	9 200	Indonesia
3	1975	Mobil	Beryl A	GBS 3 shafts	118 m	52 000	North Sea (UK)
4	1975	Shell	Brent B	GBS 3 shafts	140 m	64 000	North Sea (UK)
5	1975	Elf	Frigg CDP1	GBS 1 shaft, Jarlan Wall	104 m	60 000	North Sea (UK)
6	1976	Shell	Brent D	GBS 3 shafts	140 m	68 000	North Sea (UK)
7	1976	Elf	Frigg TP1	GBS 2 shafts	104 m	49 000	North Sea (UK)
8	1976	Elf	Frigg MCP-01	GBS 1 shaft, Jarlan Wall	94 m	60 000	North Sea (N)
9	1977	Shell	Dunlin A	GBS 4 shafts	153 m	90 000	North Sea (UK)
10	1977	Elf	Frigg TCP2	GBS 3 shafts	104 m	50 000	North Sea (N)
11	1977	Mobil	Statfjord A	GBS 3 shafts	145 m	87 000	North Sea (N)
12	1977	Petrobras	Ubarana-Pub 3	GBS caisson	15 m	15 000	Brazil
13	1978	Petrobras	Ubarana-Pub 2	GBS caisson	15 m	15 000	Brazil
14	1978	Petrobras	Ubarana-Pag 2	GBS caisson	15 m	15 000	Brazil
15	1978	Shell	Cormorant A	GBS 4 shafts	149 m	120 000	North Sea (UK)
16	1978	Chevron	Ninian Central	GBS 1 shaft, Jarlan Wall	136 m	140 000	North Sea (UK)
17	1978	Shell	Brent C	GBS 4 shafts	141 m	105 000	North Sea (UK)
18	1981	Mobil	Statfjord B	GBS 4 shafts	145 m	140 000	North Sea (N)
19	1981	Dome Petroleum	Tarsuit	Concrete Island, LWA	16 m	8 800	Beaufort Sea
20	1982	Phillips	Maureen ALC	Concrete base artic. LC	92 m	3 500	North Sea (UK)
21	1983	Texaco	Schwedeneck A*	GBS Monotower	25 m	3 620	North Sea (D)
22	1983	Texaco	Schwedeneck B*	GBS Monotower	16 m	3 060	North Sea (D)
23	1984	Mobil	Statfjord C	GBS 4 shafts	145 m	130 000	North Sea (N)
24	1984	Global Marin	Beaufort Sea **	GBS caisson, Arctic	16 m	14 300	Sakhalin (R)
25	1986	Statoil	Gullfaks A	GBS 4 shafts	135 m	125 000	North Sea (N)
26	1987	Statoil	Gullfaks B	GBS 3 shafts	141 m	101 000	North Sea (N)
27	1988	Norsk Hydro	Oseberg A	GBS 4 shafts	109 m	116 000	North Sea (N)
28	1989	Statoil	Gullfaks C	GBS 4 shafts, Skirt Piles	215 m	244 000	North Sea (N)
29	1989	Hamilton Bros	N. Ravenspurn	GBS 3 shafts	42 m	9 800	North Sea (UK)
30	1989	Phillips	Ekofisk P.B.	Protection Ring	75 m	105 000	North Sea (N)
31	1996	Elf Congo	N'Kossa	Concrete Barge	170 m	26 500	Congo
32	1993	NAM	F3-FB	GBS 3 shafts	43 m	23 300	North Sea (NL)
33	1992	Saga	Snorre CFT	Suction anchors, 3 cells	310 m	7 800	North Sea (N)
34	1993	Statoil	Sleipner A	GBS 4 shafts	82 m	77 000	North Sea (N)
35	1993	Shell	Draugen	GBS Monotower	251 m	85 000	North Sea (N)
36	1994	Conoco	Heidrun Found.	Suction anchor, 19 cells	350 m	28 000	North Sea (N)
37	1996	BP	Harding	GBS Foundation/ Storage	109 m	37 000	North Sea (UK)
38	1995	Shell	Troll A	GBS 4 shafts, Skirt Piles	303 m	245 000	North Sea (N)
39	1995	Conoco	Heidrun TLP	Concrete TLP, LWA	350 m	63 000	North Sea (N)
40	1995	Norsk Hydro	Troll B	Semisub	325 m	43 000	North Sea (N)
41	1996	Esso	West Tuna	GBS 3 shafts	61 m	29 000	Australia
42	1996	Esso	Bream B	GBS 1 shaft	61 m	14 000	Australia
43	1996	Ampolex	Wandoo	GBS 4 shafts	54 m	28 000	Australia
44	1997	Mobil	Hibernia	GBS 4 shafts, Ice Wall	80 m	165 000	Canada
45	1999	Amerada Hess	South Arne	GBS	60 m	35 000	North Sea (DK)
46	2000	Shell	Malampaya	GBS 4 shafts	43 m	34 000	Philippines
47	2005	SEIC	Sakhalin LUN-A	GBS 4 shafts, Arctic	48 m	35 500	Sakhalin (R)
48	2005	SEIC	Sakhalin PA-B	GBS 4 shafts, Arctic	30 m	28 000	Sakhalin (R)
49	2008	ExxonMobil	Adriatic LNG	LNG terminal	29 m	95 000	Adriatic Sea (I)

Notes:
* The unit has been removed and demolished by the end of its life
** Relocated from Beaufort Sea to Sakhalin.

Figure 2.2: *Existing offshore concrete structures for oil and gas production [12]*

Subfigure 2.3a illustrates the first and to the present date, only concrete semi-submersible moored with catenary anchors, while a tension leg platform with a concrete hull is shown in subfigure 2.3b. They are built of high performance lightweight aggregate concrete.

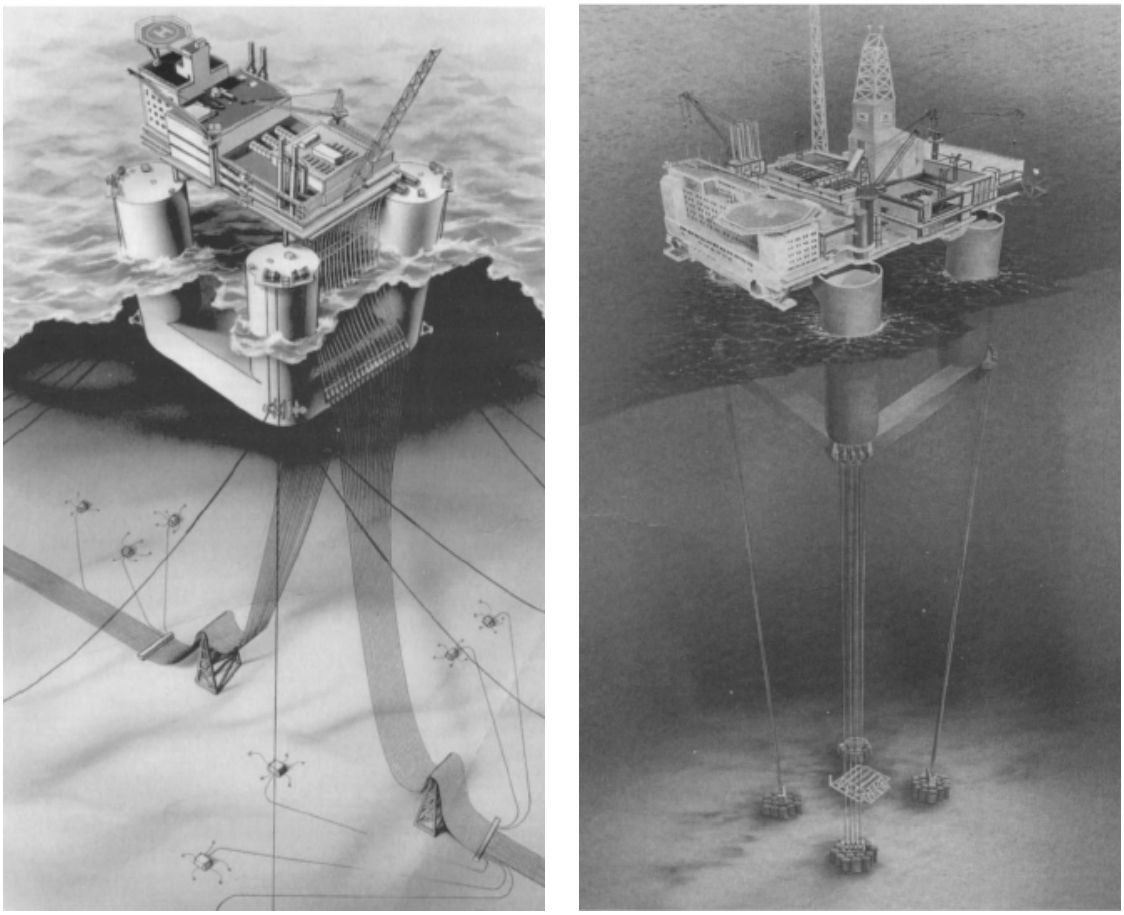

(a) Catenary anchored semi-submersible. Concrete volume $43000m^3$. (Troll B, North Sea)

(b) Tension leg platform. Concrete volume $66000m^3$. (Heidrun, North Sea)

Figure 2.3: *Floaters with concrete hulls [17]*

Analyzing and producing a detailed design of such structures is a challenging task. However, in hostile environments they are usually favored over steel jackets and floating hulls, for hydrocarbons exploitation. This is not always the case in sites with moderate water depth and more benign climatic conditions.

All the above mentioned structures are fabricated of heavily reinforced high strength/ high performance concrete which is subjected to extensive quality control procedures. These are important requirements in order to achieve the desired performance and durability of the slender structural elements, ensured through a careful materials selection and adequate mix design. Their construction is normally carried out in a benign inshore location, ensuring cost efficiency. Once completed they are towed to their final destination in deep water with exposed conditions. Standard test methods are available to verify all relevant concrete properties. In service inspections of existing platforms show an excellent

performance with little or no maintenance required for the concrete hull. Examination of cores drilled out from several North Sea platforms after 20 years of service have revealed a low chloride content near the steel, below the critical threshold value for the initiation of rebar corrosion, according to [19]. The steel reinforcement is well protected from corrosion by an adequate concrete cover, in accordance with the relevant code requirements for the intended exposure class and design life.

By comparison, the presence of concrete floaters in the wind industry is yet shy. The most noticeable contribution so far, comes from the University of Maine, where a scaled demonstration project has been deployed off the coast in June, 2013. The braced prototype known as VolturnUS is depicted in figure 2.4 during its construction and ready for towing.

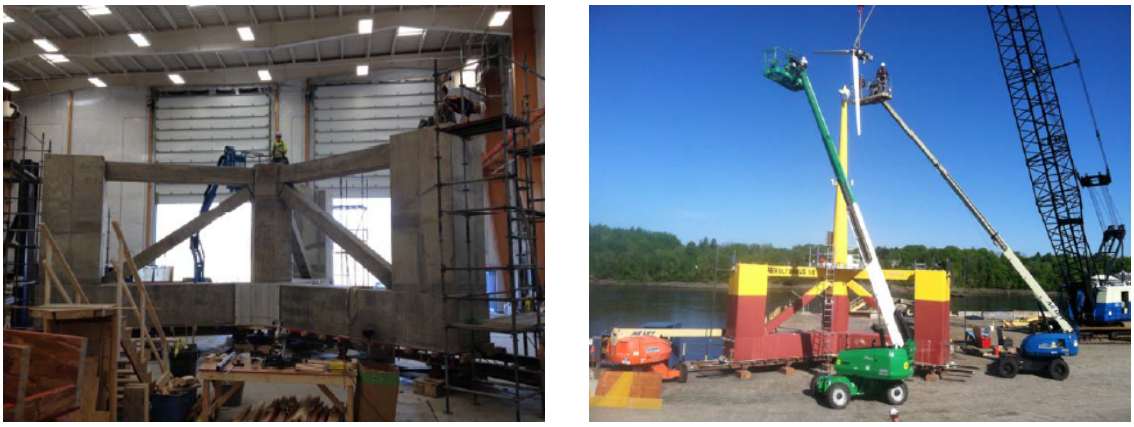

(a) During construction (b) Ready for deployment

Figure 2.4: *VolturnUS in scale 1:8 [5]*

The turbine respects a 1:8 geometric scaling of a 6MW design, while the floater is claimed to obey Froude laws. In full scale, the system is designed to be constructed and assembled dockside. Its overall properties are summarized in table 2.1.

Parameter	Value in full scale
Operational draft [m]	20
Towing draft [m]	9
Hub height [m]	100
Rotor diameter [m]	152
Rated power [MW]	6
Mooring lines	3
Hull material	Prestressed concrete
Tower material	Light-weight composite
$H_{S,50}$ [m]	12.2
$T_{P,50}$ [s]	14.1
Water depth [m]	80-100

Table 2.1: *General properties and design conditions of the VolturnUS [5]*

Chapter 3

Theories for modeling membrane and shell reinforced concrete elements

In order to ensure the safety of the floater, its structural response under extreme environmental loads is crucial. For being able to predict it, the substructure is conceptualized as composed of simpler elements acting together. How the load is shared between these component parts is answered in the global analysis. For this task, sophisticated global structural analysis procedures and computational power are available. Most challenges occur in the next step, when attempting to describe how does each of these elements respond to its applied loads, at the element analysis level. Over the last 40 years, several models have been developed for predicting the load-deformation response of membrane and shell reinforced concrete elements. Most of the differences occur from how the cracks are accounted for. Hereafter, in the present chapter a brief overview is attempted. None of these approaches is generally accepted, hence their application has to be carefully assessed with special attention to the assumptions.

3.1 Lower bound theory of plasticity for membrane elements

When it comes to designing a box/ trapezoidal cross section, it can be regarded as being composed of 4 thin concrete plates. Each of these can be designed separately as plain concrete plates reinforced in 2 orthogonal directions, based on the respective shear and normal stress which they are to be carrying, based on [28]. The concrete takes the compression, whereas the steel takes the tension. Consequently, the initial step is determining a reasonable cross sectional stress distribution over the box girder. The procedure starts from expressing the equilibrium of an infinitesimal element, as illustrated in figure 3.1.

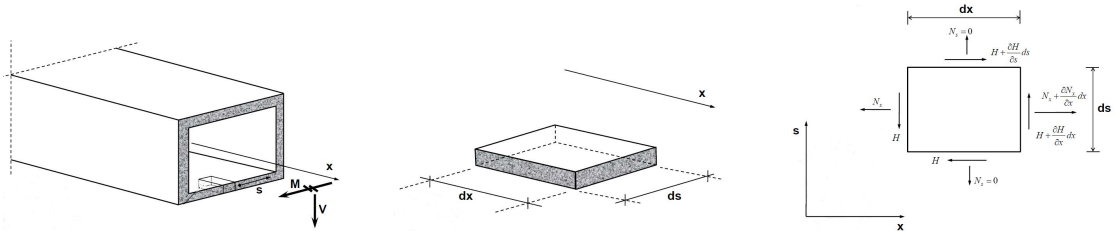

Figure 3.1: *Equilibrium of an infinitesimal element in a thin walled section under M and V*

Consequently, the equilibrium in x direction is expressed as shown in equation 3.1.

$$(N_x + \frac{\partial N_x}{\partial x}dx)ds - N_x ds + (H + \frac{\partial H}{\partial s}ds)dx - Hdx = 0 \tag{3.1}$$

By manipulating the above equation it results equation 3.2:

$$(\frac{\partial N_x}{\partial x} + \frac{\partial H}{\partial s})dxds = 0 \tag{3.2}$$

This is true if equation 3.3 is satisfied, from which it results equation 3.4.

$$\frac{\partial N_x}{\partial x} + \frac{\partial H}{\partial s} = 0 \tag{3.3}$$

$$\frac{\partial \sigma}{\partial x} + \frac{\partial \tau}{\partial s} = 0 \tag{3.4}$$

When the distribution of σ is chosen, the τ distribution can be calculated based on 3.4.

For illustrative purposes, a simple lower bound solution for a box girder subjected to bending moment and shear force (M and V respectively), as illustrated in subfigure 3.2a, is developed next. Initially, it is assumed the normal stresses σ follow a Navier distribution, as illustrated in subfigure 3.2b.

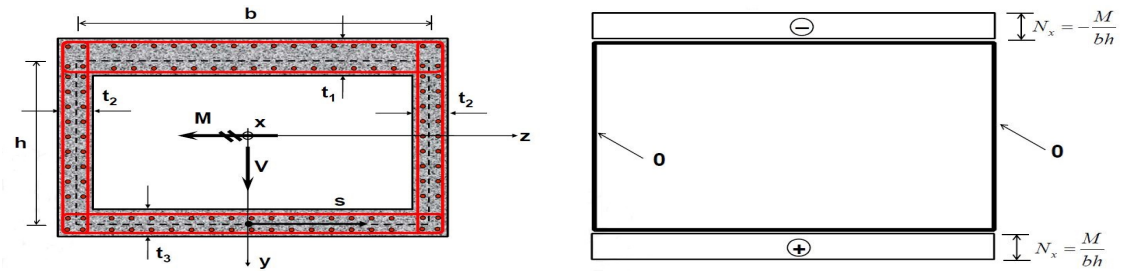

(a) Box girder characteristics

(b) Nx cross sectional distribution due to M

Figure 3.2: *Box girder under M and V*

σ_x corresponding to any point *1* in the upper flange, *2* in the vertical flange and *3* in the lower flange is expressed:

$$\sigma_{x,1} = -\frac{M}{bht_1} \qquad \sigma_{x,2} = 0 \qquad \sigma_{x,3} = \frac{M}{bht_3} \tag{3.5}$$

For the bottom flange, substituting the values obtained by equation 3.5 into equation 3.4 yields:

$$\frac{\partial(\frac{M}{bh})}{\partial x} + \frac{\partial H}{\partial s} = 0$$

$$\frac{V}{bh} + \frac{\partial H}{\partial s} = 0$$

$$\frac{\partial H}{\partial s} = -\frac{V}{bh} \quad (3.6)$$

It results that:

$$H = -\frac{V}{bh}s + k \qquad H = 0 \quad for \quad s = 0 \quad due \quad to \quad simmetry$$

$$k = 0$$

$$H = -\frac{V}{bh}s \quad (3.7)$$

In the vertical webs we have assumed $N_x = 0$. Therefore H must be constant. The final shear force distribution is illustrated in figure 3.3.

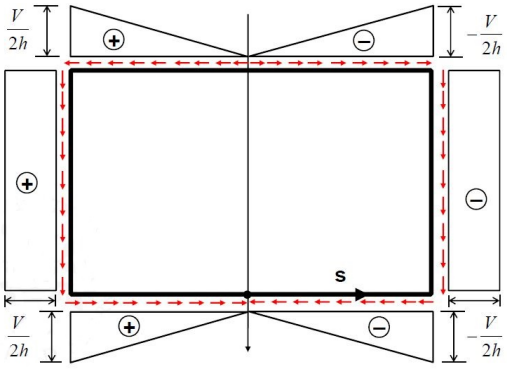

Figure 3.3: *H cross sectional distribution due to V*

It results the following:

$$\tau_{max,1} = \frac{V}{2ht_1} \qquad \tau_{max,2} = \frac{V}{2ht_2} \qquad \tau_{max,3} = \frac{V}{2ht_3} \quad (3.8)$$

Furthermore, when considering an additional action of a constant normal force $N_{x,add}$ (tension or compression) on the box girder along the x axis, the corresponding normal stresses are added to the already existing values as calculated in 3.5, assuming a constant distribution over the reinforced concrete area. The additional contribution is:

$$\sigma_{add,1} = \sigma_{add,2} = \sigma_{add,3} = \frac{N_{x,add}}{A} \quad (3.9)$$

where A represents the total reinforced concrete area.

Moreover, a hollow and thin walled cross section could also be subjected to a torsional moment T around the x axis, as illustrated in figure 3.4. This will lead to a constant

flow of shear stresses τ. The additional shear stress, to be added to the already obtained shear as shown in equation 3.8, can be calculated by use of Bredts formula, as shown in equation 3.10.

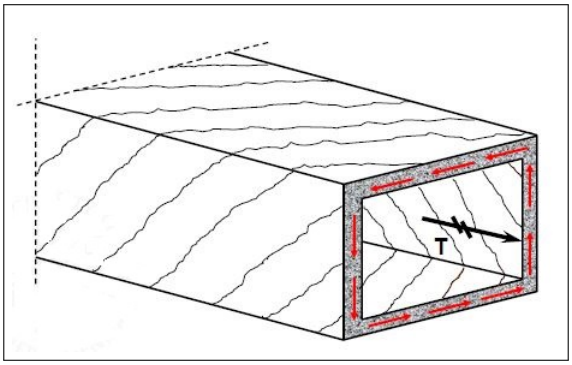

Figure 3.4: *Thin walled cross section subjected to torsional load T*

$$\tau_{add,1} = \frac{T}{2bht_1} \qquad \tau_{add,2} = \frac{T}{2bht_2} \qquad \tau_{add,3} = \frac{T}{2bht_3} \tag{3.10}$$

Consequently, with known σ_x and τ_{max} in each of the 4 concrete discs (the vertical flanges are assumed identical in the present example), it is now possible to design the reinforcement and check the concrete stresses against the allowable limits. Such a concrete disk, with the corresponding reinforcement and stresses, is illustrated in figure 3.5. It is here remarked that in our box girder design $\sigma_y = 0$ in all concrete disks.

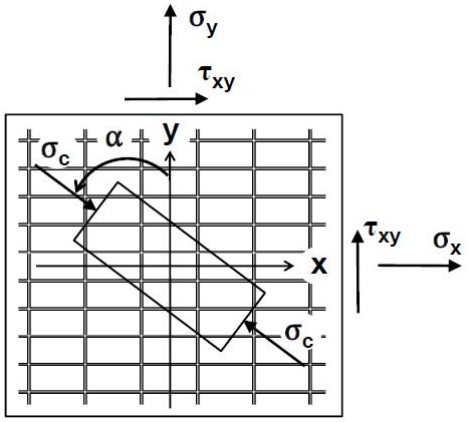

Figure 3.5: *Orthogonal reinforced concrete disk*

The following assumptions are made in the ULS design:

- Require the reinforcement to yield in tension, which means $\sigma_{sx} = f_y$
- The uniaxial concrete compression stress σ_c, forms the angle α with the y axis.
- The reinforcement is evenly distributed. A_{sl} is area per length in x direction and A_{st} is area per length in y direction, respectively.

The overall design procedure valid also for $\sigma_y \neq 0$, is summarized and followed for each concrete disk, in all points of interest:
General: $\sigma_x \leq \sigma_y$

- Case 1: $\sigma_x \geq -|\tau_{max}|$
  $A_{sl} = (\sigma_x + |\tau_{max}|)\,\frac{t}{f_{yd}}$
  $A_{st} = (\sigma_y + |\tau_{max}|)\,\frac{t}{f_{yd}}$
  $\sigma_c = 2|\tau_{max}| \leq \nu f_c$
- Case 2: $\sigma_x < -|\tau_{max}| \quad \& \quad \sigma_x\sigma_y \leq (\tau_{max})^2$
  $A_{sl} = 0$
  $A_{st} = \left(\sigma_y + \frac{(\tau_{max})^2}{|\sigma_x|}\right)\frac{t}{f_{yd}}$
  $\sigma_c = |\sigma_x|\left(1 + \left(\frac{\tau_{max}}{\sigma_x}\right)^2\right) \leq \nu f_c$
- Case 3: $\sigma_x < -|\tau_{max}| \quad \& \quad \sigma_x\sigma_y > (\tau_{max})^2$
  $A_{sl} = 0$
  $A_{st} = 0$
  $\sigma_c = |\frac{1}{2}(\sigma_x + \sigma_y) - \sqrt{\frac{1}{4}(\sigma_x - \sigma_y)^2 + \tau_{max}^2} \leq \nu f_c$

It is further remarked that if $\sigma_x > \sigma_y$ the index x is replaced with y, in the cases above described. Also, A_{sl} becomes A_{st} and the other way around, respectively. If $\sigma_c \leq \nu f_{cd}$ is not fulfilled, the cross sectional thickness t is adjusted such that the crushing of the concrete is avoided, in each critical point of the concrete discs. The value of $\nu \approx 70\%$.

This was the modeling approach adopted during the pre-project work, when it has been applied in three representative cross sections along the pontoon, based on forces determined in the center point of it, through a frequency domain hydrodynamic analysis. However, it is remarked that this approach does not account for the out of plane shear, nor does it account for the local bending, so it is not entirely suitable for modeling the floater, unless the transverse stresses are accounted for separately. Besides its limitations, the main advantage of such an approach is that it is very logical, with clear steps and provides a safe solution.

3.2 Lower bound theory of plasticity for shell elements

Unfortunately, such a theory has not been yet developed according to [28], though it would have been very useful.

3.3 Modified compression field theory and its relation to ShellDesign

For the original technical paper the reader is kindly referred to [13]. MCFT proposes an analytic model suitable for predicting the load-deformation response of reinforced concrete elements subjected to in-plane shear and normal stresses (i.e. membrane stresses). Hence it is fit for structures idealized as an assemblage of membrane elements, among which offshore gravity based structures, as illustrated in figure 3.6.

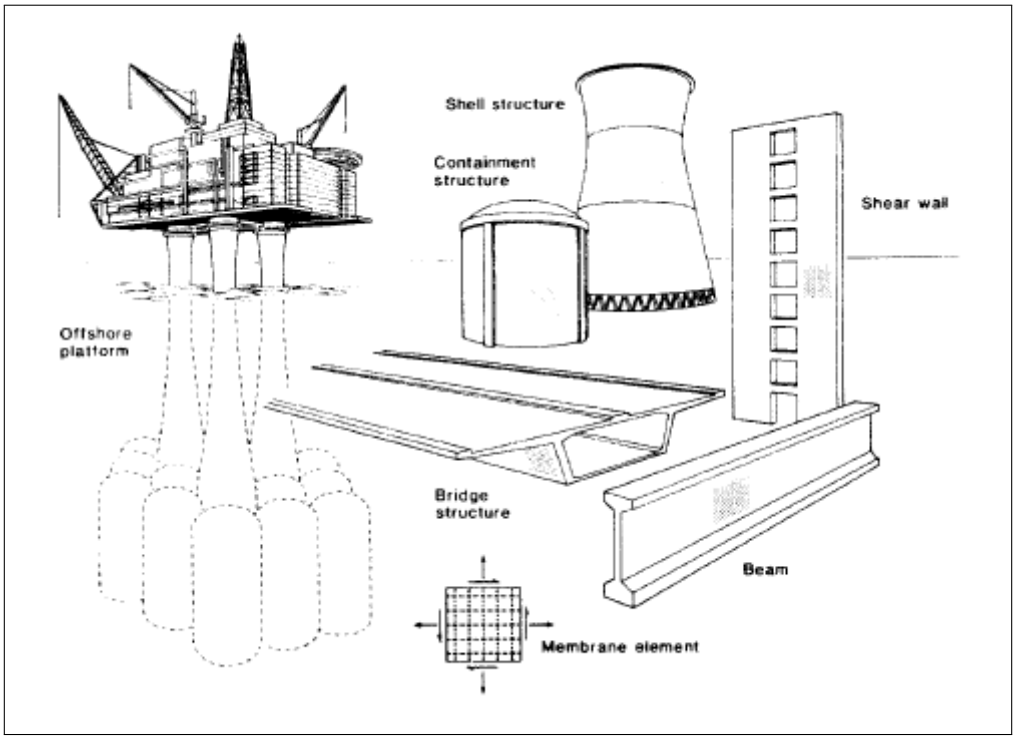

Figure 3.6: *Structures composed of membrane/ shell elements [13]*

It has been developed based on the compression-field theory [24] which is fit for reinforced concrete beams in torsion and shear. In both approaches, the cracked concrete is treated as a new-material with its own stress-strain curve. Compatibility, equilibrium and stress-strain relationships are expressed in terms of average stresses and strains.

According to specialized literature [14], it has been observed in experiments that plain uniaxially compressed concrete (i.e. concrete cylinder) exhibits a higher stiffness and strength capacity, compared to cracked reinforced concrete in compression. This effect is known as compression softening and is illustrated in figure 3.7.

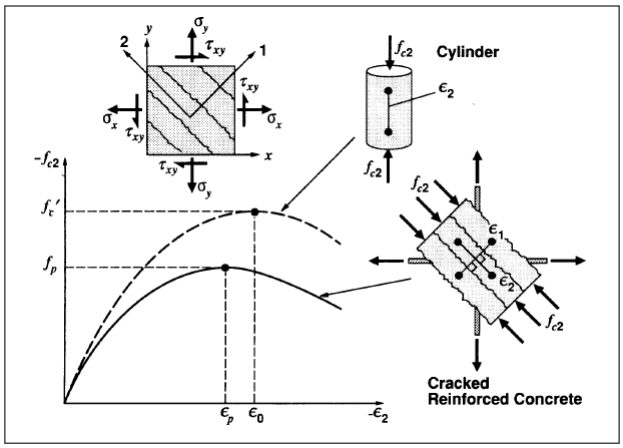

Figure 3.7: *Deteriorated compression response in cracked reinforced concrete elements [14]*

It is related to the degree of transverse cracking and tensile straining present in the structural member. This phenomena is not accounted for in the original compression field theory.

The refinements introduced by the authors in the modified compression field theory [13], are summarized next:

- Constitutive model for concrete in compression, reflecting the compression softening effects.
- Constitutive model for cracked concrete in tension, reflecting the tension stiffening effects.
- Check of local stress conditions at crack locations.

To date, besides the MCFT, a number of other analytic models have been proposed to represent these listed effects, according to [14]. Naturally, there is some disagreement with regard to the degree of softening which occurs and as to what factors influence it exactly. Hence, the suggested compression strength reduction coefficient differs slightly from one theory to another, though they universally agree that including some degree of softening is crucial for accurately modeling the behavior of cracked reinforced concrete structures.

This is basically the theory behind the post-processor ShellDesign, without tension stiffening (neglect the concrete tensile strength). The design for the in-plane stresses is handled separately of the out of plane ones, as further described.

Design for in-plane stresses. Non-linear sectional response

The 8 forces for a design section are illustrated in figure 3.8, in relation to their coordinate system. They are expressed as forces and moments (per unit meter, kN/m and kNm/m), referred to the local section coordinate system, *1,2,3* axis system.

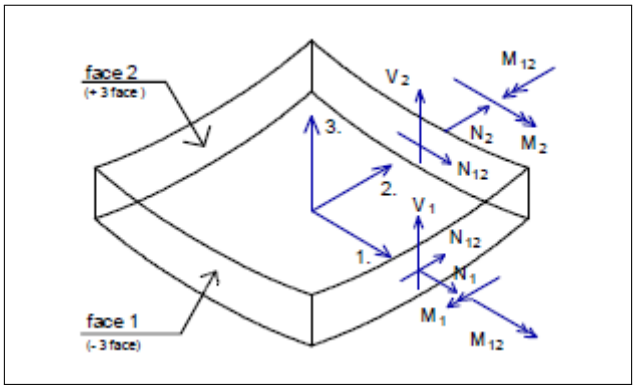

Figure 3.8: *Sectional forces in an infinitesimal shell section [32]*

The calculation of in-plane strain and stresses in a design section is based on non-linear sectional response due to the non-linear material behavior of reinforced concrete. The

result of the sectional analysis for in-plane stresses is a state of strain satisfying the specified non-linear material requirements, the geometric requirements of compatibility and the equilibrium conditions for the shell element. The design for the in-plane stresses is based on the following assumptions:

- In-plane sectional forces due to load effects are known: N1, N2, N12, M1, M2 and M12.
- Linear strain distribution over the thickness of the shell section.
- The stress-strain relationships for concrete and reinforcement are known (non-linear).

In order to integrate the concrete stresses in cracks into stress resultants, the shell section is divided into layers of equal thickness. As the stress-strain relationship is not linear, the satisfaction of the equilibrium equation 3.11 is solved by an iteration of the strain distribution procedure.

$$F_L = F_R \tag{3.11}$$

where F_L are the stress resultants due to load effects and F_R is the response, i.e. stress resultants due to stresses in concrete and reinforcement.

The Newton-Raphson iteration method is used to a specified degree of accuracy. The stresses are then derived based on non-linear sectional response.

Design for transverse stresses

It is based on a beam analogy approach accepted by NS3473, also referred to as a "simplified method". This includes the sectional transverse forces V_1 and V_2. A "uniaxial" condition (Nα, Mα, Vα) is determined for all directions (α) in steps of 5 deg, in accordance with the following equations (NS3473):

$$V_\alpha = V_1 cos(\alpha) + V_2 sin(\alpha)$$

$$N_\alpha = N_1 cos^2(\alpha) + N_2 sin^2(\alpha) + 2N_{12} sin(\alpha) cos(\alpha)$$

$$M_\alpha = M_1 cos^2(\alpha) + M_2 sin^2(\alpha) + 2M_{12} sin(\alpha) cos(\alpha)$$

$$A_{s\alpha} = A_{sx} cos^4(\alpha) + A_{sy} cos^4(\alpha)$$

Based on the in-plane stresses, the tension shear capacity is calculated in accordance with the standard. When the capacity is exceeded, shear reinforcement is required. A similar approach is adopted for determining the compression shear capacity.

Chapter 4

Design basis

In the present work, a concrete semi-submersible floater is analyzed and designed to support a DTU 10MW reference wind turbine. It is a development compared to the pre-project design, to represent a baseline design for further optimization. In terms of the overall shape, the semi-submersible is star shaped. It consists of one central column supporting the wind turbine and three side columns, connected to the central column by three submerged pontoons. There are no braces, nor water ballast considered in this concept. The columns and pontoons are to be fabricated of reinforced concrete. In order to attempt this target, to provide solid grounds for the analysis and design work, a design basis is developed over the present chapter.

It starts by outlying the adopted safety philosophy. Next is formulating the main functional requirements of such a floating structure. The chapter also covers the extreme environmental data for ULS sectional design checks. Following, the stability and motion requirements are set. It also contains a section on materials and construction techniques. Last but not least, some of the environmental aspects of realizing such constructions are investigated.

It is further remarked that the principles, technical requirements and guidance for design and construction of floating wind turbine structures are not yet extensively outlined by the international standardization companies. The only document available at the present time which is specific for undertaking such a task is [10]. Relevant for designing offshore concrete structures are [9] and NS3473, of which the latter is implemented in ShellDesign. Consequently, the following findings are not based solely on one document, but rather represent a mix of logic and best practices from multiple fields, as found through extensive literature study.

4.1 Loads and materials safety factors

According to [10], structural safety of floating wind turbines is ensured by use of a safety class methodology. The structure is to be designed to normal safety class. This requirement reflects that it is unmanned during severe environmental loading conditions,

so the consequences of failure are mainly of an economic nature. The different safety classes applicable for different parts of the floating units are reflected in terms of different requirements for load factors. The requirements for material factors usually remain unchanged regardless of which safety class is applicable for the structure in question. These target safety levels apply to structures which are correctly planned and built, i.e. without systematic errors.

The load factors are defined in accordance with [10] with dominating environmental load and normal safety class, as summarized in the following table:

Limit state	G	E
ULS	1	1.35
SLS	1	1
G= Permanent load E= Environmental load		

Table 4.1: *Load factors γ_f*

The material factors used in Norway according to NS3473 are defined in table 4.2, as found in [17].

Limit state	ULS	SLS
Concrete	1.25	1
Reinforcement	1.15	1

Table 4.2: *Material factors*

4.2 Functional requirements

4.2.1 Determined by the wind turbine

The main functional design constraints of the floating wind assembly are based on the wind turbine information. The DTU 10MW reference wind turbine is thoroughly assessed based on the reports from DTU Wind Energy [11]. The main findings of interest in the present study are summarized in table 4.3.

Description	Unit	DTU 10MW
General info		
• Wind regime		IEC Class IA
• Configuration		Upwind,3 blades
• Control		Collective pitch
• Drive train		Multiple stage gearbox
• Power rating	[MW]	10
• Maximum average wind power thrust	[kN]	1500
• Rated wind speed	$[\frac{m}{s}]$	11.4
• Cut-in, cut-out wind speed	$[\frac{m}{s}]$	4, 25

• Cut-in, rated rotor speed	[rpm]	6, 9.6
• Rated tip speed	$[\frac{m}{s}]$	90
Geometry info		
• Rotor, hub diameter	[m]	178.3, 5.6
• Hub height	[m]	119
• Tower height	[m]	115.63
Mass info		
• Single blade	[T]	41.716
• Hub	[T]	105.520
• Nacelle	[T]	446.036
• Steel tower	[T]	628.442
Tower info		
• Base outer diameter	[m]	8.3
• Top outer diameter	[m]	5.5
• Average outer diameter	[m]	6.9

Table 4.3: *10MW DTU Reference wind turbine data*

Based on the cut-in and rated rotor speeds, the 1P and 3P rotational frequencies of the wind turbine are computed with a 10% safety margin. The results are illustrated in figure 4.1. The "dry" eigen frequencies of the support structure vibrating in air resulting of this project, are aimed to be either between the 1P and 3P or larger than the 3P, in order to avoid its dynamic excitation in interaction with the operational loads. The range of eigenfrequencies that should be avoided is quite broad since the selected DTU 10MW wind turbine has a relatively wide range of operational rotational frequencies.

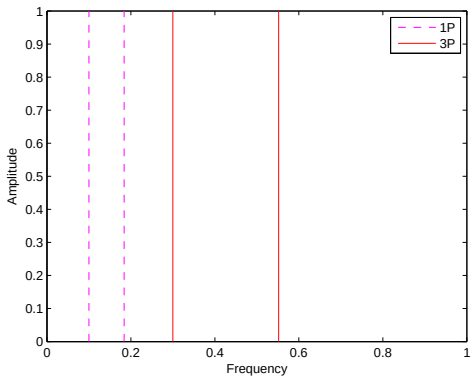

Figure 4.1: *1P and 3P rotational frequencies of the DTU 10MW reference wind turbine*

Detailed cross sectional turbine tower and blade data is provided for the reader's reference in the project appendix A. Based on it, the center of mass of the different elements is computed in Microsoft Excel, as summarized in table 4.4, with $z = 0$ at the still waterline level.

	Unit	X	Y	Z
CM of blades	[m]	7.1	0	119
CM of hub	[m]	7.1	0	119
CM of nacelle	[m]	-2.687	0	121.45
CM of steel tower	[m]	0	0	42.56

Table 4.4: *Centers of mass*

Consequently, the main functionality criteria are outlined. They ought to be ensured throughout the wind turbine lifetime (assumed 20 years):

- Provide enough space to ensure a proper blades fit.
- Maintain the wind turbine tower design. Ensure a minimum of 8.3 m diameter for the floater central column, in order to connect the tower base.
- Maintain the hub height suggested in the DTU design.
- Provide space for cables and other system components.

4.2.2 Stability and motion

In general, the semi-submersible has to be capable of maintaining intact stability at all phases of its design life. However, the stability investigations in the present work are limited to the floater in operation, under maximum average wind thrust. To conduct a reliable stability analysis for the floater in operation under extreme wind gust, a full time domain coupled analysis should be set up. It is expected that such a condition might be critical for the operation phase.

The maximum average wind heeling moment is determined by the thrust force of the wind turbine still in operation at the rated wind speed (1500 kN), acting at the rotor hub level (119 m), with respect to the buoyancy center.

For semi-submersibles, the area under the righting moment curve to the angle of down-flooding has to be equal to or greater than 130% of the area under the wind heeling moment curve to the same limiting angle, as illustrated in figure 4.2.

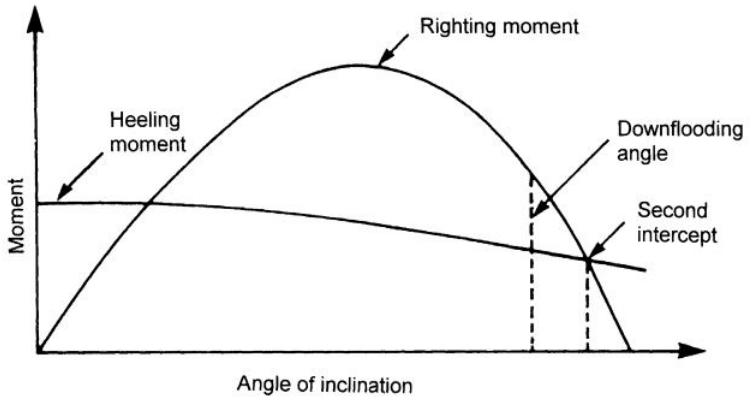

Figure 4.2: *Righting moment and wind heeling moment curves [10]*

The response characteristics (motions) in the vertical plane of the floating support structure are of interest in the present work, in order to ensure they are outside of the waves

frequencies and also do not interact with the wind turbine operational frequencies. The present semi-submersible is a column-stabilized unit consisting of large-diameter support columns attached to submerged pontoons. Usually, semi-submersibles have small water-plane areas, which give rather high natural periods in vertical modes. The natural period in heave is usually outside the range of wave periods even in extreme sea states. This implies that a semi-submersible normally has relatively small vertical motions compared to a monohull floater such as a barge. Depending on the location and the sea state, ocean waves contain substantial energy in the spectral period range 3 to 20s. For a floater, the natural periods of motion are key features, which reflect the design philosophy. In general, the natural period for semi-submersibles in heave is above 20 s and below 5 s for a TLP. In surge, sway and yaw the natural frequencies are typically above 100s and are governed by the station keeping system.

To conclude, the stability criteria for the maximum average operational conditions are formulated as follows:

- Determine the design overturning moment under the average wind thrust at the rated wind speed. Limit the heeling angle below 10 deg under the determined design overturning moment. This is found to be a reasonable value when compared to other existing designs [21] and is intended in order to limit the accelerations in the nacelle, which are associated with possible negative effects on the wind turbine.
- Ensure the area under the righting moment is over 130% compared to the area under the design over turning moment.

The motions response limiting criteria are as follows:

- Ensure a heave natural period greater than 20 s. This is required in order to avoid resonance at wave frequency motions, as most energy in the wind waves would be found at lower periods.
- Ensure roll and pitch natural periods greater than 25 s.

4.3 Environmental data for ULS

Environmental conditions consist of all natural phenomena (wind, waves, current) which influence the design of the floating wind turbine substructure, by governing its loading, hence its rigid body motions and flexible structural response. They are site-specific, i.e. are referring to a specific location. In order to select a suitable offshore location for positioning the wind floater, document [20] is studied. It presents joint environmental data at 5 European offshore locations, out of which 2 are in the North Sea. Based on the water depth and distance to shore, they are compared and site Norway 5 is selected for positioning the wind floater. Furthermore, it is assumed that the extreme loads in extreme wind and wave conditions are governed by the wave loads. Consequently, the main site characteristics are selected and presented in table 4.5.

Area	Name	Water depth [m]	Distance to shore [km]	50-year wind speed at 10m height [m/s], V_{50}	50-year significant wave height [m], $H_{S,50}$	Mean value of T_p [s]
North Sea	Norway 5	202	30	31.2	15.6	14.5

Table 4.5: *General site information and statistics*

This data is compared to reference values for 3 hours provided in [10] and is seen in good agreement.

In order to conduct a true probabilistic design of the floater which has to withstand the effects of the environmental loads, it would be necessary to provide a simultaneous probabilistic model of all the three load generating sources mentioned above. In principle, the most accurate ULS design approach is based on long-term statistics of response. This is very computationally expensive. Alternatively, a simplified conservative approach is adopted. In accordance with [8], the 50 year environmental conditions can be represented by the 50-year wave and mean wind speed, combined with the 10-year current. In the present work the current load is not considered, as no relevant data is available and its effects are assumed of secondary importance during extreme conditions.

4.3.1 Design wave load

The extreme wave load effects in the ULS design are estimated by the "50-year wave" method. This is understood as a wave with a height $H_{max,50}$ being exceeded on the average only once every 50 years. For this approach to be valid, it is required that the load effect is primarily of quasistatic nature, which is ensured by avoiding resonant conditions.

The design wave height is established in accordance with [10]:

$$H_{max,50} = 1.86 H_{S,50} \tag{4.1}$$

The shallow water wave breaking limit is calculated as:

$$H_{break,shallow} = 0.78d \tag{4.2}$$

With d=202 m, it leads to H_{break}=157 m. With the value of $H_S, 50$ extracted from table 4.5 and in accordance with equation 4.1, it returns $H_{max,50}$=29 m. This is seen as smaller compared to the shallow water braking limit, so it becomes the final value for the design wave height. It also demonstrates that the selected site Norway 5 is not in shallow waters.

Next, a suitable range of corresponding wave periods is established, as follows:

$$\sqrt{6.5H_{max,50}} \leq T \leq \sqrt{11H_{max,50}} \tag{4.3}$$

where the left hand side of the equation is based on a limiting wave steepness $\frac{H}{\lambda} \leq \frac{1}{10}$. Filling in the terms, leads to wave periods T between 14 s and 18 s. Assuming deep water conditions, the wave lengths are computed as $\lambda_1 = 1.56T_1^2$=305.76 m and $\lambda_2 = 1.56T_2^2$=505.44 m, respectively. The steepness of the first wave is calculated accordingly as $\frac{H}{\lambda}$=0.09 which is seen to fulfill the mentioned limiting criterion. Shorter period waves of this height would simply break. However, based on the fact that $\frac{\lambda_2}{2} \geq d$, it is reasoned that the site is not deep water either and the wave "feels" the sea bottom. Consequently, a more detailed assessment is carried out based on figure 4.3.

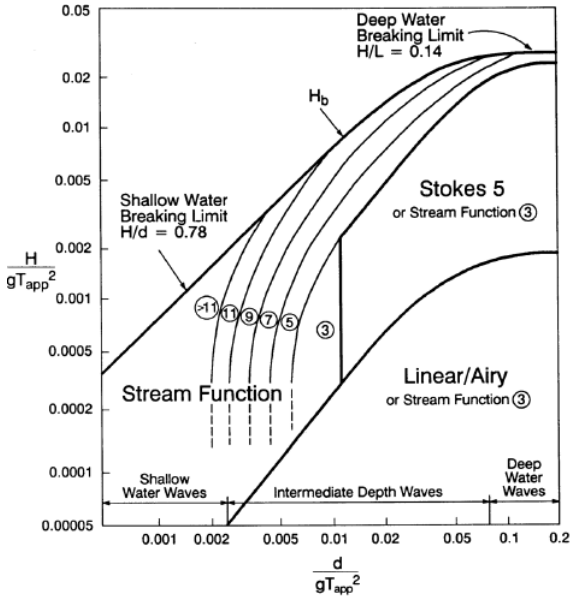

Figure 4.3: *Applicability ranges of various wave theories [25]*

With a ratio $\frac{d}{gT_2^2}$=0.06 it is concluded the site has intermediate water depths, where Airy wave theory is valid. In this approach, the wave particle velocities and accelerations are linearly dependent on the wave amplitude. These assumptions are utilized in the environmental analysis, for determining the water particle motions and the corresponding loads, as further described in the software overview section of chapter 7.

Effects of water pressure in concrete cracks are neglected for structural elements exposed to less than 100 m of waterhead, according to [9].

4.3.2 Wind load

The 50 year wind load on the wind turbine assembly is determined. Generally, this load could be composed of the wind turbine thrust and the tower drag, corresponding to the 50 year wind speed. In the present case, by examining the data already presented in table 4.5, it is seen that the 50 year wind is exceeding the turbine cut-out speed, which means that the turbine is idle in extreme conditions. Hence, the only load component left to consider is the tower drag force. This is computed based on the following equation:

$$F_D = 0.5 C_D \rho_{air} A \int_0^{116} {V_{50}}^2 \tag{4.4}$$

where ρ_{air}=1.229 $\frac{kg}{m^3}$ and A=799 m^2, given by the average tower diameter multiplied with it's height. V_{50} is extrapolated at the hub height with a logarithmic variation, as illustrated in figure 4.4, and integrated accordingly.

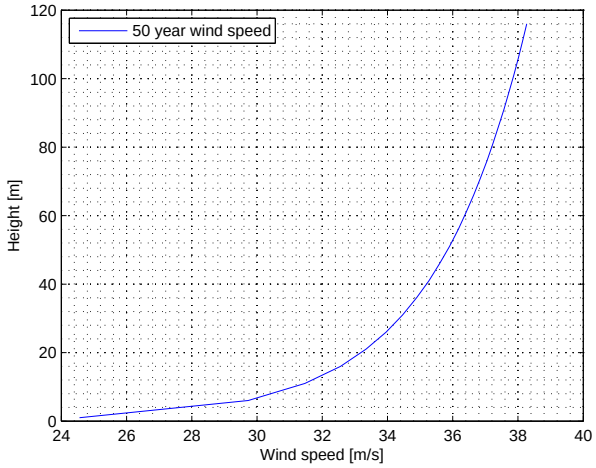

Figure 4.4: *Vertical wind profile*

C_D is the drag coefficient and in order to determine it, a few other concepts have to be introduced first as follows:

- **Inertia force** The inertial force is proportional to the mass of the fluid times its change of velocity in time. This force could also be seen as the force required to stop a moving mass of fluid over a distance L.

$$F_I \propto \rho L^3 \frac{\Delta v}{\Delta t} = \rho L^3 \frac{U}{L/U} = \rho L^2 U^2 \tag{4.5}$$

- **Viscous force** The viscous force depends on the dynamic viscosity μ and on the rate of change of velocity with distance times the surface area of the element. The force on a particle is represented by equation 4.6.

$$F_v \propto \mu \frac{\Delta v}{\Delta z} L^2 = \mu L U \tag{4.6}$$

Based on the forces acting on the fluid, a non-dimensional parameter is defined next, which indicates the relative importance of the forces. The Reynolds number is the ratio of the inertial forces over the viscous forces and is represented by equation 4.7.

$$Re = \frac{\text{inertial}}{\text{viscous}} = \frac{\rho L^2 U^2}{\mu L U} = \frac{V_{50} D}{\nu_{air}} \tag{4.7}$$

For the definition of the Reynolds number, the kinematic viscosity is introduced. This is the dynamic viscosity μ divided by the density ρ_{air}.

$$\nu_{air} = \frac{\mu}{\rho_{air}} \tag{4.8}$$

Filling in the specific data, the calculation returns Re=13E+6. Consequently, C_D=0.5 according to figure 4.5, which illustrates experimental data.

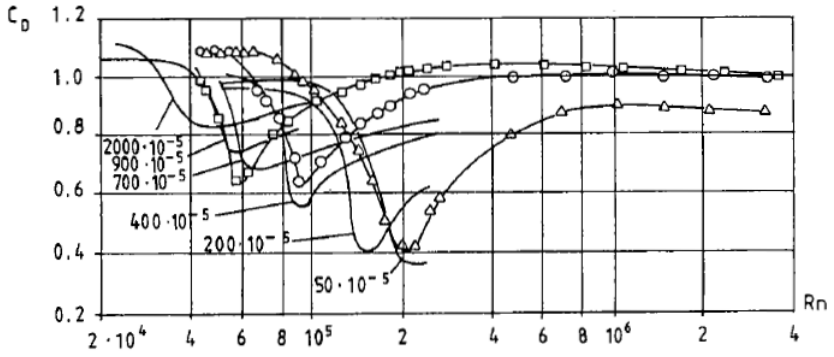

Figure 4.5: *△ C_D Drag coefficient for smooth circular cylinder [15]*

Substituting all values into equation 4.4 returns F_D=306 kN. It is assumed the application point of this static force is at two thirds of the tower height, at 77 m.

4.4 Materials

In the present section, the main construction materials and methods to be utilized in manufacturing the wind turbine floater are described. The approach is mostly from a historical and state-of-the-art perspective. Nevertheless, some innovative ideas are also introduced, which are meant to possibly lead to cost savings.

Concrete

Concrete is an extensively used composite construction material which consists of a hard, chemically inert particulate substance, known as an aggregate (usually sand and gravel) which is bonded together by cement and water. These component raw materials are illustrated in figure 4.6. Concrete is appreciated for its versatility and it can be used structurally in many different scenarios. Structural concrete may be : mass (no reinforcement), reinforced (usually with steel bars) or prestressed (with pre- or posttensioned steel strands).


(a) Coarse aggregate


(b) Fine aggregate


(c) Portland cement


(d) Water

Figure 4.6: *Concrete raw materials*

Mass concrete is a timeless construction material, first being introduced by the Assyrians, who used clay as a bonding substance. Later on, the Egyptians used lime and gypsum cement. The modern era for concrete is considered to have started in 1824, with the discovery of the Portland cement by the English inventor Joseph Aspdin the first truly artificial cement obtained by combined burning of ground limestone and clay. The other major part that constitutes the bulk of the concrete is the aggregate. The common types of aggregates include sand, crushed stone, gravel, slag and ashes. Fine aggregate is mostly used when a smooth final surface is desired. For massive cement structures, coarse aggregate is mainly employed. Mass concrete is mostly used in applications such as foundations, dams, retaining walls.


(a) Mass concrete poured around a precast shaft


(b) Retaining wall


(c) Water dam

Figure 4.7: *Examples of applications of mass concrete*

Reinforced concrete is a type of concrete, which incorporates different types of reinforcement (most commonly bars, grids, plates, fibers) in order to strengthen the concrete in tension. This concept was patented in 1867 by Joseph Monier, a Parisian gardener who first noticed that concrete is strong when in compression, but cracks when subjected to tension loads. He solved this issue by adding a wire mesh to the base of his flower pots and garden tubes, inventing the concept of reinforced concrete. Ever since, a lot of engineers and architects have shown confidence and interest in developing this construction material. By the end of the 19th century it would have already been used in several private housing projects, in both Europe and the United States. With the advancement of the technology, monolithic frame constructions were introduced, designed especially for the industrial segment. As a next step, reinforced concrete permitted the development of an completely new building shape: the thin shell. The year of 1962, with the erection of the Chicago 60 story Marina Bay towers designed by Andy Warlhol, marked the beginning

of the use of reinforced concrete in modern high rise. At the same time, this represents the moment when competition for the steel frame started as well. Nowadays the tallest building in the world, the Burj Khalifa, standing 828m tall, is using reinforced concrete as its primary structural system.

As previously illustrated in chapter 2, it is also an important construction material for the offshore structures. Concrete quality utilized in marine constructions has evolved considerably over time. For example, in 1973 when the Ekofisk tank was completed, the highest strength class allowed by the Norwegian Standard was C45 [17]. For comparison, in more recent structures the strength grades are around C 80-85, which is considered high strength/ high performance concrete. For this increase to be possible, a series of elements are required, as enumerated next:

- High-quality aggregates of suitable size, strength, grading and mineral composition.
- High strength/ low heat cement.
- Low water/ binder ratios and high workability.
- Pozzolanic additives (fly ash, slag, silica fume).
- Chemical admixtures (superplasticizers, set retarders, air entraining agents).

The use of light weight aggregate concrete (LWAC) is a suitable alternative for marine structures and it can lead to significant weight reductions (lower material density) whilst maintaining high strength and durability. It can be produced in most batching plants, similar to the one illustrated in figure 4.8.

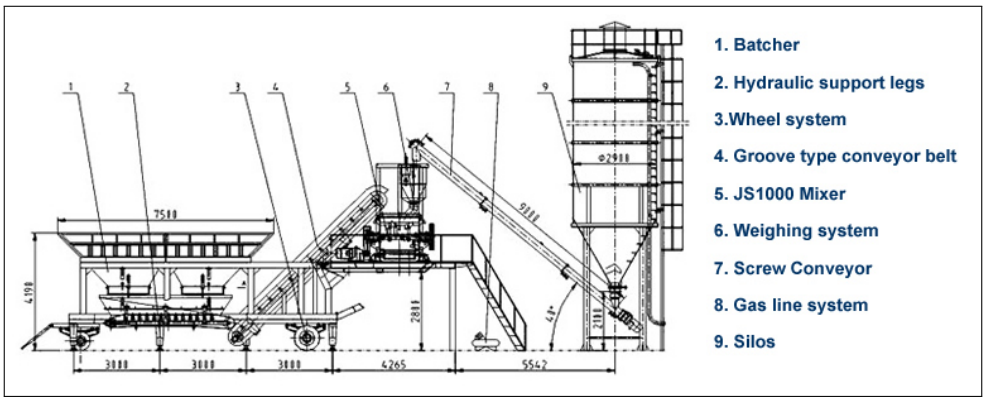

Figure 4.8: *Concrete batching plant*

The concrete mix is to be fine-tuned in order to be compatible with the chosen plant, construction procedures and the prevailing climate. The quality assurance procedures are important, in order to ensure adequate control of the aggregate grading and other admixtures. An adequate durability is also secured through the concrete mix design, combined with details which facilitate placing and compaction, proper curing and adequate cover of the reinforcement.

The chosen mix should lead to concrete of different qualities to be used throughout the floater, depending on the local stress levels. This will give the project some reserves in

the highly stressed areas. Thus, a higher class of concrete may be utilized locally in order to ensure the strength requirements, without having to increase the cross sectional thickness. The required concrete class in the critical design section is the outcome of the post-processing. However, it is here mentioned that classes of strength between C10 - C95 are allowed by the standard NS3473, for normal weight concrete; the lightweight concrete is limited between C12 - C75.

Reinforcement

Offshore structures are subjected to severe loading conditions, which is why they require to be heavily reinforced. According to [12], densities of 300 - 400 $[\frac{kg}{m^3}]$ are not uncommon and may locally rise to 700 - 800 $[\frac{kg}{m^3}]$. This leads to congested areas, especially at the intersection of different structural elements. In this context, the planning together with the production drawings become extremely important. In order to improve the concrete placing into the forms and its compaction, small diameter aggregates are used in combination with large diameter reinforcement bars. For constructing the floater, it is intended to use hot-rolled ribbed bars of weldable quality and high ductility.

Moreover, special reinforcement couplers are to be placed at the congested joints in order to reduce the overlapping length bar splices and the total construction time. Examples of such couplers are illustrated in figure 4.9.

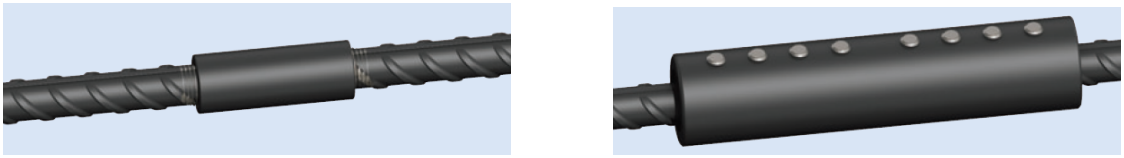

(a) Standard tapered thread (b) Mechanically bolted

Figure 4.9: *Reinforcement couplers[4]*

A standard tapered thread coupler, as shown in sub-figure 4.9a, is suitable for connecting two bars, where one can be rotated. Like its name suggests, it has an internally threaded sleeve with two right hand threads which are tapered towards the middle of the coupler. The bars require some preparation work, its ends are square cut and a tapered thread is cut onto it. In the threading shop, the couplers are torqued onto the reinforcement. The continuation bar is connected by means of a torque wrench. Alternatively, in order to avoid these reinforcement preparations, especially for the larger diameters, the solution illustrated in sub-figure 4.9b is proposed. In this case, the bars are fixed to the coupler by means of conical lock-shear bolts and internal serrated saddles. When the predetermined tightening torque for the bolts is reached, the heads shear off leaving the top of the installed bolt slightly proud of the coupler. This is a good visual check of correct installation. For more details on reinforcement couplers characteristics and installation procedure, the reader is referred to a technical brochure from a possible manufacturer [4].

Instead of conventional shear reinforcement (stirrups), T-headed bars are advised, to further reduce the congestion and to facilitate the placing of concrete. This is standard reinforcement with a friction plate welded on to the ends. Their use is generally in

basements of high rise buildings or airport apron slabs. An example is illustrated in figure 4.10. For more details on the subject, the reader is referred to a technical brochure from a possible manufacturer [33].

Figure 4.10: *Reinforcement arrangement of a deep slab, with T-bars [33]*

Bars of grade 500 MPa are selected to be utilized for reinforcing the floater.

4.5 Construction methods

Offshore concrete structures are constructed based on conventional and proven methods developed by the construction industry over time and then further developed to suit the particular features and requirements of the offshore projects. It is advised to construct as much as possible of the floater, inshore. Work offshore is more costly on both the men and the machines. The erection is expected to be very crane intensive, due to the relatively large footprint with tall columns the floater has. Furthermore, it would also involve simultaneous execution of many activities, some of which at a considerable height. For these reasons, work planning and safety are top priorities.

Where available, erection in a dry-dock is the preferred option. Some of the docks utilized in the previous projects are still in existence [12]. Dry docks are commonly 10 to 15 m deep, some even 20m, closed by simple bund walls or re-floatable caissons. Experience from previous projects shows that in order to establish a new dry dock, some six to eight months are required for site development, besides the time necessary for permitting. Alternatively, a floating barge could be used with the same purpose as a dry dock for smaller concrete structures.

Else, a construction site with a special foundation has to be set up similarly to the one shown in figure 4.11. Though this option would bring in additional costs, it might make sense given that economy of scale is achieved (tailor made high output production line).

Figure 4.11: *GBS under construction in Belgium, Thornton Bank Project [1]*

Starting the construction inshore and continuing it afloat the water is another option worth investigating, especially when having to compensate for reduced land availability. For this purpose, an additional floating construction rig with a fleet of supply vessels and ferries, is required.

In terms of the construction technique, slip forming is suggested. This is a fast method, though relatively labor intensive. The columns and pontoon walls are produced in a continuous lifting process, eliminating all horizontal construction joints. The reinforcement is installed near the top of the climbing forms, providing easy access for inspection. Uninterrupted materials supply is crucial and the compatibility between the setting time of the fresh concrete, with the lifting rate of the formwork assembly, has to be ensured. It is further remarked that pouring concrete with slip forming requires a careful control of the concrete consistency in order to ensure the construction quality, by avoiding flaws in the concrete surfaces. This method can be applied to both vertical and non-vertical walls of variable diameters and cross sectional thickness. Slip-forming of complex shapes can be performed within strict geometrical tolerances.

In marine structures, it is essential that the construction joints are watertight. If one of the compartments is flooded, the floating stability is lost. This line of thinking in design is not common in connection with ship design. Consequently, it is recommended that any injection/ grouting procedure is thoroughly tested in order to ensure that the selected materials, method and equipment work as planned.

The required completion time is relative to the exact size and complexity of the floater, together with the available resources. Work (concreting) can be carried out at sub zero temperatures for extended periods of time, given that appropriate measures are taken. Particularly frost sensitive operations are scheduled for milder weather. Historically, the project schedules have generally been respected in the oil and gas industry, with registered completion times between 18 months and 3 years, according to [12].

Nowadays, in the civil engineering industry quite some interest is seen into the use of robots and self-compacting concrete for uniquely shaped structures, as shown in [22] and [27] . The automatic manufacturing refers to both the reinforcement and 3D curved molds production. These forms come in variate shapes, from relatively small to large ones such as the bridge underside illustrated in figure 4.12. They are manufactured of plywood or

other materials which are easy to mill and able to withstand the surface pressure generated by concrete pouring.

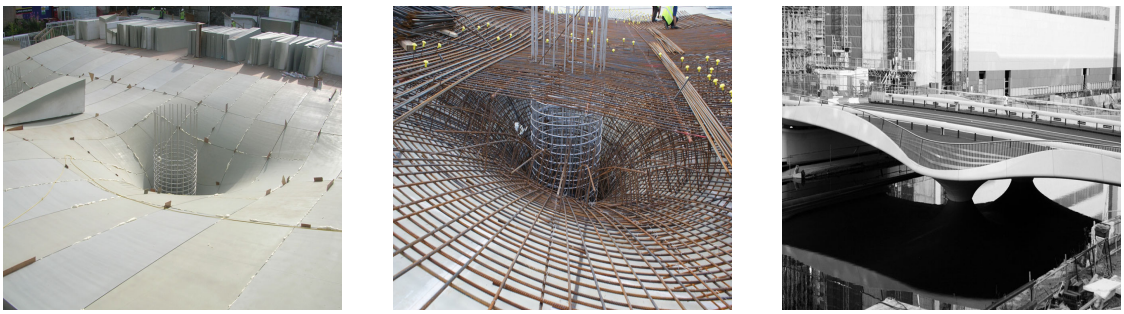

Figure 4.12: *Spencer dock bridge Dublin [2]*

All the operations related to the reinforcement production are also intended to be robotized. Such a robot bending bars is illustrated in figure 4.13.

Figure 4.13: *Reinforcement production setup prototype [3]*

Over time, such a highly automated approach could become an efficient alternative to the traditional slip forming technique coupled with a reinforcement workshop, which is currently the state-of-the-art in the offshore concrete industry, with a great potential for cost savings.

Regardless of the chosen production method, when the floater is completed, it is mated with the wind turbine and its steel tower, at the same inshore location. With the electrical components tested, the assembly is ready to be commissioned. This eliminates the need for large crane vessels, which are both expensive and with a limited availability.

Consequently, the completed platform is towed to the desired operation position offshore, at the design draft, as no ballast is utilized for achieving stability. This installation procedure requires a forecast weather window of roughly a couple of days. In parallel, the sea floor preparations are completed and the mooring system is installed. As a last step, the wind turbine is hooked-up to the electricity export cable, ready for production.

4.6 Durability

Assuming the mix design rules are respected and the construction techniques adequate, reinforced concrete in seawater has adequate durability. A floater built in this technical solution would not have the need to dry dock over its design life, giving it great life cycle costs. For this to be possible, the essentials are a concrete with a low permeability, together with adequate and uniform reinforcement cover.

Considering that the corrosion of the permanently submerged members is initiated by chlorides from sea water, an exposure class XS2 is defined for them, according to [9]. Similarly, for the remaining marine parts in the tidal, splash and spray zone, an exposure class XS3 is defined. For the sake of being conservative, an exposure class XS3 is finally adopted for the entire semi-submersible at this stage, as it is seen to bring more stringent limitations.

It is expected to tie the reinforcement in bundles. The maximum number of bars at any time in a bundle is 4. The ratio between the largest and smallest diameter bar in a bundle can not exceed 1,7. The minimum free distance between reinforcement bundles in one layer , with respect to the exposure class XS3, is defined as 45 mm and between layers 35 mm. When splicing is required a minimum development length should be ensured and the bars should be staggered.

In order to protect the steel reinforcement against corrosion and to ensure its structural performance, the reinforcement has a minimum concrete cover and the nominal characteristic crack width is also limited. Based on requirements for corrosion protection the concrete cover shall not be less than 50 mm, for an XS3 exposure class, with reinforcement slightly sensitive to corrosion and a design service life of 50 years. For protecting other attached or embedded steel parts, a cathodic protection system could be added.

Furthermore, the use of mineral additions to the concrete mix (fly ash, blast furnace slag, silica fume) would further reduce the ingress of chlorides and reduce the risk of thermal cracking, improving the overall durability of the floater. A proper installation of the prestressing system (if required) is vital to the performance and durability of the structure. It should be performed by specialized subcontractors and subjected to rigorous quality control.

4.7 Environmental aspects

Environmental impact

Producing concrete involves the emission of CO_2,SO_2 and NOx which are green house gases. They are toxic and considered by many as not beneficial for the planet we inhabit. For this reason, the life time environmental impact of the floater becomes of interest. Table 4.6 summarizes some typical numbers for estimated equivalent CO_2 impact of some of the available building materials.

Material	Kg of CO_2 equivalent/ tonne material
Concrete	122
Wood	40
Steel (from scrap material)	710
Steel	3215
Cement	656

Table 4.6: *CO_2-equivalent for some building materials [12]*

Accordingly, based on the resulting total mass of the floater, the emission of CO_2 involved in its construction should be computed. The resulting values are to be compared to available alternative solutions.

Removal, demolition and recycling

After decommissioning, the floater has to be removed from the offshore site, through a reverse installation procedure. This is not expected to be a straight forward task, especially as the condition of the platform might not be top-notch, at the end of its design life. In this context, extensive studies of safety precautions are called for, including possible extra strength members and/ or additional buoyancy. Hence, decommissioning and removal may bring in major cost issues, which are weighed up against significantly longer design life and substructure's adaptability to changing functions and requirements during operation (topside design and weight). Nonetheless, according to [12], in the UK the operators are currently required to provide a financial guarantee which covers the future costs of complete platform removal.

With the floater safely brought back to shore, it can either be refurbished or dismantled into sections. The second option is the most common. The sections are subsequently either reused (coastal systems) or demolished and recycled, as reinforcement steel and crushed concrete; currently these are mostly utilized as land fill and in the road building industry, but not for manufacturing new structural concrete, hence a material down-grading.

Chapter 5

Updated floater concept

A calculation spread-sheet has been developed in Microsoft Excel during the pre-project, based on simple analytic formulas which are introduced in section 5.1. With its use, the main dimensions and characteristics of the initial concept were determined. Part of the thesis work, due to the additional requirements and modifications introduced in the design basis, an updated concept is developed based on a similar approach. The initial values have been already introduced in chapter 1.

5.1 Floating bodies main theory and approach

A floating structure is said to be in equilibrium when the resultant of all the forces acting on it is zero and the resulting moment of these forces is also zero. A vertical downward movement (sinking deeper) results in an increase of the buoyant force which will tend to force the structure back upwards; it tends to return the structure to its original state of equilibrium so that the structure is stable for this type of disturbance. Archimede's principle holds for the vertical equilibrium between buoyancy and gravity forces [18]:

$$\rho g \nabla = gm \tag{5.1}$$

For this purpose the total mass of the semi-submersible is computed, as the sum of the light ship weight and the dead weight (ballast, spare parts, etc.). The light ship weight comprises of the weight of each structural component, together with the weight of the turbine tower and the rotor nacelle assembly. The later are treated as point masses, connected by massless beams. Each point mass is assumed to act in its corresponding center of gravity. The above enumerated quantities are adjusted until equation 5.1 is fulfilled. This leads to a displaced volume of water ∇.

For ensuring the vertical stability, Vcg the position of the vertical center of gravity is computed, for the entire structure considering the correct mass distribution. The magnitude of the keel-buoyancy KB distance follows from the underwater geometry of the

structure. The buoyancy-metacenter BM is computed in accordance with equation 5.2:

$$BM = \frac{Ix}{\nabla} \tag{5.2}$$

where Ix is the moment of inertia with respect to the longitudinal axis, which for the present concept is seen to be equal to Iy the moment of inertia with respect to the transverse axis. Next, the gravity-metacenter is computed as:

$$GM = KB + BM - Vcg \tag{5.3}$$

The value of the heeling moment is determined as the product between the maximum thrust force and the lever:

$$M = Thrust_{max}(z_{hub} - KB) \tag{5.4}$$

The resulting angle under the heeling moment is computed as:

$$\phi = atan\left(\frac{M}{\nabla GM}\right) \tag{5.5}$$

The 2D added mass in heave, A_{33}^{2D} is approximated based on the simple solution for a horizontal flat plate long $2C$ in infinite fluid, $A_{33}^{2D} = \rho\pi c^2$. The restoring is also computed as $C_{33} = \rho g Aw$ where Aw is the total water plane area, given by the central and the 3 other offset buoyancy columns. The natural periods of the semi-submersible are computed based on:

$$T_{nn} = 2\pi\sqrt{\frac{Mass + A_{nn}^{2D}}{C_{nn}}} \tag{5.6}$$

5.2 Updated model dimensions and characteristics

Over the present section the updated global model main dimensions and characteristics are established. With a design tool based on the formulas and approach presented in the previous section, numerous configurations are investigated.

Finally, a suitable update is achieved by increasing the column to column distance, while reducing the water plane area of the offset columns which gives the restoring, in order to maintain the hydrostatic properties. At the same time, the width of the base slab is not much reduced, in order to provide similar added mass, while the top slab width is decreased to minimize the overall mass and to match with the offset column diameter, resulting in a pontoon with a trapezoidal box cross section. However, these changes still translate into an increased mass. Hence, to balance the buoyancy requirements, the offset columns are tapered towards a larger base diameter. Also, the free board height is reduced to 16 m, equal to $H_{S,50}$. It is calculated that at this height over the mean water level, under a heeling angle of 10 deg, the offset column top would move 2.77 m horizontally and 0.25 m vertically downwards, ensuring it does not get submerged. Furthermore, for satisfying the strength requirements, the material characteristics are adjusted and wall thickness is varied. For the structural joints, which are expected to be subjected to higher stress levels, a concrete with an increased density is defined. At the same time, the cross

sections are thicker in these areas and internal reinforced concrete bulkheads are also accounted for in order to provide a higher stiffness. The results are summarized in table 5.1. It is remarked that the total mass of reinforced concrete is reduced by 7 % compared to the pre-project values.

	Unit	Value
Central column diameter	[m]	Variable: 10 at top, 12 at bottom
Offset column diameter at still water level	[m]	9
Pontoon height	[m]	5
Base pontoon width	[m]	12
Top pontoon width	[m]	10
Free board	[m]	16
Overall length on x	[m]	91.5
Overall length on y	[m]	103.799
Cross sectional thickness	[m]	Variable: 0.4, 0.5, 0.6, 0.7
Total mass of reinforced concrete	[T]	10726

Table 5.1: *Main characteristics of the updated concept*

A top view of the updated floater is presented in figure 5.1.

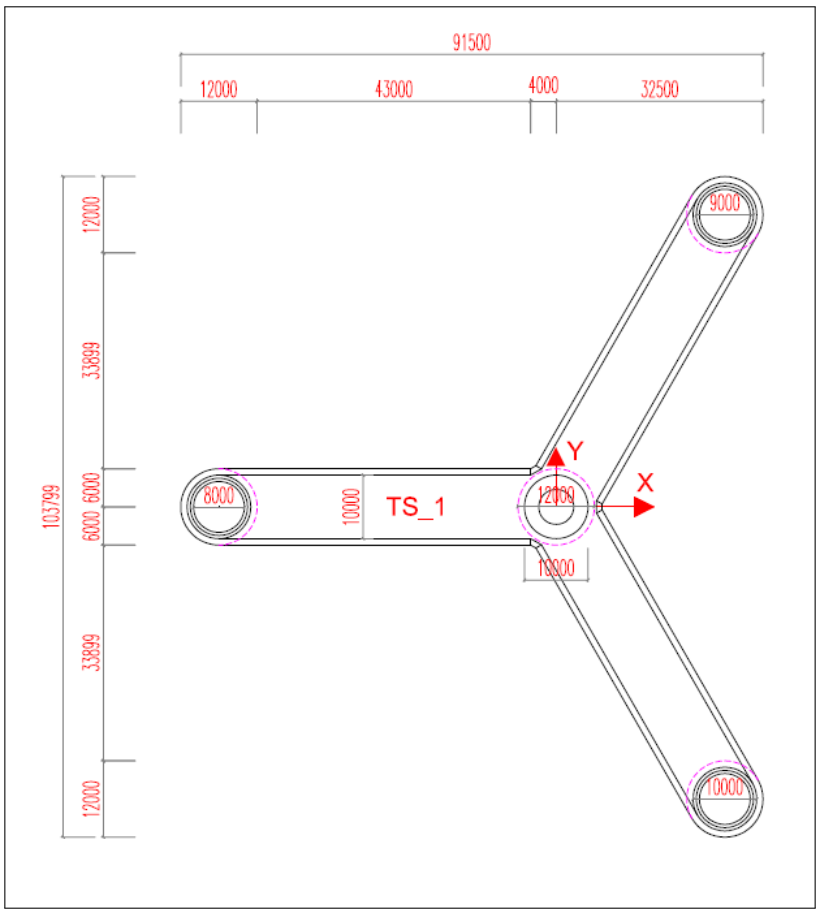

Figure 5.1: *Top view of the updated concept*

Furthermore, an identification system is defined for the concrete substructure to help with tracking the work, as follows:

- AW_{ij} for the angled walls of the pontoons, where i represents the pontoon number and j stands for the wall number.
- BS_i for the base slabs of the pontoons, where i represents the pontoon number.
- TS_i for the top slabs of the pontoons, where i represents the pontoon number.
- CC for the central column.
- CO_i for the offset columns, where i represents the column number related to the pontoon number.

Chapter 6

Finite element and panel models generation

This chapter focuses on the pre-processing work carried out in order to support the environmental and structural analysis, illustrated in chapters 7 and 8, respectively. It is organized in several section. In the first, the reader is introduced with the utilized computer software.

The actual modeling process starts with defining the structural properties such as cross sectional shapes, thickness and materials. Consequently, the entire 3D model is constructed based on guidance points and planes, ensuring the correct mass distribution. It represents an updated version of the pre-project solution. Moreover in GeniE, the user defines the ULS static load, namely the tower drag force. Also, the model boundary conditions are defined. These steps are detailed over section 6.2.

Last but not least, the automatic meshing capabilities of the program are utilized in order to generate finite element and panel models. These represent input for the environmental and structural analysis and are illustrated in section 6.3.

6.1 Brief software overview: Pre-processor DNV Sesam GeniE V6.5

This is an integrated pre-processing software tool, which is useful in designing and analyzing the offshore wind concrete floater modeled as shells, beams and point masses - which define the necessary material to carry the loads and at the same time, enough volume to give buoyancy. It is a relatively user friendly solution, with an interactive graphic user interface. The data are persistent enabling the engineer to do efficient iterative re-design of the structure. However, it is remarked that compared to general purpose post-processors, it is rather limited in options and control. For more information, the reader is kindly referred to the program user manual [29].

6.2 Global structural model

The updates to the global model are detailed over the following paragraphs, which illustrate the step-by-step GeniE implementation of the global structural model. Initially, GeniE is run and the design premises are set up for the database. The working units are set to kN and m as dictated by post-processor requirements.

Materials

Following, the updated linear construction materials are defined, as illustrated in table 6.1.

Name	Density $[\frac{T}{m^3}]$	Young Modulus [kPa]	Poisson coefficient	Thermal $[delC^{-1}]$	Damping $[\frac{kNs}{m}]$
Reinforced concrete	2.1	3e+007	0.2	1e-005	3e-005
Reinforced concrete connections	2.2	3e+007	0.2	1e-005	3e-005
Reinforced concrete top offset columns	2	3e+007	0.2	1e-005	3e-005
Steel turbine tower	8.5	2.1e+008	0.3	1.2e-005	6.28e-005
Massless	0.001	2.1e+008	0.3	1.2e-005	6.28e-005

Table 6.1: *Material properties*

The cross sectional thicknesses are also created for the different structural parts of the floater, as shown in table 6.2.

Name	Use	Average thickness[m]
$Pontoon_{700}$	4	0.7
$Pontoon_{600}$	11	0.6
$Column_{700}$	13	0.7
$Column_{500}$	6	0.5
$Column_{400}$	3	0.4
$Tower_{38}$	4	0.038
$Tower_{36}$	1	0.036
$Tower_{34}$	1	0.034
$Tower_{32}$	1	0.032
$Tower_{30}$	1	0.030
$Tower_{28}$	1	0.028
$Tower_{26}$	1	0.026
$Tower_{24}$	1	0.024
$Tower_{22}$	1	0.022
$Tower_{20}$	1	0.020
Total elements	50	

Table 6.2: *Thickness of structural elements*

Guiding geometry

Guiding points and planes are created next, based on the updated conceptual dimensions previously presented in table 5.1. The results are illustrated in figure 6.1. This grid represents the backbone of the geometrical model.

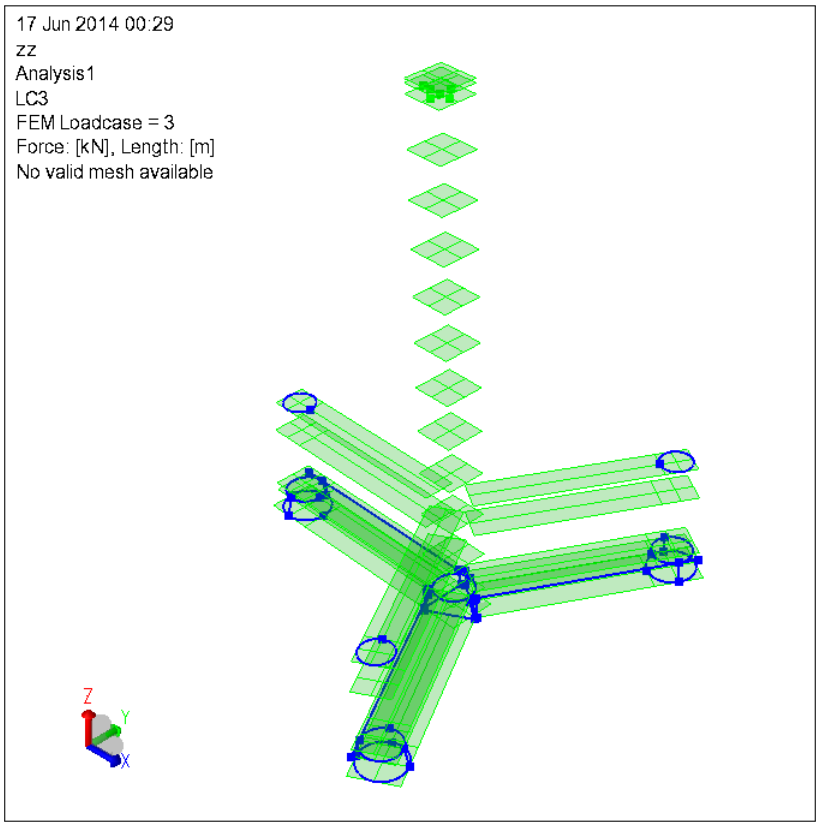

Figure 6.1: *Guiding geometry for the global model*

With the guiding geometry, 2nd order shell elements are defined next, mostly by *skin* command. In total, the floater comprises of 50 shell elements and 7 massless beam elements, meant for connecting the wind turbine components which are modeled as point masses, at their appropriate spatial position. The global model is illustrated in figure 6.2.

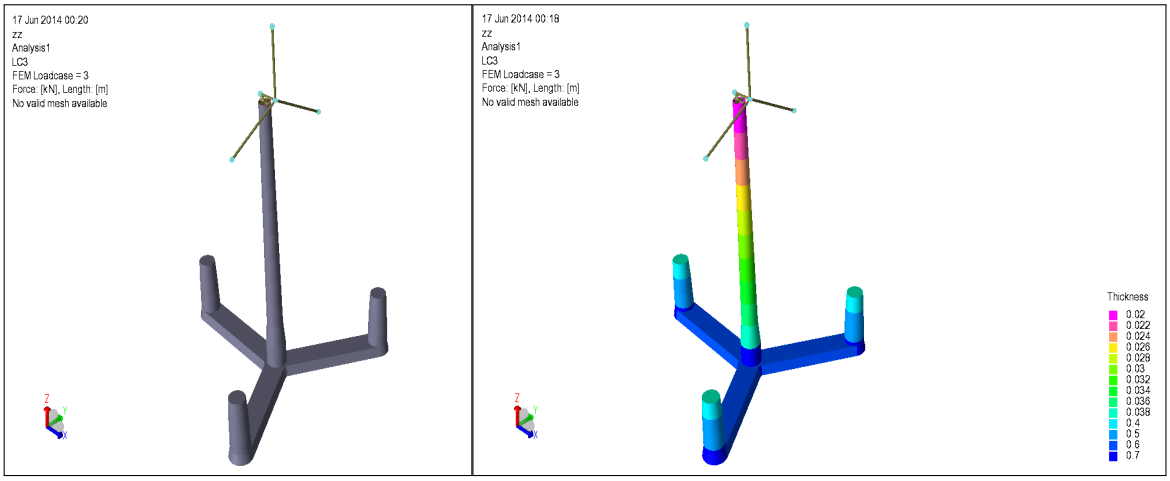

(a) Overall view (b) Structural element thickness

Figure 6.2: *Global structural model*

Figure 6.3 shows the internal reinforced concrete bulkheads, defined at the floater joints for adequately transferring the applied loads, highlighted in red.

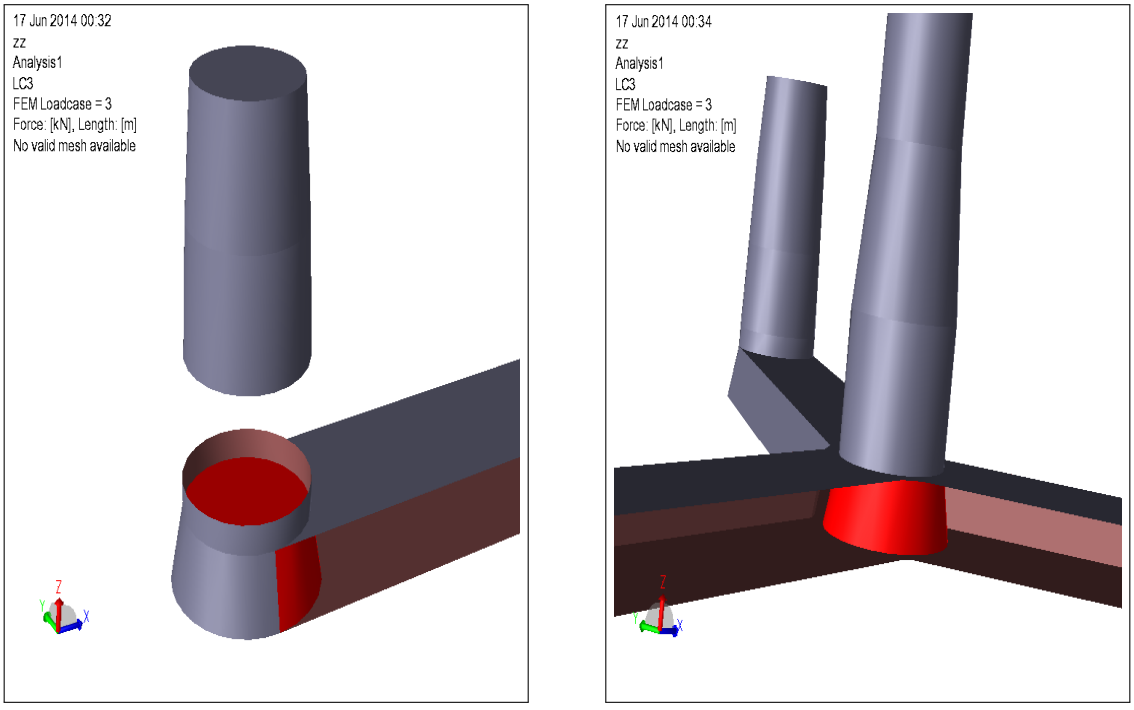

(a) Below offset column (b) Below central column

Figure 6.3: *Reinforced concrete bulkheads*

Environmental loads: wind

A point load F_D=306 kN is defined to be acting at the height of 77 m, along negative x direction, as load case LC3. Its value represents the 50 year wind turbine tower drag, in accordance with the design basis.

Boundary conditions

At this step, the essential boundary conditions are defined in the form of support constraints. They directly restrain the structure against rigid body motions, during the structural analysis. The global model is supported in 3 points at the underside of the pontoons at their intersection with the offset columns, as illustrated in figure 6.4.

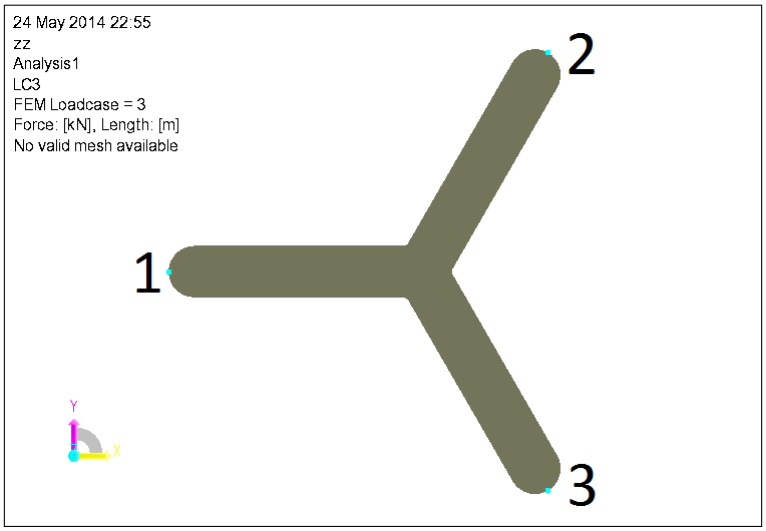

Figure 6.4: *Supports location*

Three vertical supports are defined by springs, representing the water plane stiffness of the structure:

$$k = \rho_w g A_w \tag{6.1}$$

where A_w=292 m^2 represents the water plane area of the semi-submersible. 10% of the vertical stiffness is applied in the horizontal direction. The spring stiffness below each column is then $k_{spring,z}$=$\frac{k}{3}$=$k_{z1,2,3}$. In addition, supporting in the horizontal plane is ensured by springs with a stiffness equal to 0.1 of the total vertical stiffness. The transverse horizontal stiffness (y-direction) is applied in two support points. One spring is applied in the longitudinal (x-direction). This boundary conditions will ensure free displacement of the platform due to wave action. This procedure is recommended by [35]. The supports characteristics in 6 DOF's are presented in **??**.

Support number	x $[\frac{kN}{m}]$	y $[\frac{kN}{m}]$	z $[\frac{kN}{m}]$	rx	ry	rz
1	293	146	976	free	free	free
2	free	146	976	free	free	free
3	free	free	976	free	free	free

Table 6.3: *Support characteristics*

6.3 Meshing and resulting models

The global structural model described in the previous section is meshed, leading to several finite element models. They are useful as input files for the environmental and structural analysis in chapters 7 and 8, respectively.

6.3.1 Structural model (Mass model)

After setting the meshing superelement type and the option for using second order elements is activated, an automatic mesh is generated with the constant length of 1 m. It results in a mesh counting 12907 elements (38238 nodes) which is overall illustrated in figure 6.5.

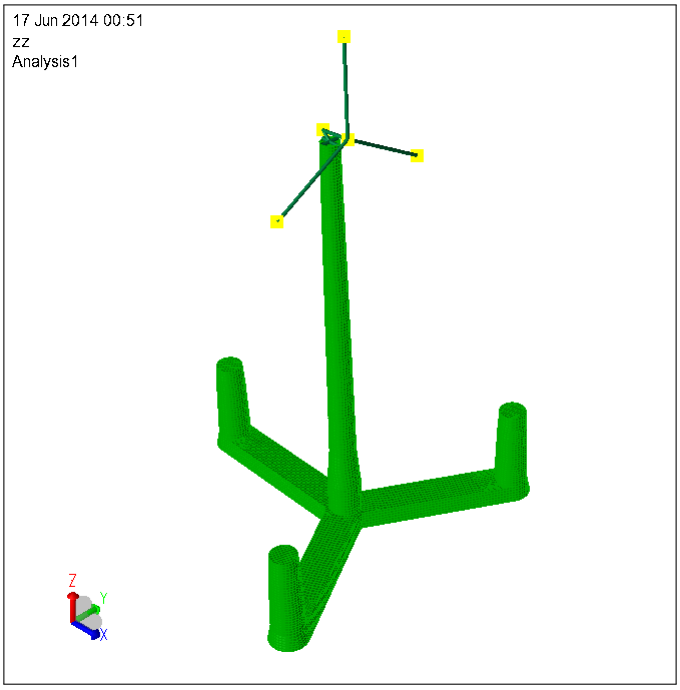

Figure 6.5: *Structural and mass model mesh*

A low quality mesh leads to large numerical errors and is strongly undesirable. Even though a complete mesh sensitivity study is not in the scope of the present project, it is here remarked that the finer the mesh, the higher the computational expense and the

lower the discretization error. However, it is still arguable the extent of how fine the mesh should be, as a too fine mesh could lead to an increased manipulation error. Hence, the designer should be aiming to balance the discretization with the manipulation error, leading to the mesh element size with the minimal total error.

At a closer inspection, the generated mesh appears of reasonable quality, with elements of limited skewness. A measure of the mesh quality is its relative jacobi, as shown in subfigure 6.6.

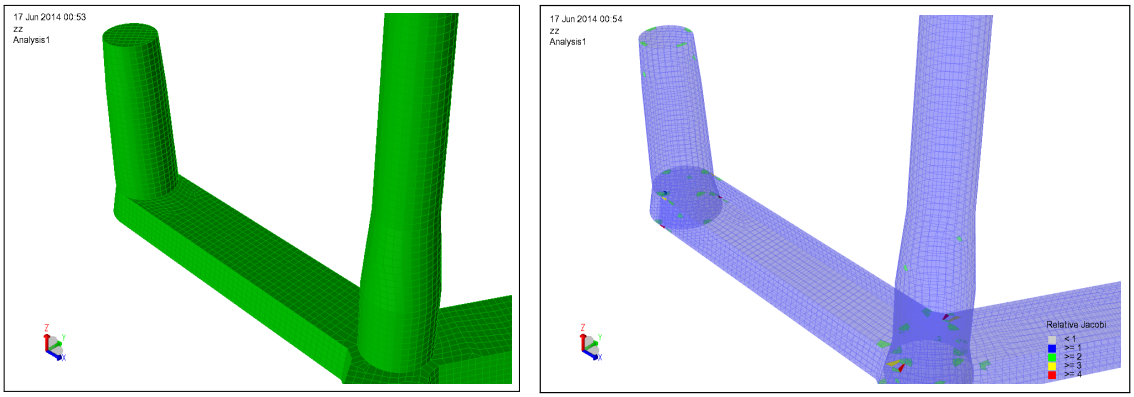

(a) Closer view of the mesh (b) Relative jacobi view of the mesh

Figure 6.6: *Mesh quality inspection*

Nevertheless, it is observed that some of the elements near the joints are not resolved properly with the adopted mesh length. They are not better resolved when reducing the overall mesh size either. The triangular elements are excluded in the post-processing work illustrated in chapter 9, due to a software limitation. In order to refine the mesh locally and be sure the work is actually better, a full mesh convergence study is required. Considering these limited drawbacks, it is concluded in agreement with ShellDesign software support representatives that the mesh is acceptable at the current stage of work. Consequently, it is exported as T3.FEM. Moreover, it is here remarked that the same T file containing the structural mesh is further utilized as the mass model also. This is acceptable considering the mass distribution is accurate for the global structural model.

6.3.2 Panel models

Two panel models are developed in GeniE, one to be used in the stability analysis and the other for the hydrodynamic analysis. More specifically, they are used by HydroD for the hydrodynamic coefficients calculation. The program computes the potential function based on a finite volume approach. The difference between the two is that the latter is generated up to the water level only, while the former includes the freeboard as well. The difference is due to a requirement in the stability analysis for ensuring the top of the columns are not submerged during the analysis.

They are created based on the structural model generated in the previous subsection, by assigning wet surface property to the concerned areas, which are predefined as sets

of elements. It is remarked that only the parts outside the column-pontoon intersection are wet surfaces and shall receive hydrodynamic loads. A consistent definition of surface normals is essential and is verified by carrying out an analysis with a dummy hydro pressure as a load case. It is desired that the front side of the shells receive the loads. In the present case this goal is achieved, the direction of the hydro pressure being shown as arrows on the geometry, as illustrated in figure 6.7.

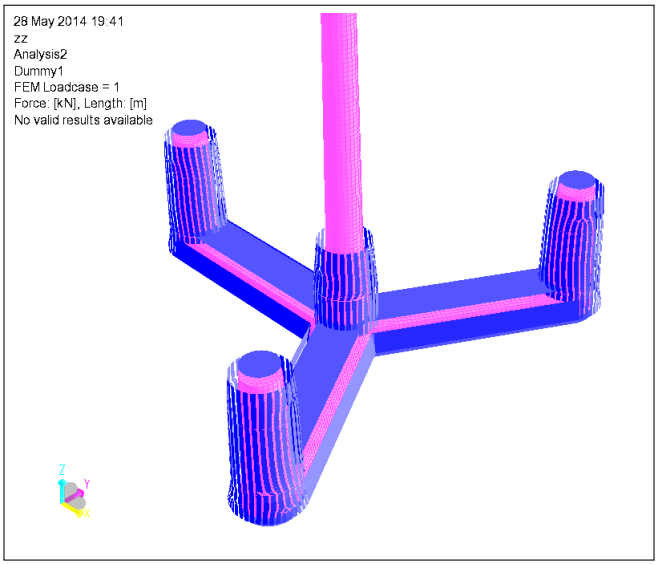

Figure 6.7: *Dummy hydro pressure along the wet surface*

Following, the panel elements for both models are automatically generated in GeniE. The super element type is set and the mesh size is kept constant at a value of 1 m. This ensures a smooth transition between the elements, with an aspect ratio close to 1. An illustration of the resulting models is presented in figure 6.8.

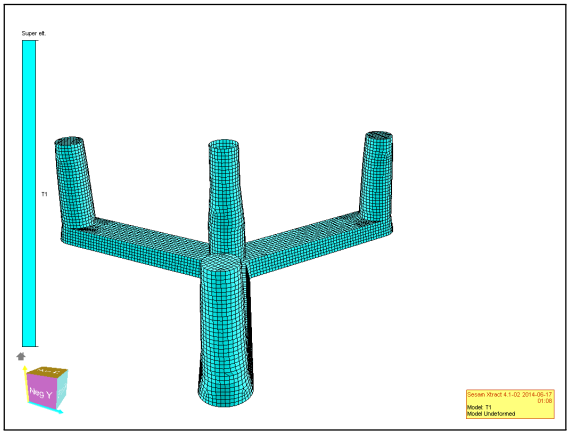

(a) 9380 Elements (9369 Nodes) panel model for the stability analysis

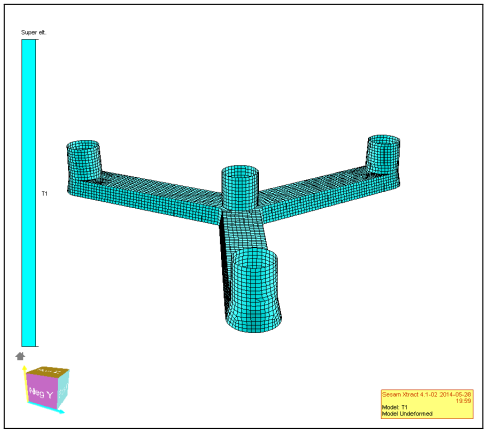

(b) 7048 Elements (7083 Nodes) panel model for the hydrodynamic analysis

Figure 6.8: *Panel models*

The mesh quality is properly verified. The mesh size requirement is the following:

$$M_{size} \leq \frac{\lambda}{4} \tag{6.2}$$

The shortest wave of interest in the present design is 3 s. In deep water, the corresponding wave length is computed as $\lambda = 1.56T^2$=14.04 m. Plugging this result into equation 6.2, it returns a maximum allowable mesh size of 3.5 m. Consequently, a mesh with 1 m resolution is expected to capture well all physical phenomena.

The panel model for the stability analysis is exported from GeniE as T1.FEM. Similarly, the other panel model for the Wadam analysis is exported as 2T1.FEM.

6.3.3 Morison model

A Morison model is also developed in GeniE in order to further utilize it during the Wadam analysis of a composite model, as shown in chapter 7, which includes both the panel model 2T1.FEM and a Morison model 2T2.FEM, in order to account for the viscous effects. It is built from scratch as a 2 node beam model with the correct material and cross section, corresponding to the part of the semi-submersible below the free water surface. It is illustrated in figure 6.9.

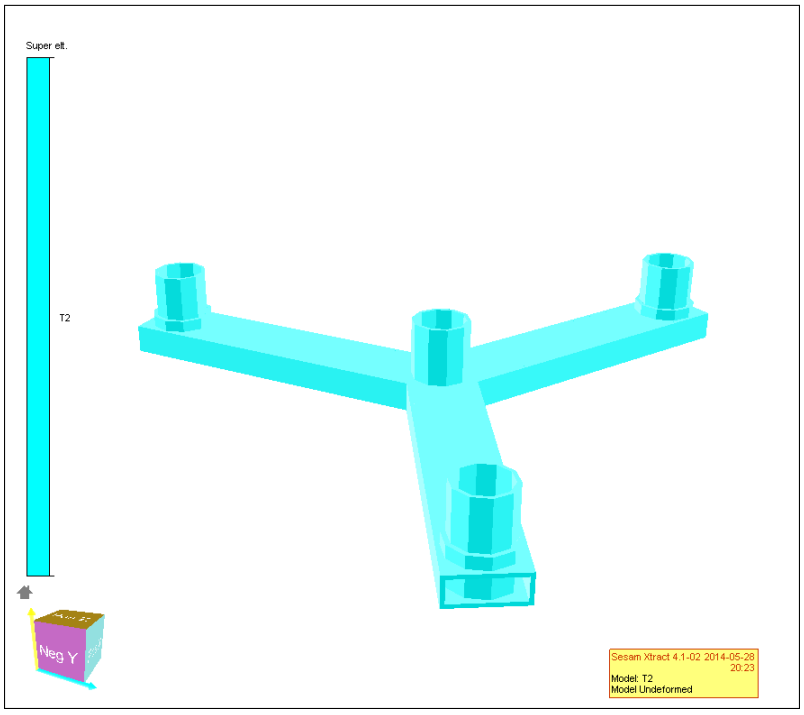

Figure 6.9: *Morison model*

Chapter 7

Environmental analysis

The environmental analysis concerning the updated global structural model of the concrete floater, consists of two types of analysis conducted in HydroD: hydrostatic stability during operation under the average thrust and hydrodynamic in frequency domain, for investigating the motions in the vertical plane. Over the present chapter, details are given on how such analysis are set up, their verification and what the outcome is.

7.1 Software overview: DNV Sesam HydroD

HydroD is an integral part of the Sesam system. It is used in order to carry out a stability analysis and frequency domain analysis of the semi-submersible which is treated as a floating rigid body. The hydrodynamic analysis outcome consists of both motion information, as well as structural loads which are further transferred to Sestra for the linear structural analysis, as detailed in chapter 8. The finite element models (T files) previously created in chapter 6, represent input files for HydroD, as further illustrated over the next sections.

The analysis work is conducted in the frequency domain, for which the system is assumed linear and in steady state according to [15]. In nonlinear and/or transient conditions, the problem must be solved in the time domain.

The basic assumptions for studying a linear wave body interaction problem are:

- Linear potential flow theory, the fluid is assumed irrotational, incompressible and inviscid.
- Deep water, validity of Airy theory.
- Regular incoming waves.
- Steady state conditions.
- Zero forward speed.

In a linear system, the output is proportional to the input, the output of a linear combination of inputs is a linear combination of the outputs to the single inputs, resulting that

the superposition principle is valid. It means that: in transient conditions, small variations in the initial conditions result in small changes in the output and can not modify the qualitative behavior of the output. In steady state conditions, if the input oscillates with a given period, the output will oscillate with the same period. A consequence of linear theory is that the response (output), i.e. body motion amplitude, is proportional to the excitation (input), i.e. incident wave amplitude.

Wadam software module in Sesam HydroD represents state of the art technology regarding its analysis features. It applies Airy wave theory and results are presented as complex transfer functions or as deterministic results for specified phases of the wave. The Wadam software is based on widely accepted linear methods for marine hydrodynamics, the 3-D radiation-diffraction theory employing a panel model and Morison equation in linearised form employing a beam model. The radiation-diffraction part of Wadam is based on software developed by Massachusetts Institute of Technology. This method is appropriate for voluminous structural parts (having typical dimensions greater than 1/5 of the wavelength). This implementation can be used for infinite and finite water depths. The free surface condition is linearised for the first order potential theory. The radiation and diffraction velocity potentials on the wet part of the body surface are determined from the solution of an integral equation obtained by using Green's theorem, with the free surface source potentials as the Green's functions. The source strengths are evaluated based on the source distribution method using the same source potentials. The integral equation is discretisised into a set of algebraic equations by approximating the body surface with a number of plane quadrilateral panels. The source strengths are assumed to be constant over each panel. Two, one or no planes of symmetry of the body geometry may be present. The solution of the algebraic equation system provides the strength of the sources on the panels. The equation system, which is complex and indefinite, is solved by a direct factorisation method or by an iterative method. Numerical difficulties, such as irregular frequencies can show up, frequencies at which the source technique does not provide any solution for a surface-piercing body.

In the linear diffraction problem the body is fixed and interacting with incident waves. The hydrodynamic loads provided are the Froude- Kriloff and diffraction loads, obtained integrating, respectively, the incident wave dynamic pressure and the diffraction dynamic pressure, along the mean wetted hull surface. In the linear radiation problem the body is forced to oscillate in its 6 degrees of freedom, with frequency ω and no incident waves. The moving body generates radiated waves associated with the radiation velocity potential and is subjected to hydrodynamic loads identified as added mass, damping and restoring terms. The restoring terms are connected with the variation of the buoyancy due to the body motions, i.e. they are connected with the hydrostatic pressure. The added mass and damping are connected with the dynamic pressure caused by the body motions. In all cases the pressures are integrated along the mean wetted hull surface. The added mass coefficient is proportional to the body acceleration whereas the damping coefficient is proportional to the velocity. The heave damping is directly linked to the amplitude of the waves generated by the body. For a semi-submersible the wave induced radiation linear damping at resonance (the inviscid solution) is small because of the long wave regime. They have a relatively long natural period, which has a low frequency and implicitly small wave induced radiation damping. Viscous effects are not considered within the potential flow theory. However, in some cases they are relevant. Based on figure 7.1, it is

remarked that for large ratios of $\frac{\lambda}{D}$ and $\frac{H}{D}$, viscous forces are predominant. λ is defined as the wave length, while D is the cross sectional diameter and H represents the wave amplitude. In this region of low frequency, the viscous damping matters. The Morison method will predict drag (viscous) forces more accurately. The user then establishes a so-called composite model. By establishing a composite model in which a structure is modeled by a beam model inside a panel model, the advantages of both methods are utilized. For more information regarding Wadam, the reader is referred to consulting the user manual [30].

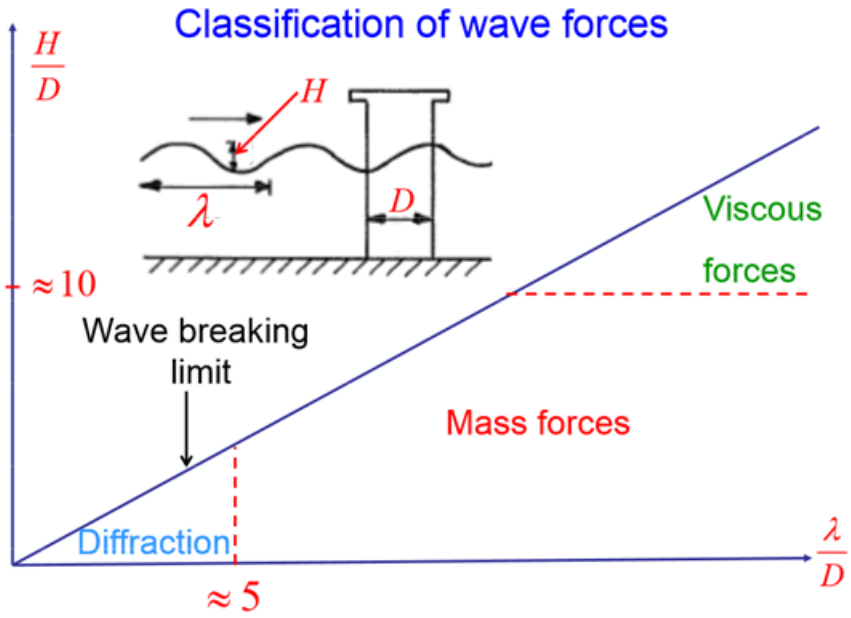

Figure 7.1: *Classification of wave forces [15]*

The global response results are usually analyzed and presented by using another tool called Postresp, also part of the DNV Sesam software suite. Consequently, the sets of data are further manipulated by means of Text, Excel and Matlab.

Furthermore, it is remarked that the static station keeping model (mooring lines) is not included in HydroD, resulting in no restoring for the horizontal motions (surge, sway, yaw).

7.2 Hydrostatic analysis and results

Hydrostatic and stability computations are run for intact conditions, in accordance with the main steps in the HydroD stability wizzard, hereafter described. The database units are set to kN and m.

Initially, a choice is made for the stability analysis to be based on the panel model T1.FEM, as obtained is subsection 6.3.2. HydroD computes the draught and heel/trim angles to ensure equilibrium, with a 5 % defined tolerance. A heeling moment curve is also specified to be included for computations of the heeling moment work and intersection points between righting moment and heeling moment. This represents the maximum average thrust force during operation. The main steps of the wizzard are summarized in table 7.1.

Step number	Input	Output
1. Define location	Based on the site conditions as defined in chapter 4	Norway 5
2. Define hydro model	Floating unit	$HydroModel_{Stability}$
3. Create panel model	T1.FEM, translate (0,0,-15)	$PM_{Stability}$
4. Create loading condition	Define waterline at z=0	$LC_{Stability}$
5. Create mass model	T3.FEM, translate (0,0-15)	$MM_{Stability}$
6. Edit stability analysis	$LC_{Stability}$, Norway 5, Auto detect rotation axis	$SA_{PanelModel}$
7. Create wind heeling moment	Constant value of 193414.596 kN*m	$WH_{Stability}$
8. Create stability analysis	Steps 1 to 7	$StabilityAnalisys_{PM}$

Table 7.1: *Main steps of the stability analysis*

Running the stability analysis at step 8 is concluded with a report. A plot showing the heeling moment curve against the GZ-curve (righting moment), is illustrated in figure 7.2.

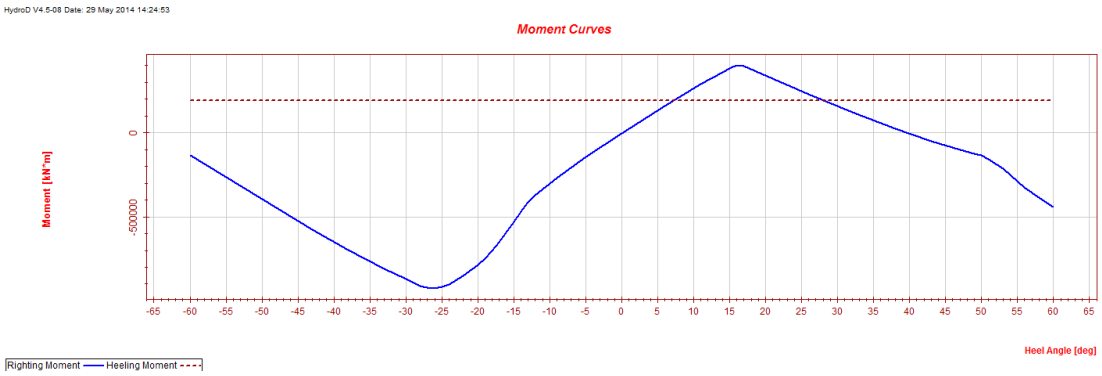

Figure 7.2: *Righting moment against heeling moment*

The overall aspect of the curve appears reasonable, without spikes. The downflooding occurs at the second intercept between the two curves, at 27.95 deg. The area under both curves is computed (between zero and the second intercept) and the results are tabulated in 7.2, which also contains the values obtained for the pre-project model, for comparison.

	Pre-project	Thesis
Total mass [T]	13322	12184
Buoyancy mass [T]	13224	12531
GM on z [m]	12.26	12.93
CoG on z [m]	3.23	0.72
CoB on z [m]	-9.91	-10.72
Deck immersion heel angle negative side [deg]	23.5	-23.62
Deck immersion heel angle positive side [deg]	17.53	15.14
1^{st} intercept angle [deg]	6.94	7.27
2^{nd} intercept angle [deg]	37.96	27.95
Righting moment area [kNm]	227631	122494
Heeling moment area [kNm]	128142	92351
Ratio of moments [%]	170	132.6

Table 7.2: *Main results of the stability analysis*

From this data, it is concluded that the total mass of the updated model is 8.5 % reduced compared to the pre-project, while the reduction in the buoyancy mass is 5 % only. This is mostly due to reducing the free board height, which also reduces the CoG, together with having bulkheads and increased material densities at the connections. A reserve of buoyancy is seen to be provided within 5 % tolerance.

The total mass is observed to have been well predicted with the theoretical approach in 5, where the result was 7 % difference. Nevertheless, it is here also remarked that a small difference in the total mass occurs even between the programs of the same suite. For example GeniE returns a value 0.5 % less, compared to the result presented in the above table and 1 % less compared to the results in the hydrodynamic analysis, as shown in the next section. This behavior is most likely due to numeric issues and is negligible.

It is remarked that the pre-project model has a slightly increased hydrostatic stability. However, this was expected. Reducing the water plane area in the thesis model, hence having a smaller restoring coefficient, decreases its stability. This effect is almost entirely compensated by increasing the distance between the columns (increase water plane area moment of inertia). Under the maximum heeling force, the pre-project model leans 6.94 deg, whereas the updated model 7.27 deg. However, the values are seen both below 10 deg, which was the upper limit imposed in chapter 4. It is reminded here that the other stability requirement for column-stabilized units such as semi-submersibles, in accordance with [10], is that the area under the righting moment curve to the angle of downflooding shall be equal to or greater than 130 % of the area under the wind heeling moment curve to the same limiting angle. Analyzing the ratios presented in the table leads to concluding that second stability requirement is also fulfilled by both models.

7.3 Hydrodynamic motion analysis and results

Analysis definition

Initially, a panel model model frequency domain analysis is conducted for observing the resonant behavior of the updated floater.

Following, a composed frequency domain analysis is conducted for determining the motion characteristics of the updated floater. The heave, roll and pitch response amplitude operators (RAO) resulting of the Wadam analyses are of interest, as they could interfere with the first order waves excitation and with the wind turbine operating frequencies.

Both frequency domain analysis for the updated floater are conducted for 48 wave periods, ranging between 3 - 30 s, as shown in table 7.3. It is remarked that the waves are concentrated around the floater's expected heave natural period, in order to capture its behavior at resonance.

3 4 5 6 7 8 9 10 11 12 13 14 14.5 15 15.5 16 16.5 17 17.5 18 18.5
19 19.25 19.5 19.75 20 20.25 20.5 20.75 21 21.25 21.5 21.75 22 22.25 22.5 22.75 23
23.5 24 24.5 25 25.5 26 27 28 29 30

Table 7.3: *List of considered wave periods*

The composite analysis is based on a composed model and is developed with the help of a wizzard, similar to the one for the stability analysis described in the previous section. The main input consists of the T files for the panel, morison and mass models, which have been developed in chapter 6.

Additionally, a 3 hours sea state is defined with a Jonswap spectrum of irregular waves, where H_S=15.6 m, T_P=14.5 s and γ=3.3, in accordance with the site conditions.

The lift and drag coefficients are determined in accordance with the standard [7], corresponding to the offset, central columns and pontoons, respectively. Their values are shown in table 7.4. Furthermore, pressure area elements are included in order to account for the end of the pontoons effects in the Morison model.

	C_{dy}	C_{dz}
Pontoon	1.5	2
Offset columns	0.7	0.7
Centralcolumn	0.7	0.7

Table 7.4: *Lift and drag coefficients [7]*

Running the global response hydrodynamic analysis leads to two results file G2.SIF.

Results verification and presentation

Before moving on to presenting the results, their correctness is assessed based on the output files. Both return the following message: "A grand total of 0 legal elements did not match with any hydrodynamic panels! No pressure have been transferred to these elements". This is self-explanatory, saying that all elements below the free surface have received hydrodynamic pressure. It is a signal of good quality of the total load transfer.

The floater's heave RAO with/ out viscous effects is presented in figure 7.3. The panel model results are plotted in subfigure 7.3a. The resonant behavior is observed at the heave frequency. A cancellation frequency is also captured. In subfigure 7.3b, a comparison is made to the results including viscous effects. It is remarked that in the high frequency region the viscous effects do not come into play and that the panel model captures the floater's response accurately, whereas in the long waves region it does not. All these effects are in accordance with the theory.

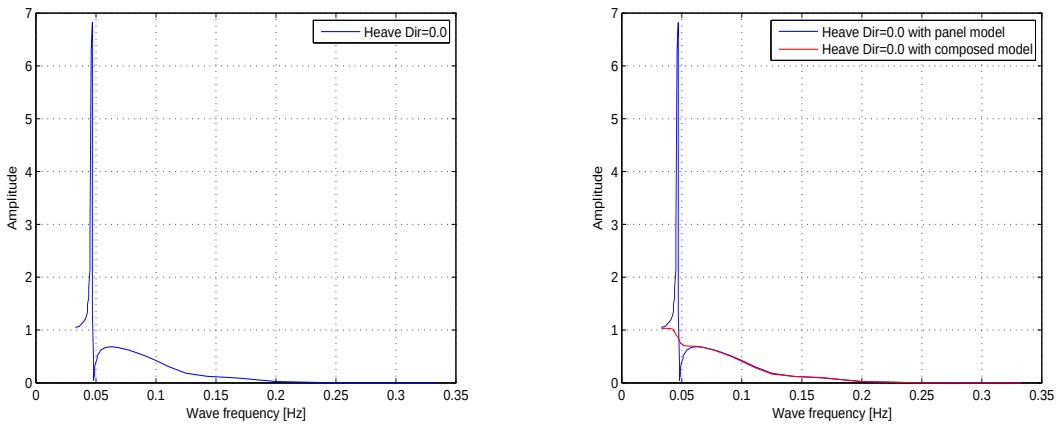

(a) With updated panel model

(b) Comparison

Figure 7.3: *Heave RAO with/ out viscous effects*

The heave, roll and pitch natural periods of the semi-submersible are computed with data retrieved from the mass, added mass and restoring matrix in Postresp. The added mass is found to be highly dependent on the frequency. This is expected, considering the semi-submersible is a large body. The calculations are based on equation 5.6. The results are illustrated in table 7.5. They are seen to be outside of the waves which contain most of the energy (over 20 s).

	Unit	Heave	Pitch	Roll
Mass	[kg]	1.219E+04	2.155E+07	2.155E+07
Added mass	[kg]	22000	105000000	105000000
Restoring	$[\frac{kg}{s^2}]$	2.906E+03	1.592E+06	1.592E+06
Natural period	[s]	21.55	56.01	56.01

Table 7.5: *Heave, roll and pitch natural periods*

Figure 7.4 illustrates a comparison of the updated composed results with the pre-project composed model, for the heave motion. It is observed that the response amplitude is lower in the updated case for the same wave direction. This is expected as it considers a higher sea-state hence more damping, compared to the pre-project. The amplitude is seen to considerably increase near the heave natural period. The heave motion is not sensitive to the incoming wave direction. The amplitude is minimum for head waves, increasing for beam seas and maximum for a wave incoming angle of 30 and 60deg, though with limited variation.

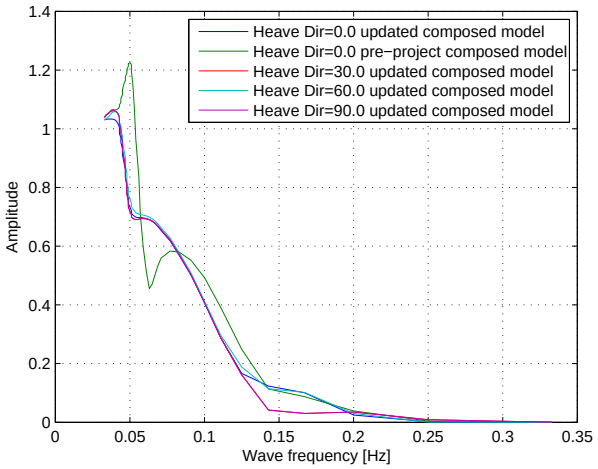

Figure 7.4: *Heave RAO*

It is concluded that by introducing viscous damping, through the Morisons equation, the resonance response amplitude in heave becomes limited, with a maximum around 1.1, which is a reasonable value.

The floaters pitch RAO including viscous effects in shown in figure 7.5.

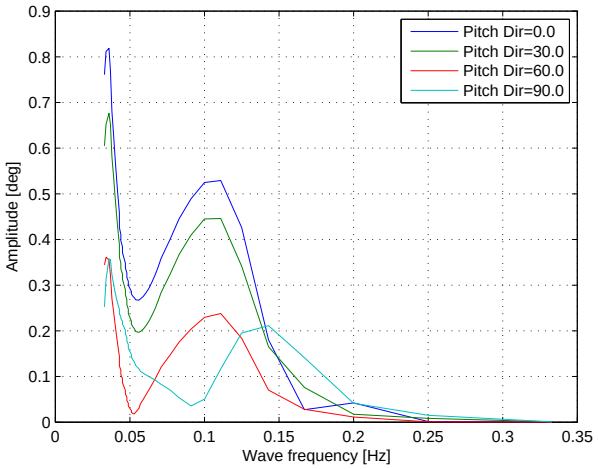

Figure 7.5: *Pitch RAO for different wave headings (composed model)*

The maximum amplitude is close to 0.9 deg for head seas, which is considered acceptable. An increase in the pitch RAO is observed around the heave natural period. The amplitude is gradually decreasing with increasing wave angle, to the minimum which occurs in beam seas, around 0.4 deg.

The floaters roll RAO including viscous effects in shown in figure 7.6.

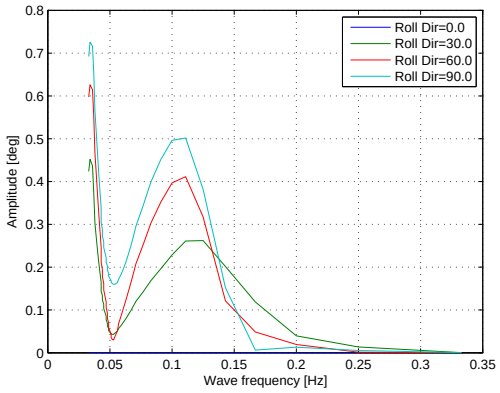

Figure 7.6: *Roll RAO for different wave headings (composed model)*

The maximum amplitude is around 0.7 deg for beam seas, which is considered an acceptable value. An increase in the roll RAO is observed around the heave natural period. The amplitude is gradually decreasing with decreasing wave angle, to zero in head seas, as expected.

A comparison plot of the motions with the wind turbine operating frequencies is provided in figure 7.7, for the critical wave direction. It is remarked that they come into the 1P range. However, the amplification factor for all concerned motions is smaller than 1 in where they overlap. Furthermore, this can not be avoided due to the wind turbine design and is accepted by the international practice. Generally, interaction with 3P is considered critical and not acceptable.

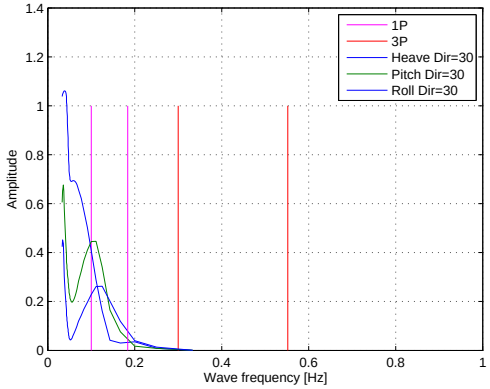

Figure 7.7: *1P and 3P vs. Motions frequencies*

7.4 Hydrodynamic loads analysis

For obtaining the hydrostatic and hydrodynamic loads acting on the floater in waves of 1 m amplitude at different relevant frequencies, a new composed model analysis is defined in HydroD (with stochastic drag and load transfer). The resulting loads file is to be further utilized in the Sestra structural analysis as illustrated in chapter 8, together with the T file for the global structural model, previously created in GeniE.

The steps involved in setting up the analysis in HydroD are similar to the ones already presented in the previous section. Due to symmetry reasons, it is considered that waves ranging from 0-120 deg in steps of 30 deg, are sufficient to capture all loading possibilities. The hydrodynamic loads selected to be transferred to the shell elements global structural model are the following:

- Include static load cases in the loads file.
- Include gravity forces in the static load cases.
- Include inertia forces on the loads file.
- Include restoring pressure (the vessel motion causes a change in draft and an additional fluid pressure) forces on the loads file.
- Include hydrodynamic load cases in the loads file.
- Include dynamic gravity. The gravity force is essentially divided into two parts, the constant gravity force and the additional force resulting from the vessel motion angles. The latter is known as dynamic gravity.

At this step, the starting number of these load cases is also mentioned, 8. Running the analysis leads to the creation of a loads file L3.FEM. It contains 248 load cases, the first 7 which have been defined in the T file. However, it is here remarked that out of these initial 7 load cases, the first represents the hydro dummy pressure for checking the panel models and the third is for the 50 year tower drag; the remaining are empty load cases. Load case number 8 represents the difference between the hydrostatic and gravity load. Starting with number 9 the wave loads are defined as complex numbers. It means there are 240 wave loads which is in accordance with the wave periods and directions defined for the analysis, namely 48 periods and 5 directions. These are complex numbers. A table with all the load cases and their meaning is added in appendix B. The list is also relevant for understanding how the design load combinations are defined in chapter 9.

Chapter 8

Structural analysis and results

This chapter is organized in three sections. In the first one, the reader is provided with a brief overview of the software utilized in the structural analysis. Some theoretical aspects behind the program are also introduced. In section 8.2, a free vibration dynamic analysis is carried out in order to determine the eigenvalues of the floater seen as a flexible body. Following, section 8.3 illustrates the procedure and results for a static structural analysis.

8.1 Brief software overview: DNV Sesam Sestra

Sestra is the program for static and dynamic structural analysis within the Sesam software system. The overall analysis capabilities of Sestra are schematically illustrated in figure 8.1.

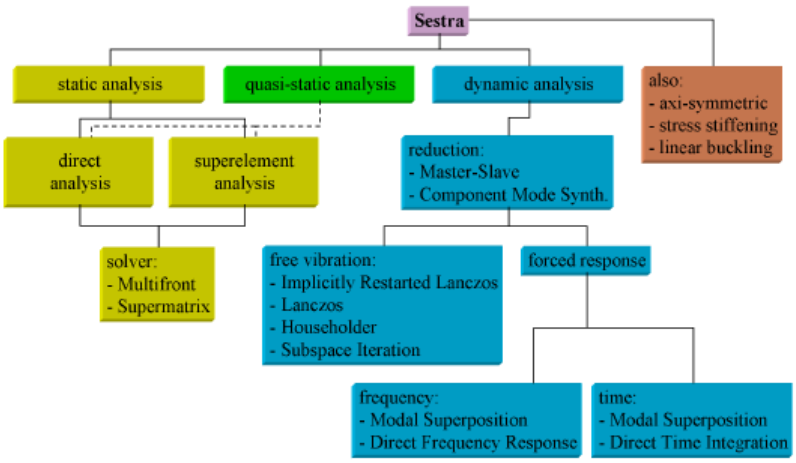

Figure 8.1: *Schematic illustration of the capabilities of Sestra [31]*

In terms of the formulation, Sestra uses a displacement based finite element approach. According to [31], in a static analysis this results in a linear system of equations:

$$Kr = R \tag{8.1}$$

where K is the global stiffness matrix formed by appropriate addition of the element stiffness matrices, r is the matrix of unknown nodal displacements and R is the nodal load matrix. The matrices r and R have one column per load case.

When boundary conditions are introduced, which represent known values for elements within r, the system is modified and reduced:

$$K_{ii}r_i = R_i \tag{8.2}$$

where i stands for the free (internal) degrees of freedom of the model. In the matrix R_i, the load components for the internal degrees of freedom, are transformed to account for the effect of given displacements, if such exist. In the present work, the Multifront solver is selected for solving the equation, which is faster and uses less disk space for sparse stiffness matrices when compared with the Supermatrix solver, according to [31].

During a free vibration analysis, applying the finite element displacement based method in space results in the algebraic initial value system:

$$M\ddot{r} + Kr = 0 \tag{8.3}$$

where $\ddot{r}$ is derivation with respect to time. The eigenvalue λ_i and the mode shape ϕ_i satisfy:

$$K\phi_i = \lambda_i M\phi_i \tag{8.4}$$

where $i = 1, ..., n$ with n degrees of freedom. The square root of the eigenvalues are denoted ω_i and they represent the eigen frequencies of the finite element model. In the present work, the implicitly restarted Lanczos method is selected, which is based on the Multifront solver and is the most efficient and reliable one, according to [31].

Sestra is interfaced with other program modules for:

- Finite element model generation - performed in the pre-processor, GeniE.
- Load calculation - performed in the environmental analysis program, HydroD.
- Results evaluation and presentation - stress presentation performed in the post-processor, Xtract.
- Cross sectional design - performed in the post-processor, ShellDesign.

An overview of the input and output of Sestra is shown in figure 8.2.

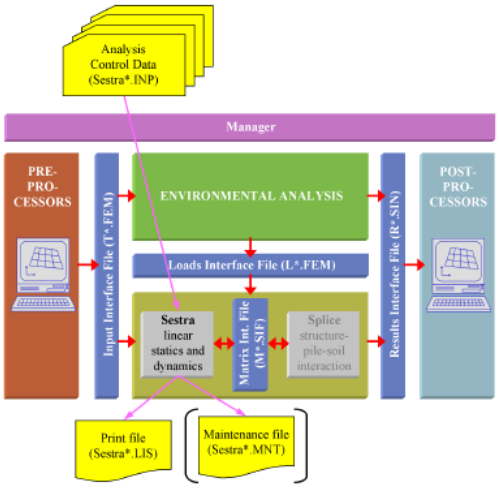

Figure 8.2: *Sestra input and output [31]*

In the present work, the following types of elements are utilized:

- 1 node GMAS (general one node mass element).
- 1 node GSPR (spring to ground element).
- 3 nodes BTTS (beam element).
- 6 nodes SCTS (subparametric curved triangular thin/ thick shell).
- 8 nodes SCQS (subparametric curved quadrilateral thin/ thick shell). Stress are calculated at eight point of the 2x2x2 Gaussian integration grid as indicated in figure 8.3.

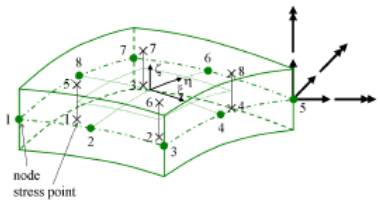

Figure 8.3: *The quadrilateral shell element SCQS with stress points [31]*

For more information on Sestra and the finite element displacement formulation supporting it, the reader is kindly referred to the program user manual [31].

8.2 Free vibration dynamic analysis and results

This section illustrates the procedure and results for a free vibration dynamic analysis carried out in Sestra. The main theoretical background was introduced in the previous section of this chapter.

Sestra is run based on the input file T3.FEM, which has been developed as described in chapter 6. This file contains the necessary model data. Other inputs consist in choosing the solver and the number of desired eigenvalues.

The Sestra free vibration dynamic analysis output files are the following:

- Print file Sestra.LIS
- Maintenance file.
- Results interface file R3.SIN (created for full computations with result calculation).

Following the successful completion of the run, the reliability of the given solution is assessed, by analyzing the print file Sestra.LIS. The types and numbers of finite elements are inspected together with the mass matrix. For a visual inspection of the mode shapes, the total displacements for the first three eigenvalues are presented in figure 8.4. These mode shapes appear to be reliable.

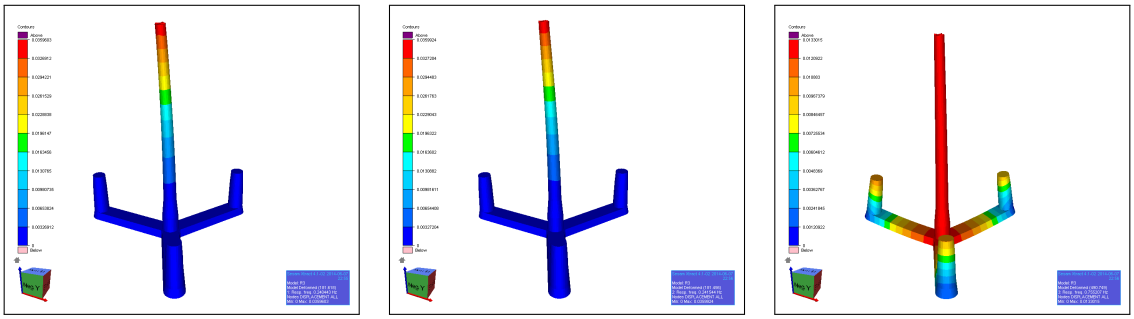

(a) First (b) Second (c) Third

Figure 8.4: *Structural mode shapes*

An overview of the eigenvalues is presented in table 8.1.

Number	Frequency [Hz]
1	0.240
2	0.242
3	0.755
4	1.167
5	1.202
6	1.610
7	1.708
8	1.777
9	1.787
10	2.220

Table 8.1: *Eigenvalues and eigen frequencies*

Next, the eigen frequencies are plotted against the 1P and 3P rotational frequencies of the wind turbine, as illustrated in figure 8.5.

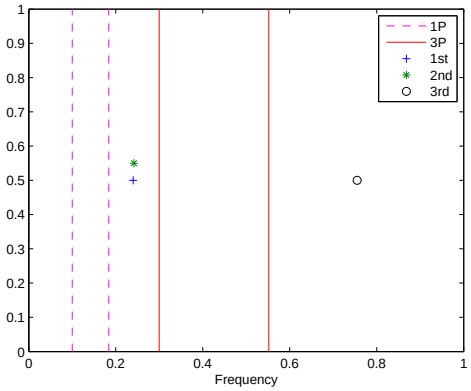

Figure 8.5: *1P and 3P vs. eigen frequencies*

The first two eigen frequencies of the support structure are seen to lay in between the wind turbine rotational frequencies, whereas the third one is greater. Consequently, the structural response due to dynamic loading may be analyzed by a quasistatic method, i.e. a static analysis in Sestra with 'quasistatic' loads, as illustrated in the following section.

8.3 Static analysis

The present section illustrates the procedure and results for a static analysis carried out is Sestra (with static and quasi-static loads). The main theoretical background behind a Sestra static analysis was introduced in the first section of this chapter. The 'quasi-static' approach involves neglecting the dynamic effects of the structure and is often referred to as stiffness controlled dynamics, as the mass and damping forces in the structure are small compared to the forces resulting from elastic and possible inelastic strains. The 'quasistatic' loads are complex numbers, corresponding to the frequency domain analysis.

Sestra is run based on the input interface file T3.FEM, created in chapter 6, and the loads interface file L3.FEM, which results of chapter 7. The former contains both complex and real loads as it has been shown already. These two files contain the necessary model and loads data.

The Sestra static analysis output files are the following:

- Print file Sestra.LIS
- Maintenance file.
- Results interface file R3.SIN (created for full computations with result calculation).

Following the successful completion of the run, the reliability of the solution is assessed, by analyzing the print file Sestra.LIS. It is seen that all 248 load cases have been transferred from the loads file. The static analysis is quality checked by comparing the sum of the loads with the sum of the reaction forces (reaction=-load). It is observed that the differences between the summed loads and reaction forces is small compared to the significant force components, with an order of magnitude 10^{-5}. Consequently, it is concluded the

solution is reliable from a numerical perspective. However, erroneous results caused by bad element shapes and a coarse element mesh, are not detected in the above mentioned check.

This is further achieved by comparing element stresses in neighboring elements using Xtract. Large differences would indicate a too coarse element mesh. Consequently, the result interface file R3.SIN is loaded into Xtract. This file contains a large amount of data. For avoiding manipulation errors, the results are analyzed separately for the different structural parts of the global model. A discussion is attempted next.

8.3.1 Stress results discussion

In general, the quality of the stresses is observed to be acceptable, with relatively large gradients occuring only at the elements intersections which have not been rounded (angled wall - angled wall). These local design details could be further improved. The corresponding stresses are not post-processed.

Local bending is observed to occur at the elements level, when inspecting the stresses on both sides. A spike is observed in σ_{xx}, occurring at the intersection between the bulkheads and base slab. The effects of the supports is seen to have been properly resolved through the method proposed in chapter 6.

Chapter 9

Post-processing and results

ShellDesign version 4.3.1 is a design tool and post processor for reinforced concrete shell structures subjected to stresses in and out of plane. Being owned, developed and supported by Dr. Techn. Olav Olsen AS, it is based on extensive development and project experience gained through a large number of offshore concrete projects (expert in thin-shell structures).

In the present work, it is utilized for conducting ULS sectional design checks in an automated fashion. It implements the following standards: NS3473 and Euro Code 2. The first is selected, considering the Euro Code 2 is not entirely suitable to offshore structures. Extensive verification reports to support the software are available.

The input consists of the sectional geometry, forces and design sections with their corresponding amount of reinforcement and material properties. The sectional design accounts for the non-linear material behavior. The amount and location of reinforcement, together with the material properties are user defined, for each desired design section. The sectional geometry and forces are fetched from the finite element analysis based on a shell element model, developed in chapter 8. The ShellDesign main input is summarized in figure 9.1.

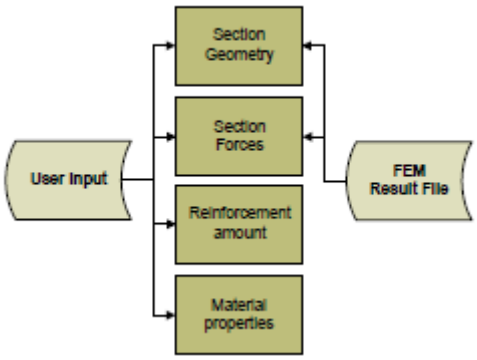

Figure 9.1: *Input to design calculations [32]*

Desired load cases are defined as part of ShellDesign, in order to simulate realistic ULS load combinations. Printed tables are useful in verifying the input data in terms of geometry, design sections and local coordinates system.

The results are presented in tables, in the form of utilization ratios of specified concrete, reinforcement and shear capacities. Results are given for the critical design sections corresponding to each relevant structural element. Following, an initial bill of quantities is developed, based on which a conservative total cost estimate is given. The cost on the environment the construction materials have, is also assessed in an environmental impact assessment.

Hereafter, all these points mentioned are further exemplified for the problem at hand. The work is based on the software user manual and feedback from Bente Skovseth Nyhus and Rikke Ellingsen, the software support contact persons. It is further remarked in this context, that similarly to most of the specialized software, this program is also lacking a graphic user interface.

9.1 Limit states and design calculations

In the present scope of work ordinary ULS checks are conducted in accordance with the implemented design code. This state relates to the risk of failure or large inelastic strains of a failure character. The basis of the involved design calculations are the sectional geometry, forces, amount of reinforcement and material properties. The carried out checks, specific for this limit state, are the following: stresses in concrete and reinforcement, shear capacity of the cross section. In general, sectional design allows for optimizing the reinforcement requirement. It is specified through the DECAS statement.

9.2 Design sections

The floater consists of columns linked to pontoons. They in turn are split into vertical/ angled column walls, angled pontoon walls and horizontal pontoon slabs. These structural elements are modeled as 8 node shell elements. A shell section is defined as a line through such an element, perpendicular to its middle surface. All design calculations refer to these sections, also known as design sections. ShellDesign is used in connection with the finite element analysis results interface file R3.SIN, so that the design sections are related to the stress points (Gauss-points) of the finite elements. For each 8 node shell element, there are 8 stress points in one element, but every 2 are located at the same line through the element thickness, hence only 4 design sections. Consequently, a design section is seen passing through pairs of Gauss points. Within each design section, the stress distribution is assumed to vary linearly over the element thickness and determined by the stresses in the Gauss points.

In practice, the identity of each shell section consists of 3 elements: part id, F and H section numbers. To start generating sections, the start element number is defined together with F and H generation directions. A local coordinate system is defined by the user for each design section, called a *1,2,3* axis system. 1 and 2 axis correspond with the directions

of the reinforcement. The generation of design sections is achieved by command SHSEC and the 1,2,3-axis are specified through SHAXE.

In total, 19648 design sections are defined for one third of the floater, as summarized in table 9.1. The remaining two thirds of the floater are dimensioned similarly, due to symmetry reasons.

Part	Design sections
BS_1	5184
TS_1	3864
$AW_1 2$	1128
$AW_1 1$	1128
CC	2584
OC_1	5760
Total: 19648	

Table 9.1: *Design sections*

For a detailed understanding of the axis and design sections definition of each relevant structural element, the reader is kindly referred to the project appendix C.

9.3 Load cases and design combinations

The following load case types are used in ShellDesign:

- OLC : Original load case. These are load cases retrieved from the finite element analysis, through the results interface file R3.SIN.
- BAS : Basic combination load case. Combine single load effects to present real load situations. Basic tool for scaling and combining load types, through the statement BASCO.

The resulting design basic load combinations with the corresponding safety factors, are tabulated in 9.2. They count 25. Furthermore, each of the waves is considered with 24 phase angles between 0-360 deg, in steps of 15 deg. This results into a total of 600 design cases.

BASCO ID	Load Factor	OLC number	Load Factor	OLC number	Load Factor	OLC number
3000	1.0	8	1.35	3	19.6	20
3001	1.0	8	1.35	3	19.6	22
3002	1.0	8	1.35	3	19.6	24
3003	1.0	8	1.35	3	19.6	26
3004	1.0	8	1.35	3	19.6	28
3010	1.0	8	1.35	3	19.6	68
3011	1.0	8	1.35	3	19.6	70
3012	1.0	8	1.35	3	19.6	72
3013	1.0	8	1.35	3	19.6	74
3014	1.0	8	1.35	3	19.6	76
3020	1.0	8	1.35	3	19.6	116
3021	1.0	8	1.35	3	19.6	118
3022	1.0	8	1.35	3	19.6	120
3023	1.0	8	1.35	3	19.6	122
3024	1.0	8	1.35	3	19.6	124
3030	1.0	8	1.35	3	19.6	164
3031	1.0	8	1.35	3	19.6	166
3032	1.0	8	1.35	3	19.6	168
3033	1.0	8	1.35	3	19.6	170
3034	1.0	8	1.35	3	19.6	172
3040	1.0	8	1.35	3	19.6	212
3041	1.0	8	1.35	3	19.6	214
3042	1.0	8	1.35	3	19.6	216
3043	1.0	8	1.35	3	19.6	218
3044	1.0	8	1.35	3	19.6	220

Table 9.2: *Factored load combinations*

With 600 design cases and 19648 design sections for one third of the floater, it is demonstrated that efficient post-processing of a concrete floater requires such an automatic procedure.

9.4 Materials

The available concrete types are in accordance with the rules of NS3473, as it was also described in chapter 4. They are specified through CMPNS and can be modified by the user.

In terms of reinforcement 2 types are specified through the program input file: normal and shear reinforcement. Additionally, prestress reinforcement could be specified, if required. The properties of the steel are determined in accordance with the rules of NS3473. The reinforcement directions are defined for each section in relation with the 1,2,3 axis system, as illustrated in figure 9.2.

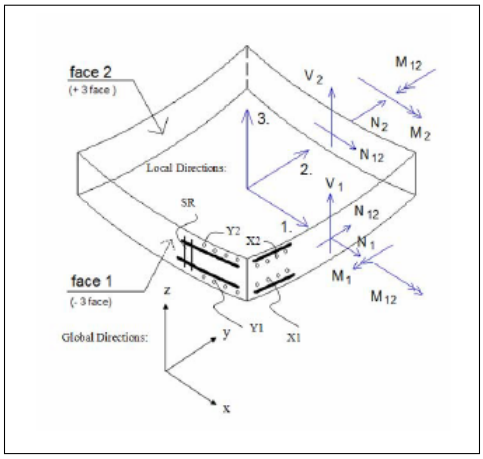

Figure 9.2: *Reinforcement directions [32]*

The reinforcement area is specified per unit meter, hence the input in ShellDesign is $[\frac{m^2}{m}]$. For example, one rebar of 25 mm diameter placed at 200 mm in one direction, returns a ShellDesign input area equal to $0.002454[\frac{m^2}{m}]$. The precise positioning of each of the four reinforcement layers is defined, considering the concrete cover requirements defined in chapter 4. The concrete cover is set to 75 mm for the base slab and 70 mm for the remaining structural elements.

9.5 ULS Results

At the current design stage, ULS results without reinforcement optimization with respect to layer and directions are presented, for each structural element. For simplicity, it is also assumed that the reinforcement type and quantity is constant over each element, as determined for the critical design sections. The same assumption is made for the the concrete grade. In a later design stage, this could obviously be optimized over the different areas, in order to maximize the utilization ratios and the average rebar utilization, but such an operation is very time consuming considering the shear size of the structure. Also, the other relevant limit states have to be checked before such an optimization is attempted. Nevertheless, it is considered that with these assumptions a conservative baseline design could be established, with a corresponding bill of quantities, materials cost estimate and environmental impact assessment. Corresponding structural drawings are attached in appendix D.

9.5.1 BS_1

An input file is built, based on the previously introduced principles, to identify the critical design sections in the pontoon base slab, in terms of concrete stresses and maximum/ minimum rebar layer stresses. Appendix C contains the design sections and local axis system definition, for the reader's referral. The main outcome is tabulated next:

Max. rebar stresses							
Part	FS	HS	ID	Reinf. area $[\frac{mm^2}{m}]$	Load ID	Phase	UR
BS_1	122	19	X11	7359	BAS 3024	75	0.95
	122	1	X21	6476	BAS 3010	180	0.69
	62	1	Y12	6476	BAS 3004	105	0.78
	59	18	Y22	6476	BAS 3004	105	1
Max. concrete stresses							
Part	FS	HS	Face	Thickness $[m]$	Load ID	Phase	UR
BS_1	66	18	1	0.7	BAS 3004	90	0.9
	29	18	2	0.7	BAS 3000	135	0.74
Max. stirrup stresses							
Part	FS	HS	ID	Reinf. area $[\frac{mm^2}{m}]$	Load ID	Phase	UR
BS_1	29	18	93	5027	BAS 3000	135	0.69
Total concrete volume $[m^3]$							442
Rebar weight/ concrete volume $[\frac{kg}{m^3}]$							306
Average rebar utilization							0.3

Table 9.3: *Utilization ratios for BS_1*

It is observed that the longitudinal reinforcement in the exterior layer is stressed the most, around the middle width section, next to the central column. This occurs for the longest design wave, at an incoming angle of 60 deg. It is also remarked that a higher reinforcement quantity is provided in this layer and direction in order to ensure an acceptable design. The transverse reinforcement in the interior layer is the second most stressed, around the middle width section, at roughly half slab length. This occurs for the shortest design wave in head direction. Also, maximum concrete stresses are seen to occur in the concrete around the middle width section, at half the slab length and close to the outer column for the other shell face respectively, in the shortest waves, at different incoming directions. Stirrups are critically stressed in the middle width section near the outer column. It is determined that the most critical is the longest design wave in head seas. Critical design sections are seen to be located in the middle width of the slab, at both ends and in the middle length. Its average utilization ratio shows room for considerable optimization. Concrete grade B50 appears to be sufficient in the critical design section and the assumed slab thickness proves to be acceptable. Both the thickness and quality should be optimized over the slab.

9.5.2 TS_1

An input file is built to identify the critical design sections in the pontoon top slab, in terms of concrete stresses and maximum/ minimum rebar layer stresses. Appendix C contains the design sections and local axis system definition, for the reader's referral. The main outcome is tabulated next:

Max. rebar stresses							
Part	FS	HS	ID	Reinf. area $[\frac{mm^2}{m}]$	Load ID	Phase	UR
TS_1	119	28	X11	6476	BAS 3010	0	0.63
	118	14	X21	6476	BAS 3000	30	0.98
	61	14	Y12	6476	BAS 3000	105	0.76
	54	1	Y22	6476	BAS 3000	120	0.57
Max. concrete stresses							
Part	FS	HS	Face	Thickness $[m]$	Load ID	Phase	UR
TS_1	29	16	1	0.6	BAS 3000	120	0.76
	61	14	2	0.6	BAS 3000	105	0.71
Max. stirrup stresses							
Part	FS	HS	ID	Reinf. area $[\frac{mm^2}{m}]$	Load ID	Phase	UR
TS_1	29	15	93	5027	BAS 3000	90	0.74
Total concrete volume $[m^3]$							269
Rebar weight/ concrete volume $[\frac{kg}{m^3}]$							345
Average rebar utilization							0.38

Table 9.4: *Utilization ratios for TS_1*

It is observed that the longitudinal reinforcement in the exterior layer is stressed the most, though less than for BS_1, around the middle width section, next to the central column. This occurs for the shortest design wave, in head seas. The transverse reinforcement in the interior layer is the second most stressed, around the middle section at roughly half slab length. This occurs for the same design wave. Also, maximum concrete stresses are seen to occur in the concrete around the middle section, at half the slab length and close to the outer column for the two shell faces respectively, in the shortest waves. Stirrups are critically stressed in the middle width section near the outer column. They are more stressed compared to the bottom slab. Critical design sections are seen to be located in the middle width of the slab, at both ends and in the middle length. The most critical load case is the shortest wave in head seas. Overall, a higher average reinforcement utilization ratio is noticed compared to the base slab. Concrete grade B50 appears to be sufficient in the critical design section and the assumed slab thickness proves to be acceptable. Both the thickness and quality should be optimized over the slab.

9.5.3 AW_{12} and AW_{11}

The angled walls are dimensioned identically, due to symmetry. Appendix C contains the design sections and local axis system definition, for the reader's referral. The adopted design is for AW_{12}, for which the main outcome is tabulated next:

Max. rebar stresses							
Part	FS	HS	ID	Reinf. area $[\frac{mm^2}{m}]$	Load ID	Phase	UR
AW_{12}	82	12	X11	6476	BAS 3010	0	0.52
	94	12	X21	6476	BAS 3010	0	0.43
	43	1	Y12	6476	BAS 3004	105	0.94
	8	1	Y22	6476	BAS 3004	105	0.25
Max. concrete stresses							
Part	FS	HS	Face	Thickness $[m]$	Load ID	Phase	UR
AW_{12}	88	11	1	0.6	BAS 3010	0	0.2
	41	1	2	0.6	BAS 3004	105	0.87
Max. stirrup stresses							
Part	FS	HS	ID	Reinf. area $[\frac{mm^2}{m}]$	Load ID	Phase	UR
AW_{12}	86	1	91	1257	BAS 3024	30	0.93
Total concrete volume $[m^3]$							144
Rebar weight/ concrete volume $[\frac{kg}{m^3}]$							345
Average rebar utilization							0.28

Table 9.5: *Utilization ratios for AW_{12}*

The transverse reinforcement in the exterior layer is stressed the most, around the bottom section in the middle of the pontoon. This is opposite to the slabs, which have been seen to be more stressed longitudinally. It occurs for the longest design wave in head seas. This is in agreement with large compression stresses in concrete interior face in the same zone and load case. The exterior layer of horizontal reinforcement is also stressed more compared to the interior one, with maximum values in the top of the wall towards the central column. They occur for the shortest design wave at an incoming angle of 30 deg. The stirrups are stressed the most at the bottom of the wall towards the central column, corresponding to the longest design wave at an incoming angle of 60 deg. Critical design sections are seen to be located both at the top and bottom over the wall height, at both ends and in the middle length. The longest design wave in head seas is the most critical. Overall, a lower average reinforcement utilization ratio is noticed compared to both slabs. A considerably reduced stirrups area is required in the walls. Concrete grade B50 appears to be sufficient in the critical design section and the assumed wall thickness proves to be acceptable. Both the thickness and quality should be optimized over the wall.

9.5.4 *CC*

An input file is built to identify the critical design sections in the central column, in terms of concrete stresses and maximum/ minimum rebar layer stresses. Appendix C contains the design sections and local axis system definition, for the reader's referral. The main outcome is tabulated next:

Max. rebar stresses							
Part	FS	HS	ID	Reinf. area $[\frac{mm^2}{m}]$	Load ID	Phase	UR
CC	66	9	X11	4906	BAS 3014	120	0.68
	2	10	X21	4906	BAS 3004	150	0.59
	6	15	Y12	6476	BAS 3034	330	0.79
	31	14	Y22	4906	BAS 3004	150	0.65
Max. concrete stresses							
Part	FS	HS	Face	Thickness $[m]$	Load ID	Phase	UR
CC	46	14	1	0.7	BAS 3034	345	0.39
	51	15	2	0.7	BAS 3000	30	0.37
Max. stirrup stresses							
Part	FS	HS	ID	Reinf. area $[\frac{mm^2}{m}]$	Load ID	Phase	UR
CC	6	15	92	2827	BAS 3034	330	0.87
Total concrete volume $[m^3]$							376
Rebar weight/ concrete volume $[\frac{kg}{m^3}]$							242
Average rebar utilization							0.38

Table 9.6: *Utilization ratios for CC*

It is observed that the longitudinal reinforcement in the exterior layer is stressed the most, near the intersection with the top slab. This occurs for the longest design wave in beam seas. The area of reinforcement required in this layer and direction is also larger compared to the others, in order to ensure an acceptable utilization ratio. The transverse reinforcement in the exterior layer is the second most stressed. This occurs for the longest design wave, at an incoming angle of 30 deg. Maximum concrete stresses are seen to occur in the concrete near the intersection with the top slab. The same is valid for the stirrups maximum utilization ratio. Critical design sections are found all around the central column, near the intersection with the top slab. Overall, a similar average reinforcement utilization ratio is noticed compared to the top slab, though the quantity per unit volume is the lowest overall. The utilization ratios with concrete grade B50 in the critical design sections are seen as relatively low. Consequently, the thickness of the section could be much reduced.

9.5.5 OC_1

An input file is built to identify the critical design sections in the outer column, in terms of concrete stresses and maximum/ minimum rebar layer stresses. Appendix C contains the design sections and local axis system definition, for the reader's referral. The main outcome is tabulated next:

Max. rebar stresses							
Part	FS	HS	ID	Reinf. area $[\frac{mm^2}{m}]$	Load ID	Phase	UR
OC_1	62	1	X11	4906	BAS 3000	60	0.61
	62	1	X21	4906	BAS 3000	30	0.36
	61	1	Y12	4906	BAS 3000	45	1
	62	1	Y22	4906	BAS 3000	15	0.28
Max. concrete stresses							
Part	FS	HS	Face	Thickness $[m]$	Load ID	Phase	UR
OC_1	14	12	1	0.7	BAS 3000	135	0.3
	60	1	2	0.7	BAS 3000	135	0.44
Max. stirrup stresses							
Part	FS	HS	ID	Reinf. area $[\frac{mm^2}{m}]$	Load ID	Phase	UR
OC_1	62	1	92	2827	BAS 3000	75	0.68
Total concrete volume $[m^3]$							489
Rebar weight/ concrete volume $[\frac{kg}{m^3}]$							297
Average rebar utilization							0.03

Table 9.7: *Utilization ratios for OC_1*

It is observed that the transverse reinforcement in the exterior layer is stressed the most, near the intersection with the bottom slab. This occurs for the shortest design wave in head seas. The longitudinal reinforcement in the exterior layer is the second most stressed, in the same region. This occurs for the shortest design wave also. Maximum concrete stresses are seen to occur in the concrete near the intersection with the bottom slab, and with the top slab respectively. The stirrups maximum utilization ratio is seen near the base slab intersection. Critical design sections are found near the intersection with the bottom slab. Overall, very low average reinforcement utilization ratio is noticed. The utilization ratios for concrete grade B50 in the critical design sections are seen also very low. Consequently, the offset columns present the most room for optimization in terms of longitudinal and transverse reinforcement as well as concrete. A moderate quantity of shear reinforcement is required, similar to the central column.

9.5.6 Bill of quantities and cost estimate

A bill of quantities is prepared in the present subsection, based on the ULS results previously presented. It is summarized in table 9.8.

Part	Rebar weight [T]	Concrete weight [T]
Bottom slabs	446	2755
Top slabs	350	1719
Angled walls	328	1691
Central column	120	727
Outer column	465	2009
Entire floater	1709	8901

Table 9.8: *Bill of quantities for the baseline concept*

Price quotes for reinforcement bars and coils have been received on www.alibaba.com from 11 Chinese companies. They have capacity to produce bars in diameters between 8 - 50 mm. The average unit price per tonne for a total quantity of 2000 T is 367 EUR. However, it is here remarked that the steel market is quite volatile and it might be best to purchase the reinforcement from a nearby manufacturer of trusted quality. Furthermore, the price per tonne is expected to decrease with an increasing required quantity. The cost of concrete B50 has been obtained from http://www.byggecentrum.dk at 0.15 $\frac{EUR}{kg}$.

With this data, the bill of quantities and information from chapter 4, a cost estimate is prepared for the materials. Their production involves an equivalent CO_2 emission which is also estimated. The results are tabulated next:

	Cost [EUR]	CO_2 equivalent [T]
Reinforcement	627 203	1213
Concrete	1 335 150	1086
Total	1 962 353	2299

Table 9.9: *Baseline materials cost and estimated equivalent CO_2 impact*

9.6 Additional features: Non-linear structural response

The information in this section presents an additional feature of ShellDesign, which it is believed that if applied would lead to less conservative design results. It is mostly relevant for SLS investigations.

The structural analysis carried out in Sestra is static linear elastic, allowing for the principle of superposition, as previously explained in chapter 8. Such an approach assumes constant element stiffness. In the design calculations, when establishing the cross sectional response, it is accounted for the actual non-linear behavior of reinforced concrete due to cracking, etc. Hence, this resulting stress of strain is not consistent with the strain profile from the linear structural analysis. Such an inconsistency is not desirable and should

consequently be avoided. For this purpose, ShellDesign has an iterative linear-elastic procedure, in which the element stiffness matrix is gradually refined for the non-linear material response, until a specified convergence criterion is reached. The main idea is that the stiffness parameters resulting of the design calculations are fed back into the Sestra finite element analysis, which is rerun several times until stiffness convergence. The design flow based on this non-linear method is illustrated in figure 9.3.

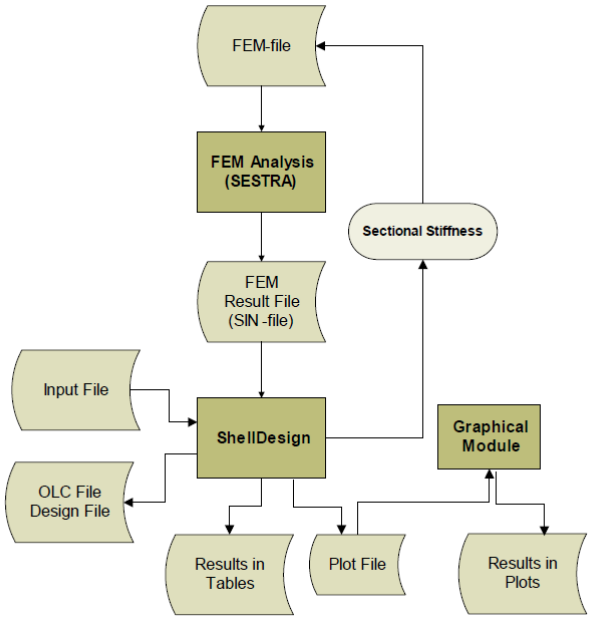

Figure 9.3: *Interaction scheme of Sestra and ShellDesign in the iterative mode [32]*

Initially, a new FEM file is created to work as input for Sestra, in which the shell elements are replaced by sandwich elements. The stiffness matrix is updated based on the cracked section analysis. Consequently, a new linear finite element analysis is carried out with Sestra based on the updated FEM file. This results in a new Sestra output file (SIN file). The procedure is repeated until convergence of the stiffness.

The actual implementation of this method is attempted in the ULS design, though without success. The main lesson learned is summarized next:

- Pre-processor GeniE assigns material numbers to the different types of elements defined. It is not possible to control this sequence explicitly. It is required by ShellDesign, that the shell elements have the highest material number. This could be solved in two ways, editing manually the material numbers in the interface file T3.FEM, or building an entire shell model - including the wind turbine. The first option is not viable due to the large number of elements which would need to be edited, while for attempting the second more detailed turbine data is required. Nevertheless, this is remarked as a serious drawback of the post-processor.

Chapter 10

Conclusions and recommendations for future work

10.1 Conclusions

A first attempt to establish an optimizable baseline design for a concrete semi-submersible supporting a 10MW DTU reference wind turbine has been made.

Initially, an extensive literature study has been conducted on the design of semi-submersibles and offshore concrete structures. Consequently, the main requirements were formulated for the floater in the form of a design basis. These included wind turbine, stability and motions functional prerequisites. The main ULS load effects due to wind and wave actions have also been determined. A theoretical review has been completed for design of membrane/ shell reinforced concrete elements. A theoretical analysis was conducted in order to establish the updated concept dimensions.

The outcome was consequently pre-processed into a shell elements global model, to support several types of numerical computations. These included stability and hydrodynamic analysis, relevant for the floater in operation. They also included linear structural analysis. The computations has been performed with DNV Sesam software and the post-processing of the results with ShellDesign.

The global stability was verified and was seen to be slightly reduced compared to the pre-project model. This has been expected due to the changes in the overall geometry and was predicted well by the analytic tool. The overall mass of material is seen to have been reduced by 8.5 %, while the buoyancy by 5 %.

Hydrodynamic analysis has been conducted in the frequency domain, with both panel and composed models, where the floater is treated as a rigid body, in order to investigate its motions in the vertical plane, susceptible to first order waves. It is established by comparison to the pre-project results, that the composed model properly captures the resonant behavior of the floater. The heave period is determined to 21.5 s which is

above the requirement of 20 s. The roll and pitch periods are calculated as 56 s. The motions are seen to interfere with the 1P operational frequencies of the wind turbine, which is considered acceptable. No interference is expected to occur with the 3P. The hydrodynamic loads corresponding to 1 m wave amplitudes were determined.

With a free vibration analysis the first 10 eigenmodes of the floater have been found. They were seen not to interfere with the operational frequencies of the wind turbine. Consequently, relevant stress results of the quasi-static analysis were briefly discussed. They were seen to exhibit a rather complex behavior which was challenging to fully explain.

A ULS sectional design check with a non-linear material response has been performed based on the linear structural analysis results, in accordance with NS3473. The stresses were post-processed and 600 representative ULS checks were performed in 19648 design sections. For this task a reliable post-processor was required. The results were hardly intuitive. The following conclusions have been established based on the main findings:

- For BS_1, it is determined that the most critical is the longest design wave in head seas. Critical design sections are found in the middle width of the slab, at both ends and in the middle length. The reinforcement is stressed the most in the longitudinal direction. Its has an average reinforcement UR of 0.3. The assumed section thickness of 0.7 m with concrete B50 is determined to be appropriate, in the critical design section. A large quantity of stirrups is required near the middle width section close to the outer column. This is the critical element over the entire structure.
- For TS_1, it is determined that the most critical is the shortest design wave in head seas. Critical design sections are found in the middle width of the slab, at both ends and in the middle length, similarly to BS_1. The reinforcement is stressed the most in the longitudinal direction, though less than for BS_1. It has an average reinforcement UR of 0.38. The assumed section thickness of 0.6 m with concrete B50 is determined to be appropriate, in the critical design sections. The maximum quantity of stirrups is required in the same zone and is identical to BS_1.
- AW_{12} and AW_{11} are dimensioned identically due to symmetry reasons. The worst for this angled wall is the longest design wave in head seas. Critical design sections are seen to be located both at the top and bottom over the wall height, at both ends and in the middle length. The transverse reinforcement is stressed the most. The wall has an average reinforcement UR of 0.28 and the assumed section thickness of 0.6 m is seen to be adequate with concrete B50. This element requires the least stirrups compared to all other structural elements.
- CC is mostly susceptible to the longest design wave in beam seas. Most of the critical sections are found to occur at the intersection with TS_1. The longitudinal reinforcement is stressed the most. The column has an average reinforcement UR of 0.38, identical to TS_1. The resulting concrete stresses are seen quite low, meaning the initially assumed thickness was to large. It requires a medium quantity of shear reinforcement.
- OC_1 appears to be only susceptible to the shortest design wave in head seas. Most of the critical sections are found to occur at the intersection with BS_1. The longitudinal reinforcement is stressed the most. The column has an average reinforcement

UR of 0.03, the lowest in all elements. It's assumed base thickness 0.7 m is found to result in relatively low concrete stresses. It requires a medium quantity of shear reinforcement.

Corresponding structural drawings have been established. The resulting bill of quantities and cost of materials estimate has been determined. The environmental impact of building such a floater has also been assessed. A conservative total quantity of required materials was determined to satisfy the ULS requirements: 1709 T of reinforcement and 8901 T of concrete. Producing the required materials would involve an equivalent CO_2 emission of 2300 T. A baseline cost estimate for the construction materials was established at 1962353 EUR.

10.2 Recommendations for future work

Since the present study was the first known attempt at establishing an optimizable baseline model for a reinforced concrete semi-submersible, there are numerous opportunities for future work. The following are specific recommendations for improving on the present study:

- Include a mooring model and non-linear wave effects, to investigate the motions in the horizontal plane. A catenary chain/ wire system with clamped weights is recommended. [15] and [23] could be used as references. Conduct a free decay test, establish the displacement-force characteristics. Check the strength of the mooring line. Conduct a coupled wind-wave time domain analysis. This could be done in Simo/ Riflex and FAST. Verify the wind controller.
- Identify and consider all relevant load cases during the design life of the floater. Focus on the SLS. Apply the non-linear structural analysis method described in chapter 9, in the critical design sections.
- Conduct a mesh convergence study and improve the model locally, especially at the angled walls intersections, where some stress concentration has been observed.
- Perform D-region design to determine the rebar anchorage and stress transfer in the discontinuity regions. These include joints and other geometric or static discontinuities such as post-tensioning anchorages, embedded items, etc. The main focus of D-regions is providing an appropriate reinforcement detailing of the section and are only applied in the case of high stresses and difficult detailing. Stresses are extracted from ShellDesign, for the critical design sections. Consequently, strut and tie numerical tools could be used, as described in [26]. This is required as part of FLS.
- Conduct experiments to investigate the floater motions and stability. Pay particular attention to scaling effects. In the detailed design phase, conduct structural experiments on critical connections.

References

[1] Internet. URL http://seco.be/fr/r%C3%A9f%C3%A9rences/ouvrages-hydrauliques?page=1.

[2] Internet, June 2014. URL http://www.nedcam.com/spencer-dock-bridge-dublin.htm.

[3] Digital fabrication techniques using automation and robot technology. Internet, June 2014. URL http://www.tailorcrete.com/27160.

[4] Ancon. Reinforcing bar couplers for the construction industry. UK, September 2012.

[5] Andrew Joseph Goupee Anthony Michael Viselli, Habib Joseph Dagher. Volturnus 1:8 - design and testing of the first grid-connected offshore wind turbine in the u.s.a. 2014.

[6] Johan Blaauwendraad. *Plates and FEM - Surprises and pitfalls*, volume 171. Springer, 2010.

[7] DNV. *Environmental conditions and environmental loads. Recommended practice DNV-RP-C205.* 2010.

[8] DNV. *Design of Offshore Wind Turbine Structures DNV-OS-J101.* September 2011.

[9] DNV. *Offshore Concrete Structures DNV-OS-C502.* September 2012.

[10] DNV. *Design of Floating Wind Turbine Structures DNV-OS-J103.* June 2013.

[11] DTU Wind Energy. The dtu 10mw reference wind turbine project site. Internet, 2013. URL https://dtu-10mw-rwt.vindenergi.dtu.dk/.

[12] Tor Ole Olsen et al. Concrete structures for oil and gas fields in hostile marine environments. Technical report, FIB, October 2009.

[13] M. P. Collins F. J. Vecchio. The modified compression-field theory for reinforced concrete elements subjected to shear. *ACI*, 83(2):219–231, 1986.

[14] M. P. Collins F. J. Vecchio. Compression response of cracked reinforced concrete. *Journal of structural engineering*, 119, 1993.

[15] O.M. Faltinsen. *Sea loads on ships and offshore structures.* Cambridge university press, 1990.

[16] Luan C. Gao Z., Moan T. Conceptual designs of a 5-mw and a 10-mw semi-submersible wind turbine with emphasis on the design procedure. *Journal of Offshore Mechanics and Arctic Engineering (Submitted 2014).*

[17] Erik Jersin Ivar Holand, Ove T. Gudmestad, editor. *Design of Offshore Concrete Structures.* Spon Press, 2000.

[18] W.W. Massie J.M.J. Journe. *Offshore hydromechanics.* Delft University of Technology, 2001.

[19] Frank Vecchio et al. Koichi Maekawa. Practitioners' guide to finite element modelling of reinforced concrete structures. Technical report, FIB, 2008.

[20] Torgeir Moan Lin Li, Zhen Gao. Joint environmental data at five european offshore sites for design of combined wind and wave energy devices. OMAE, June 2013.

[21] Main(e) International Consulting LLC. *Floating offshore wind foundations: Industry consortia and projects in the United States, Europe and Japan. An overwiev.* 32 Blueberry lane, Bremen ME 04551, USA, May 2013.

[22] D. Mathiesen L.N. Thrane, T.J. Andersen. The use of robots and self-compacting concrete for unique concrete structures. *Tailor Made Concrete Structures - Walraven & Stoelhorst (eds)*, pages 801–806, 2008.

[23] Norsk Hydro M. MOrland and Kwemer Engineering a.s O. Frydenhsnd. Design, fabrication and installation of the mooring system for the troll b concrete oil production platform. *OTC*, pages 255–266, 1996.

[24] D. Mitchell M. P. Collins. Shear and torsion design of prestressed and non-prestressed concrete beams. *PCI*, 25(5):32–100, 1980.

[25] Le Mehaute. *An introduction to hydrodynamics and water waves.* Springer, 1976.

[26] Aurelio Muttoni Miguel Fernandez Ruiz. On development of suitable stress fields for structural concrete. *ACI structural journal*, pages 495–502, 2007.

[27] Fabian Scheurer Silvan Oesterle Matthias Kohler Fabio Gramazio Nicholas Williams, Hanno Stehling. A case study of a collaborative digital workflow in the design and production of formwork for non-standard concrete structures. *International journal of architectural computing*, issue 03, volume 9:223–240.

[28] Hoang L.C. Nielsen M.P. *Limit analysis and concrete plasticity.* C R C Press LLC, 2011.

[29] Det norske veritas. *Sesam user manual: GeniE Volume 1 Concept design and analysis of Offshore Structures.* DNV, valid from program version 6.5 edition, June 2013.

[30] Det norske veritas. *Sesam user manual: Wadam*. DNV, valid for program version 9.0 edition, February 2013.

[31] Det norske veritas. *Sesam user manual: Sestra*. DNV, valid for program version 8.6 edition, February 2013.

[32] Dr. Techn. Olav Olsen. *Shell Design - Design tool for Reinforced Concrete Shell Structures. User Manual*, version 1.7 edition, 08 2013.

[33] RFA-TECH. Technical solutions for reinforced concrete. UK, 2013.

[34] Miguel Lamas Pardo Rodrigo Perez Fernandez. Offshore concrete structures. 2012.

[35] Hans Helle Berg Sigmund Rine. Use of probabilistic methods for planning of inspection for fatigue cracks in offshore structures. appendix b: Fatigue analysis of semi-submersibles. Technical report, Det norske veritas, 2011.

Appendix A

DTU 10MW reference wind turbine

This appendix contains detailed wind turbine blade and tower data.

BLADES

The blade is designed from scratch
Operating at maximum CP pitch=0.0deg

OVERALL DATA

Rotor radius (In hub-coordinate system)	89.166 m			
Blade length (Projected onto hub-coordinate system z-axis)	86.366 m			
Blade length (Accumulated length along blade axis)	86.466 m			
Overall (Integrated) Mass	41,716 kg		This is the mass of the composite and sandwich core materials. Additional mass for adhesives and other secondary structures was not considered.	
Structural Damping Ratio (All Modes)	3 log.decr [%]			
Body Center of gravity (Blade coordinates	x_B [m]	y_B [m]	z_B [m]	
	-1.18E-01	-3.60E-01	2.62E+01	

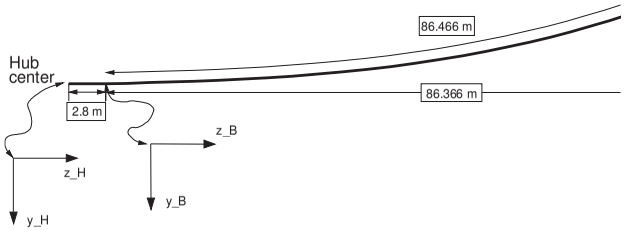

Blade planform properties (Coarse N=40)

Blade Coordinates defined relative to the Hub coordinate system
Cone angle not included
2.5 deg coning should be applied relative to hub center to both hub and blade
Twist is defined positive nose up
To run rotor with no coning of pre-bend simply set all y-coordinates of the blade axis = 0

Blade Axis x [m]	Blade Axis y [m]	Blade Axis z [m]	Twist [deg]	Chord [m]	Pitch axis aft LE (x/c) [-]	Relative thickness [-]
0.00000000E+00	0.00000000E+00	0.00000000E+00	0.00000000E+00	5.38000000E+00	5.00000000E-01	1.00000000E+02
0.00000000E+00	7.00600379E-05	2.80000000E+00	-1.45000000E+01	5.38000000E+00	5.00000000E-01	1.00000000E+02
0.00000000E+00	-1.05323899E-02	5.44301756E+00	-1.45000000E+01	5.38028982E+00	4.99997510E-01	9.96786635E+01
0.00000000E+00	-2.34489635E-02	8.17976984E+00	-1.45000000E+01	5.37996054E+00	4.99986212E-01	9.53328682E+01
0.00000000E+00	-3.87046869E-02	1.10027383E+01	-1.44320088E+01	5.45248001E+00	4.93766259E-01	8.60491476E+01
0.00000000E+00	-5.71797917E-02	1.39031430E+01	-1.38888157E+01	5.63544064E+00	4.71390872E-01	7.38688686E+01
0.00000000E+00	-7.95730259E-02	1.68710210E+01	-1.25459743E+01	5.86600432E+00	4.40125062E-01	6.10969583E+01
0.00000000E+00	-1.06658246E-01	1.98953357E+01	-1.06086877E+01	6.07065431E+00	4.12123725E-01	5.03586826E+01
0.00000000E+00	-1.39166815E-01	2.29641225E+01	-8.89245229E+00	6.18451124E+00	3.90733922E-01	4.30356446E+01
0.00000000E+00	-1.77828132E-01	2.60646653E+01	-7.80180235E+00	6.20300884E+00	3.75466967E-01	3.82518611E+01
0.00000000E+00	-2.23300638E-01	2.91836994E+01	-7.02416237E+00	6.14288001E+00	3.64741493E-01	3.49081138E+01
0.00000000E+00	-2.76148772E-01	3.23076383E+01	-6.38219779E+00	6.01996243E+00	3.57594872E-01	3.24150527E+01
0.00000000E+00	-3.36817765E-01	3.54227943E+01	-5.77685701E+00	5.84906854E+00	3.52895338E-01	3.05392762E+01
0.00000000E+00	-4.05606390E-01	3.85156384E+01	-5.22750216E+00	5.64532333E+00	3.50031082E-01	2.90526152E+01
0.00000000E+00	-4.82646481E-01	4.15730197E+01	-4.67357583E+00	5.42189119E+00	3.49983146E-01	2.78103477E+01
0.00000000E+00	-5.67888084E-01	4.45823887E+01	-4.08859635E+00	5.18582938E+00	3.50009929E-01	2.67860200E+01
0.00000000E+00	-6.61096253E-01	4.75319957E+01	-3.48775508E+00	4.94282736E+00	3.49994957E-01	2.59618700E+01

0.00000000E+00	-7.61854536E-01	5.04110617E+01	-2.88655238E+00	4.69821952E+00	3.50002205E-01	2.53179760E+01
0.00000000E+00	-8.69580952E-01	5.32099164E+01	-2.29907925E+00	4.45677501E+00	3.49999159E-01	2.48339879E+01
0.00000000E+00	-9.83553269E-01	5.59201011E+01	-1.73617493E+00	4.22269122E+00	3.50000277E-01	2.44898176E+01
0.00000000E+00	-1.10292858E+00	5.85344352E+01	-1.20718981E+00	3.99867965E+00	3.49999926E-01	2.42644205E+01
0.00000000E+00	-1.22679942E+00	6.10470477E+01	-7.18703543E-01	3.78608059E+00	3.50000013E-01	2.41416069E+01
0.00000000E+00	-1.35419022E+00	6.34533643E+01	-2.73076262E-01	3.58570648E+00	3.50000002E-01	2.41009086E+01
0.00000000E+00	-1.48401153E+00	6.57500952E+01	1.30379615E-01	3.39809449E+00	3.49999997E-01	2.40986815E+01
0.00000000E+00	-1.61520846E+00	6.79351584E+01	4.93278807E-01	3.22348972E+00	3.50000001E-01	2.41005850E+01
0.00000000E+00	-1.74683969E+00	7.00075977E+01	8.19565193E-01	3.06189968E+00	3.50000000E-01	2.40998537E+01
0.00000000E+00	-1.87799733E+00	7.19674921E+01	1.11392478E+00	2.91304006E+00	3.50000000E-01	2.41000000E+01
0.00000000E+00	-2.00775569E+00	7.38158535E+01	1.38270442E+00	2.77627915E+00	3.50000000E-01	2.41000206E+01
0.00000000E+00	-2.13524633E+00	7.55545098E+01	1.63109081E+00	2.65069499E+00	3.50000000E-01	2.40999908E+01
0.00000000E+00	-2.25985399E+00	7.71859743E+01	1.86195876E+00	2.53594729E+00	3.50000000E-01	2.41000016E+01
0.00000000E+00	-2.38101986E+00	7.87133469E+01	2.07762680E+00	2.43077140E+00	3.50000000E-01	2.41000006E+01
0.00000000E+00	-2.49808632E+00	8.01402166E+01	2.28007940E+00	2.33143176E+00	3.50000000E-01	2.40999995E+01
0.00000000E+00	-2.61073474E+00	8.14705231E+01	2.46899667E+00	2.23241582E+00	3.50000000E-01	2.41000001E+01
0.00000000E+00	-2.71869829E+00	8.27084849E+01	2.64408409E+00	2.12906893E+00	3.50000000E-01	2.41000000E+01
0.00000000E+00	-2.82165682E+00	8.38585215E+01	2.80296482E+00	2.01909559E+00	3.50000000E-01	2.41000000E+01
0.00000000E+00	-2.91948162E+00	8.49251565E+01	2.94507068E+00	1.90332250E+00	3.50000000E-01	2.41000000E+01
0.00000000E+00	-3.01214554E+00	8.59129575E+01	3.07008508E+00	1.77610767E+00	3.50000000E-01	2.41000000E+01
0.00000000E+00	-3.09964246E+00	8.68264859E+01	3.17732896E+00	1.62601186E+00	3.50000000E-01	2.41000000E+01
0.00000000E+00	-3.18195178E+00	8.76702529E+01	3.27095596E+00	1.44011918E+00	3.50000000E-01	2.41000000E+01
0.00000000E+00	-3.25920748E+00	8.84486629E+01	3.35752648E+00	1.18359898E+00	3.50000000E-01	2.41000000E+01
0.00000000E+00	-3.33150994E+00	8.91660000E+01	3.42800000E+00	6.00000000E-01	3.50000000E-01	2.41000000E+01

Tower

The tower is designed from scratch

OVERALL DATA

Hub height	119.0	m	
Tower Top Height (from ground)	118.38	m	
Tower Height	115.63	m	
Overall (Integrated) Mass	628,442	kg	
c.g. Location	47.6	m	
Structural Damping Ratio (All Modes)	6.28	log.decr [%]	
Young's Elasticity Modulus	2.10E+11	Pa	
Poisson's ratio	0.3	-	
Effective Density	8500	kg/m^3	(account for some secondary structures)

DISTRIBUTED PROPERTIES

global height z [m]	Outer diameter [m]	Wall thickness	Cross section area [m2]	Mass per length [kg/m]
0.000	8.300	38.0	0.9863	8383.7
11.500	8.022	38.0	0.9531	8101.2
11.501	8.022	36.0	0.9031	7676.7
23.000	7.743	36.0	0.8716	7409.0
23.001	7.743	34.0	0.8234	6999.2
34.500	7.465	34.0	0.7937	6746.4
34.501	7.465	32.0	0.7472	6351.2
46.000	7.186	32.0	0.7192	6113.3
46.001	7.186	30.0	0.6744	5732.8
57.500	6.908	30.0	0.6482	5509.7
57.501	6.908	28.0	0.6052	5143.9
69.000	6.629	28.0	0.5807	4935.7
69.001	6.629	26.0	0.5394	4584.5
80.500	6.351	26.0	0.5166	4391.2
80.501	6.351	24.0	0.4770	4054.7
92.000	6.072	24.0	0.4560	3876.2
92.001	6.072	22.0	0.4182	3554.3
103.500	5.794	22.0	0.3989	3390.8
103.501	5.794	20.0	0.3628	3083.6
115.630	5.500	20.0	0.3443	2926.7

Appendix B

Basic load cases

A list of the basic (original) load cases with their signification, is presented in the following table. These are transferred from the hydrodynamic analysis to the structural analysis. The list is also relevant for understanding how the design load combinations are defined in chapter 9.

OLC number	Type	Explanation	
1	Real	Dummy hydrostatic pressure	
2		Empty	
3		50 year wind turbine tower drag force	
4		Empty	
5		Empty	
6		Empty	
7		Empty	
8		Gravity and buoyancy	
9	Complex	Incoming direction 0 deg, 1 m wave amplitude	3 s
10			4 s
11			5 s
12			6 s
13			7 s
14			8 s
15			9 s
16			10 s
17			11 s
18			12 s
19			13 s
20			14 s
21			14.5 s
22			15 s
23			15.5 s
24			16 s
25			16.5 s
26			17 s
27			17.5 s
28			18 s
29			18.5 s
30			19 s
31			19.25 s
32			19.5 s
33			19.75 s
34			20 s
35			20.25 s
36			20.5 s
37			20.75 s
38			21 s
39			21.25 s
40			21.5 s
41			21.75 s
42			22 s
43			22.25 s
44			22.5 s

45			22.75 s
46			23 s
47			23.5 s
48			24 s
49			24.5 s
50			25 s
51			25.5 s
52			26 s
53			27 s
54			28 s
55			29 s
56			30 s
57	Complex	Incoming direction 30 deg, 1 m wave amplitude	3 s
58			4 s
59			5 s
60			6 s
61			7 s
62			8 s
63			9 s
64			10 s
65			11 s
66			12 s
67			13 s
68			14 s
69			14.5 s
70			15 s
71			15.5 s
72			16 s
73			16.5 s
74			17 s
75			17.5 s
76			18 s
77			18.5 s
78			19 s
79			19.25 s
80			19.5 s
81			19.75 s
82			20 s
83			20.25 s
84			20.5 s
85			20.75 s
86			21 s
87			21.25 s
88			21.5 s
89			21.75 s
90			22 s
91			22.25 s

92			22.5 s
93			22.75 s
94			23 s
95			23.5 s
96			24 s
97			24.5 s
98			25 s
99			25.5 s
100			26 s
101			27 s
102			28 s
103			29 s
104			30 s
105	Complex	Incoming direction 60 deg, 1 m wave amplitude	3 s
106			4 s
107			5 s
108			6 s
109			7 s
110			8 s
111			9 s
112			10 s
113			11 s
114			12 s
115			13 s
116			14 s
117			14.5 s
118			15 s
119			15.5 s
120			16 s
121			16.5 s
122			17 s
123			17.5 s
124			18 s
125			18.5 s
126			19 s
127			19.25 s
128			19.5 s
129			19.75 s
130			20 s
131			20.25 s
132			20.5 s
133			20.75 s
134			21 s
135			21.25 s
136			21.5 s
137			21.75 s
138			22 s

139			22.25 s
140			22.5 s
141			22.75 s
142			23 s
143			23.5 s
144			24 s
145			24.5 s
146			25 s
147			25.5 s
148			26 s
149			27 s
150			28 s
151			29 s
152			30 s
153	Complex	Incoming direction 90 deg, 1 m wave amplitude	3 s
154			4 s
155			5 s
156			6 s
157			7 s
158			8 s
159			9 s
160			10 s
161			11 s
162			12 s
163			13 s
164			14 s
165			14.5 s
166			15 s
167			15.5 s
168			16 s
169			16.5 s
170			17 s
171			17.5 s
172			18 s
173			18.5 s
174			19 s
175			19.25 s
176			19.5 s
177			19.75 s
178			20 s
179			20.25 s
180			20.5 s
181			20.75 s
182			21 s
183			21.25 s
184			21.5 s
185			21.75 s

186			22 s
187			22.25 s
188			22.5 s
189			22.75 s
190			23 s
191			23.5 s
192			24 s
193			24.5 s
194			25 s
195			25.5 s
196			26 s
197			27 s
198			28 s
199			29 s
200			30 s
201	Complex	Incoming direction 120 deg, 1 m wave amplitude	3 s
202			4 s
203			5 s
204			6 s
205			7 s
206			8 s
207			9 s
208			10 s
209			11 s
210			12 s
211			13 s
212			14 s
213			14.5 s
214			15 s
215			15.5 s
216			16 s
217			16.5 s
218			17 s
219			17.5 s
220			18 s
221			18.5 s
222			19 s
223			19.25 s
224			19.5 s
225			19.75 s
226			20 s
227			20.25 s
228			20.5 s
229			20.75 s
230			21 s
231			21.25 s
232			21.5 s

233			21.75 s
234			22 s
235			22.25 s
236			22.5 s
237			22.75 s
238			23 s
239			23.5 s
240			24 s
241			24.5 s
242			25 s
243			25.5 s
244			26 s
245			27 s
246			28 s
247			29 s
248			30 s

Table B.1: *Original load cases transferred from HydroD to Sestra*

Appendix C

Post-processing. Design sections and local axis system definition

BASE SLAB 1:

MESH:

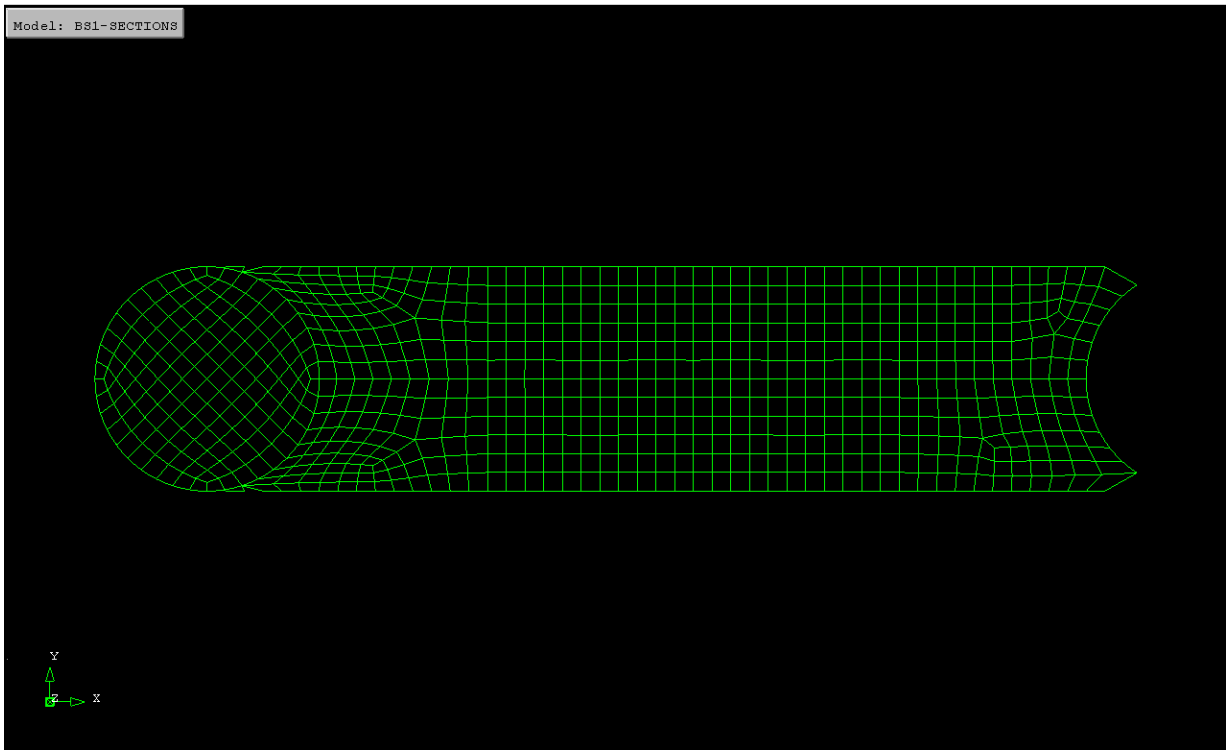

F-SECTION:

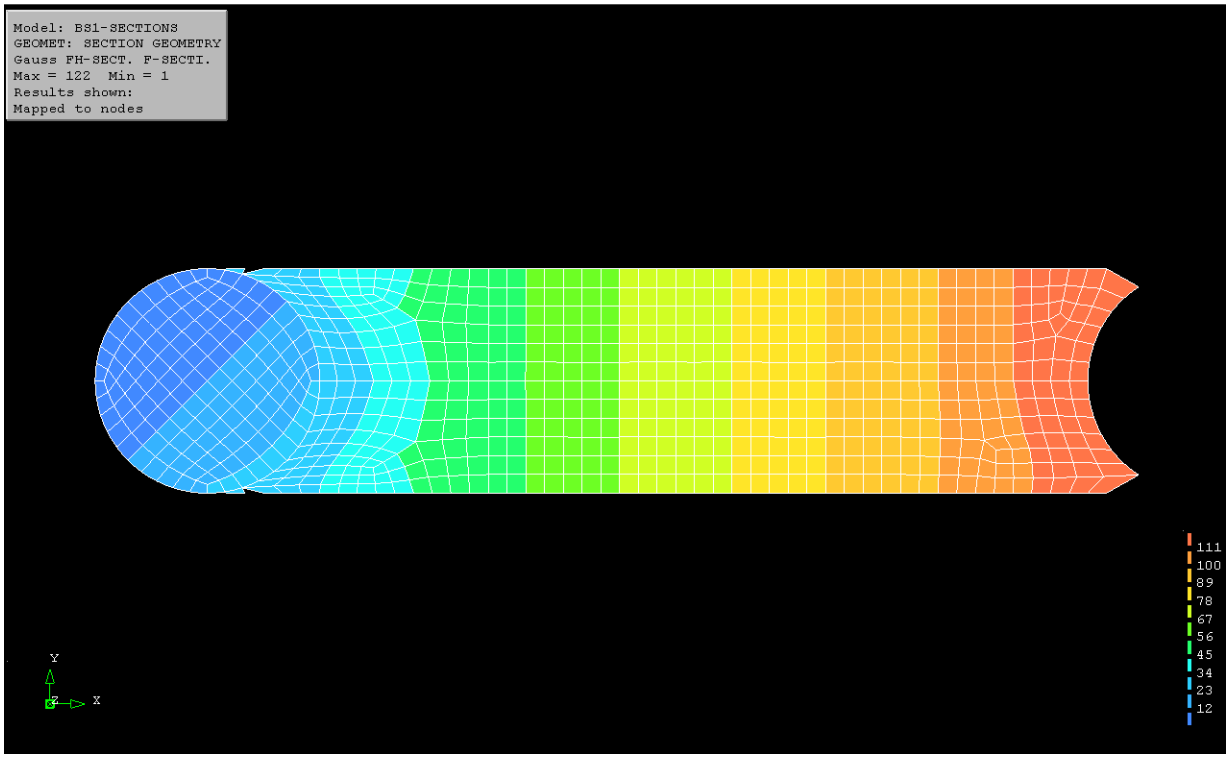

H-SECTION:

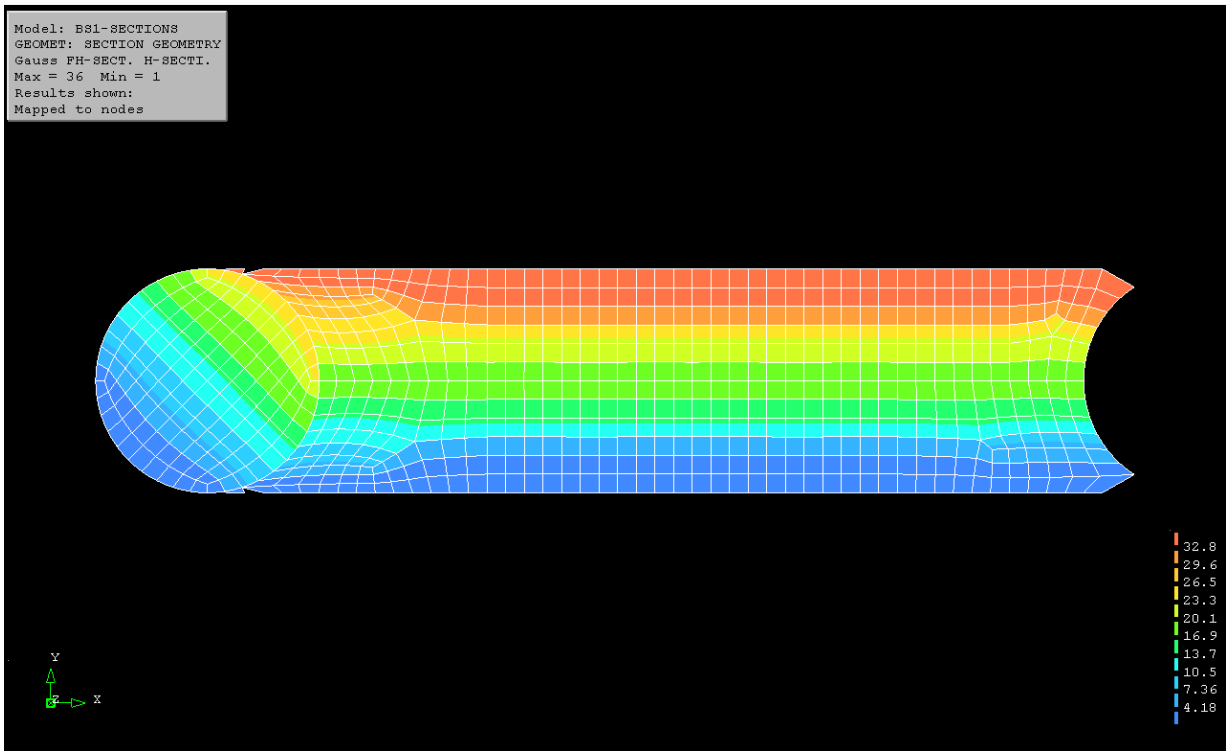

1-AXIS:

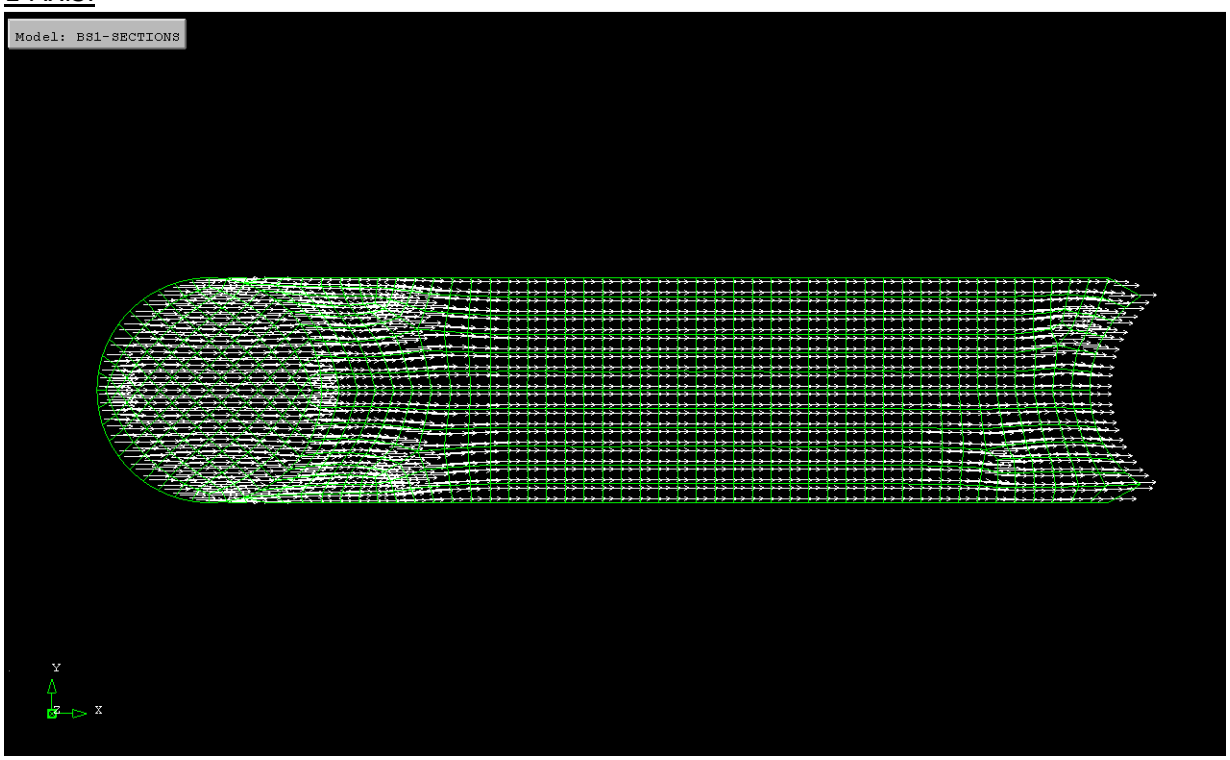

2-AXIS:

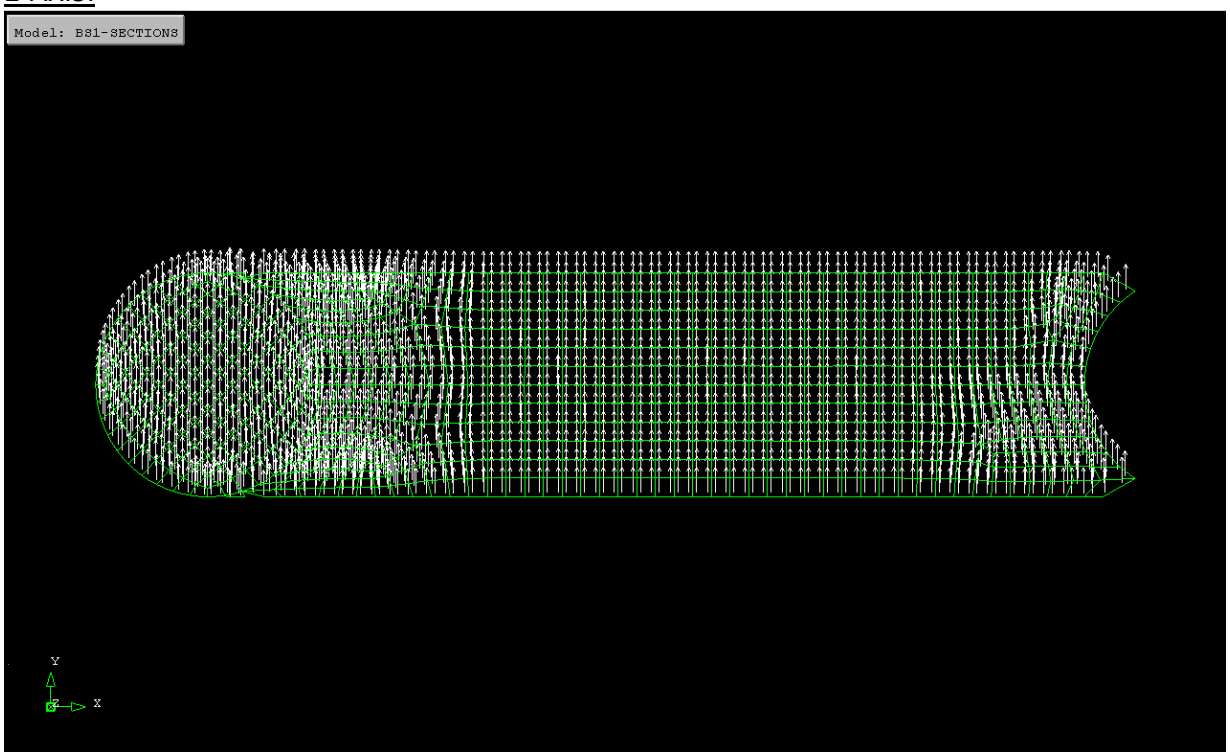

3-AXIS:

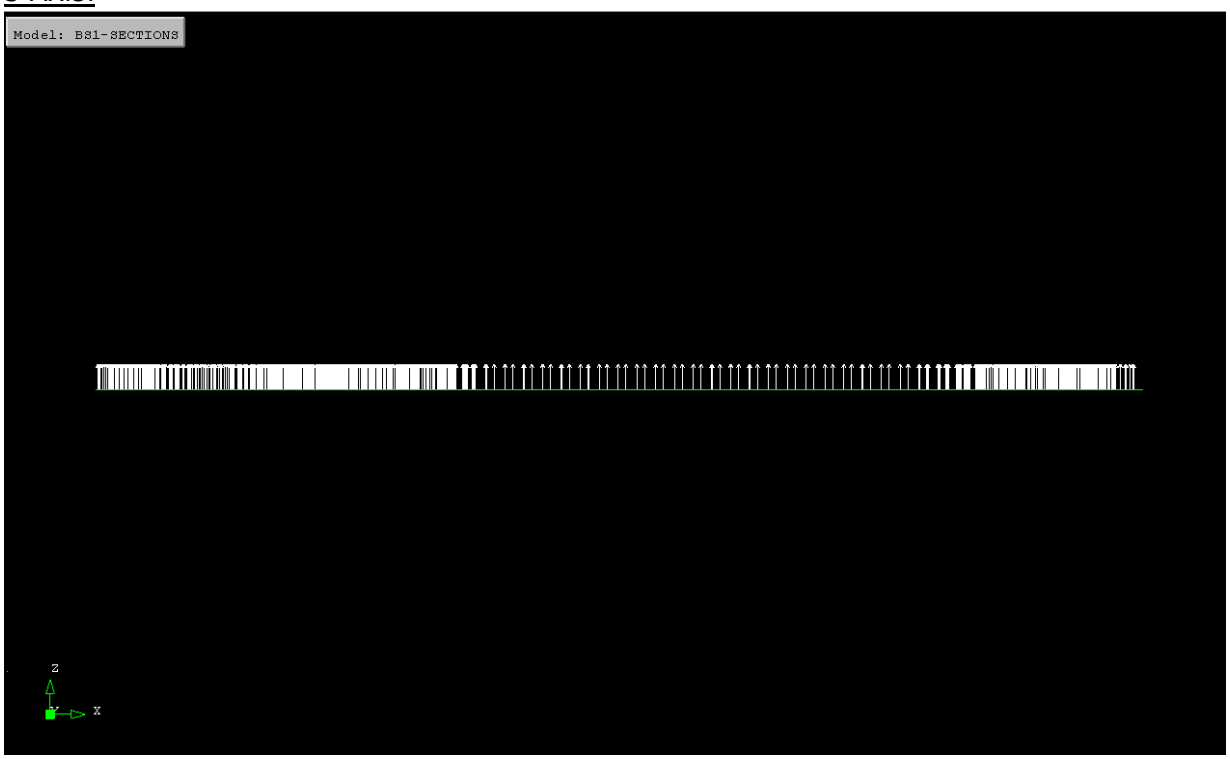

TOP SLAB 1:

MESH:

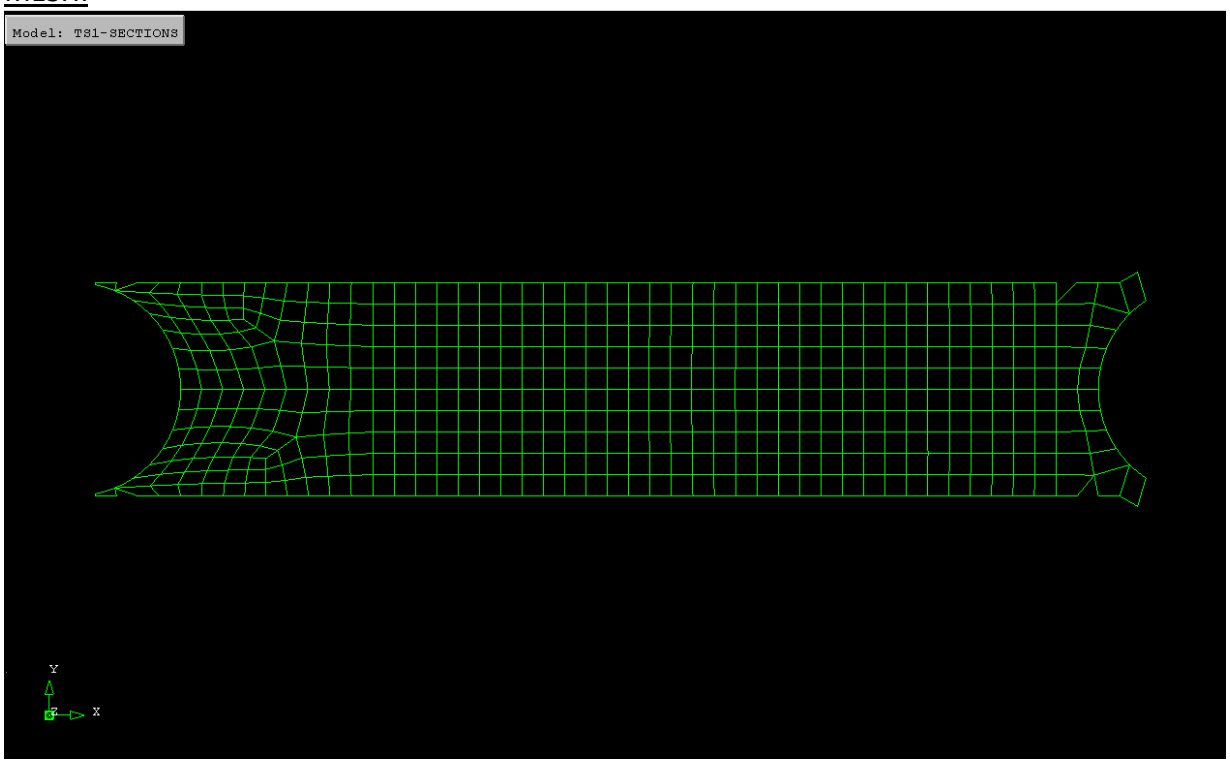

F-SECTION:

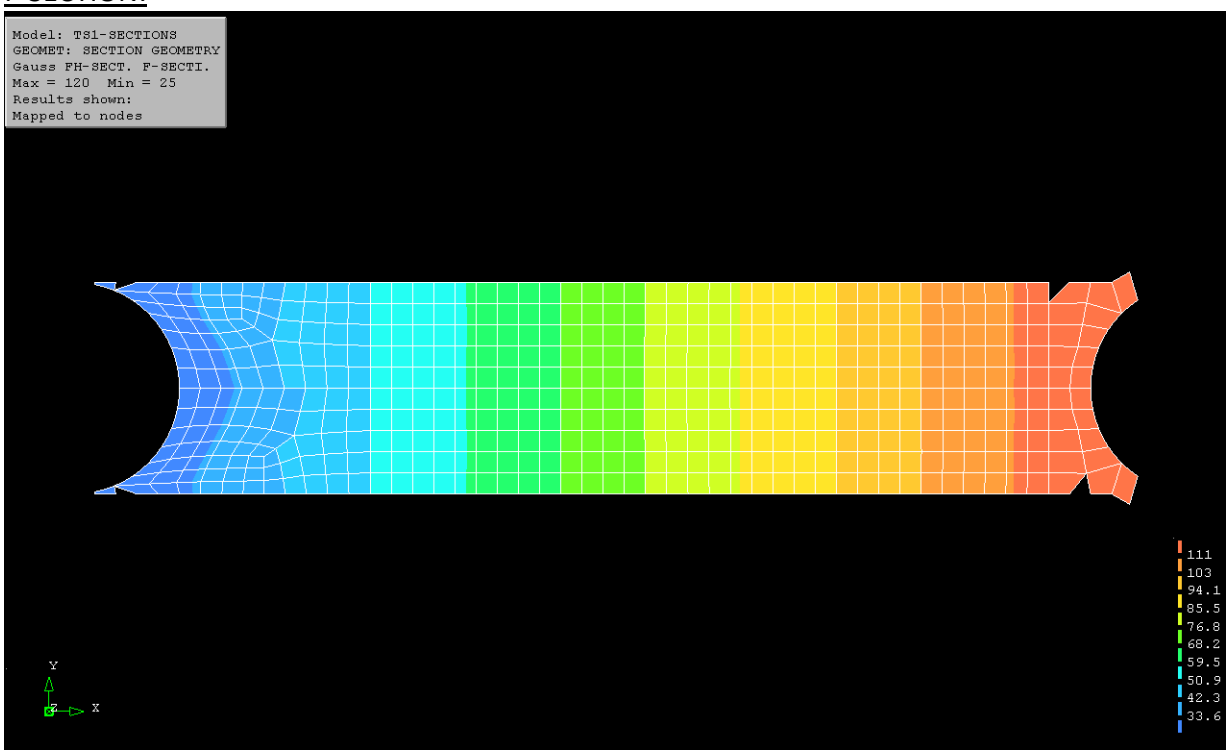

H-SECTION:

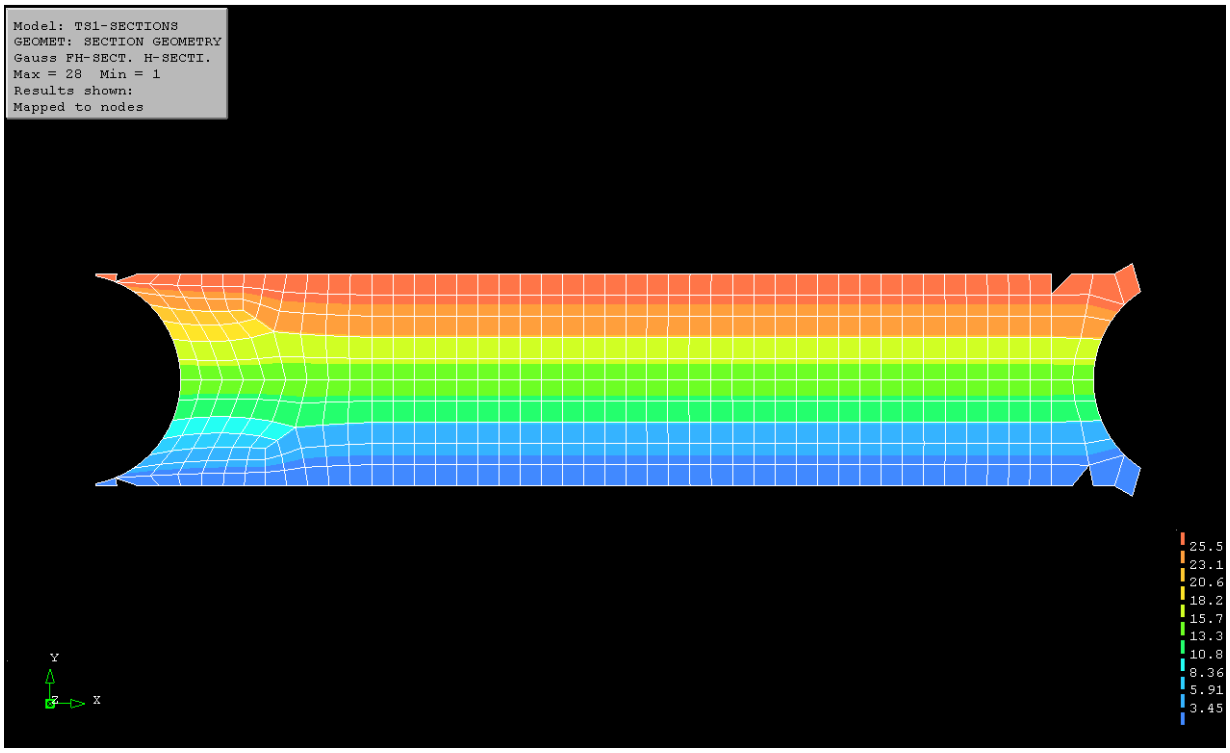

1-AXIS:

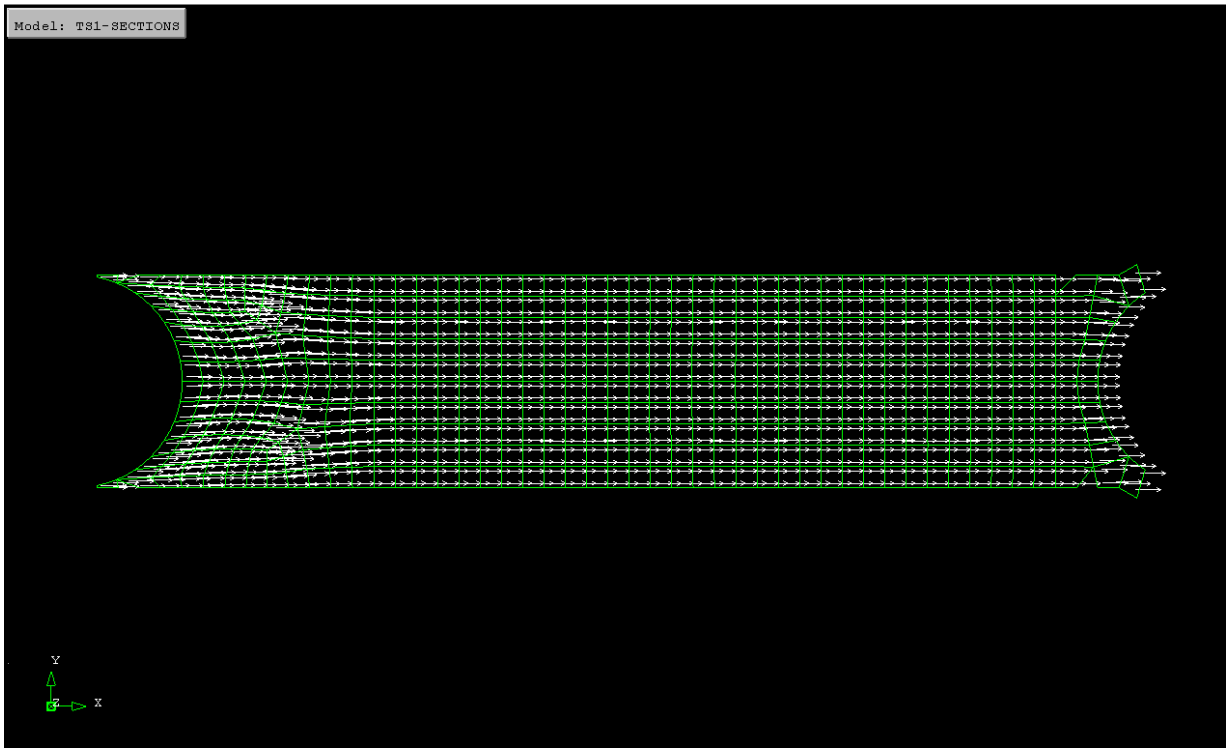

2-AXIS:

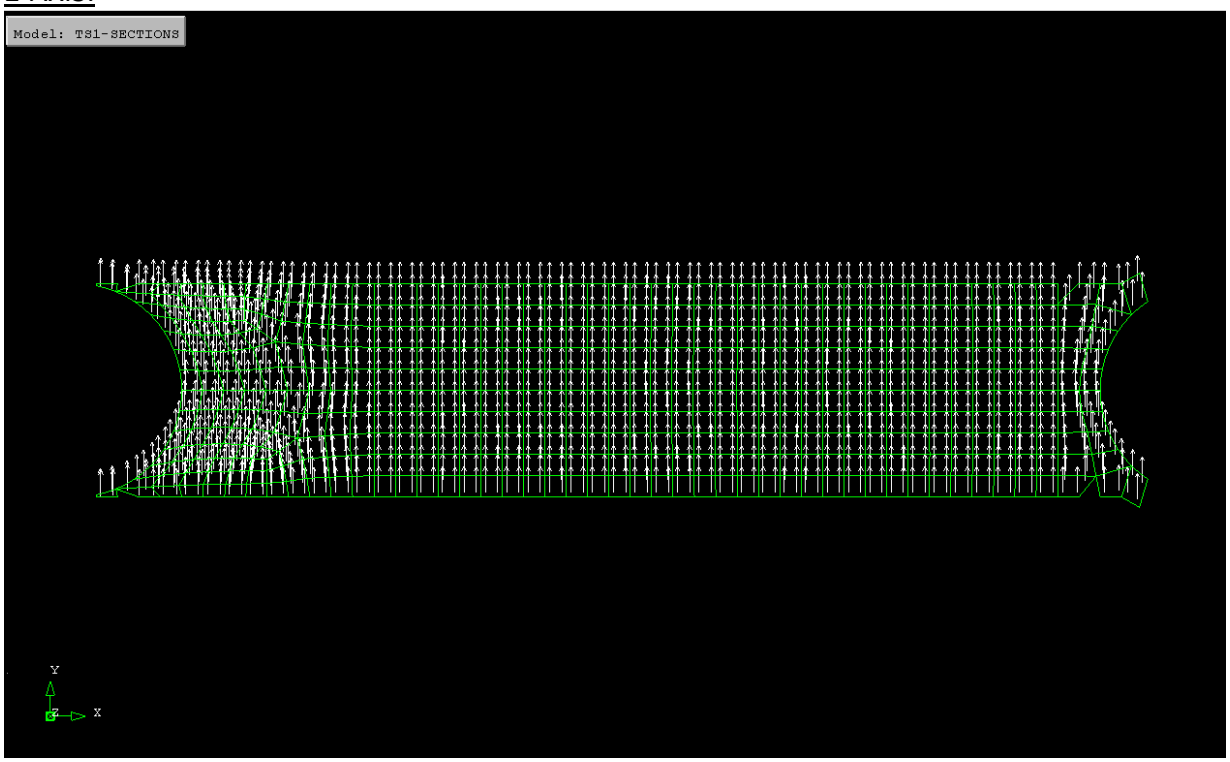

3-AXIS:

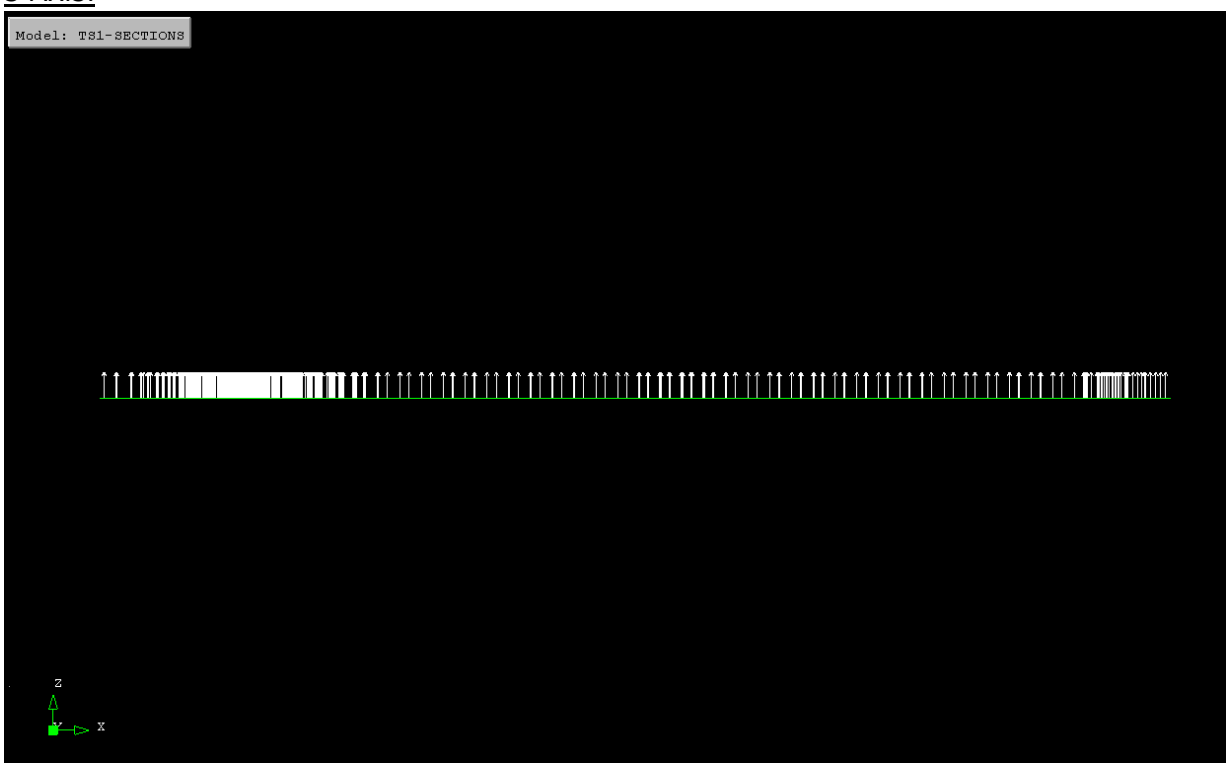

Outer Column OC_1:

F-SECTION:

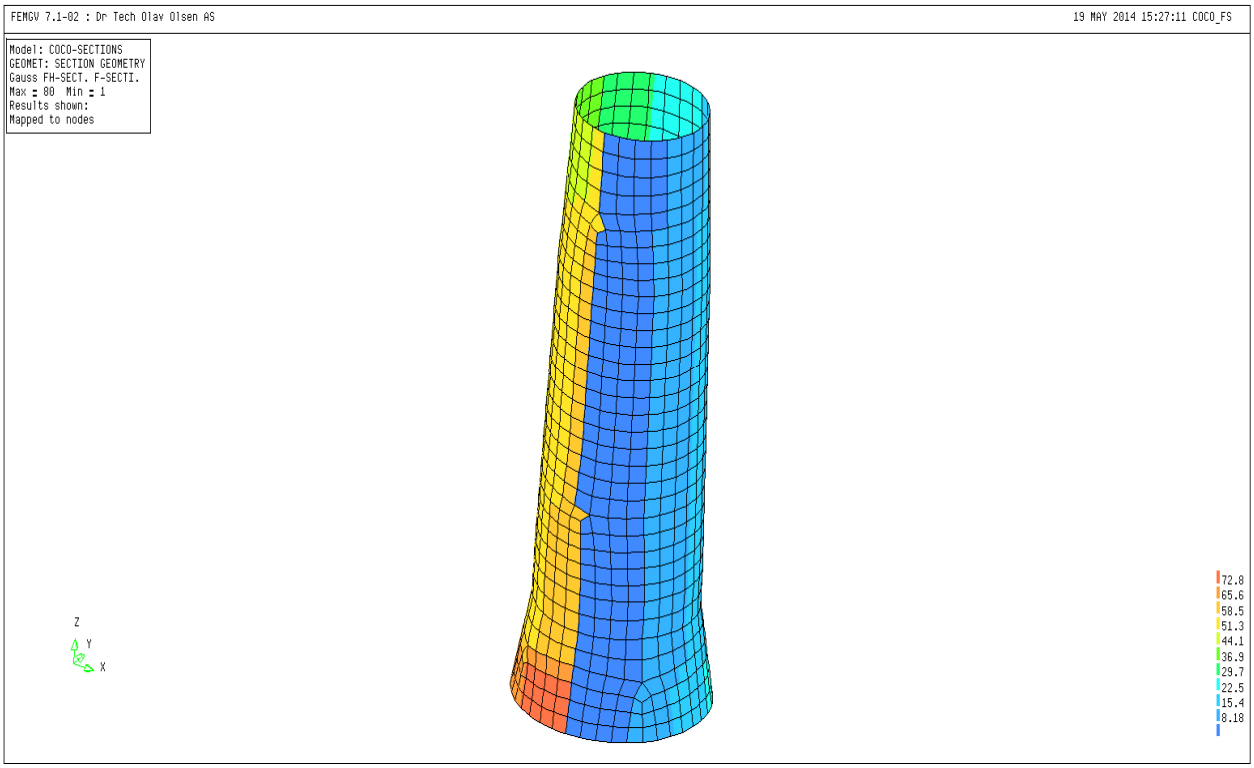

H-SECTION:

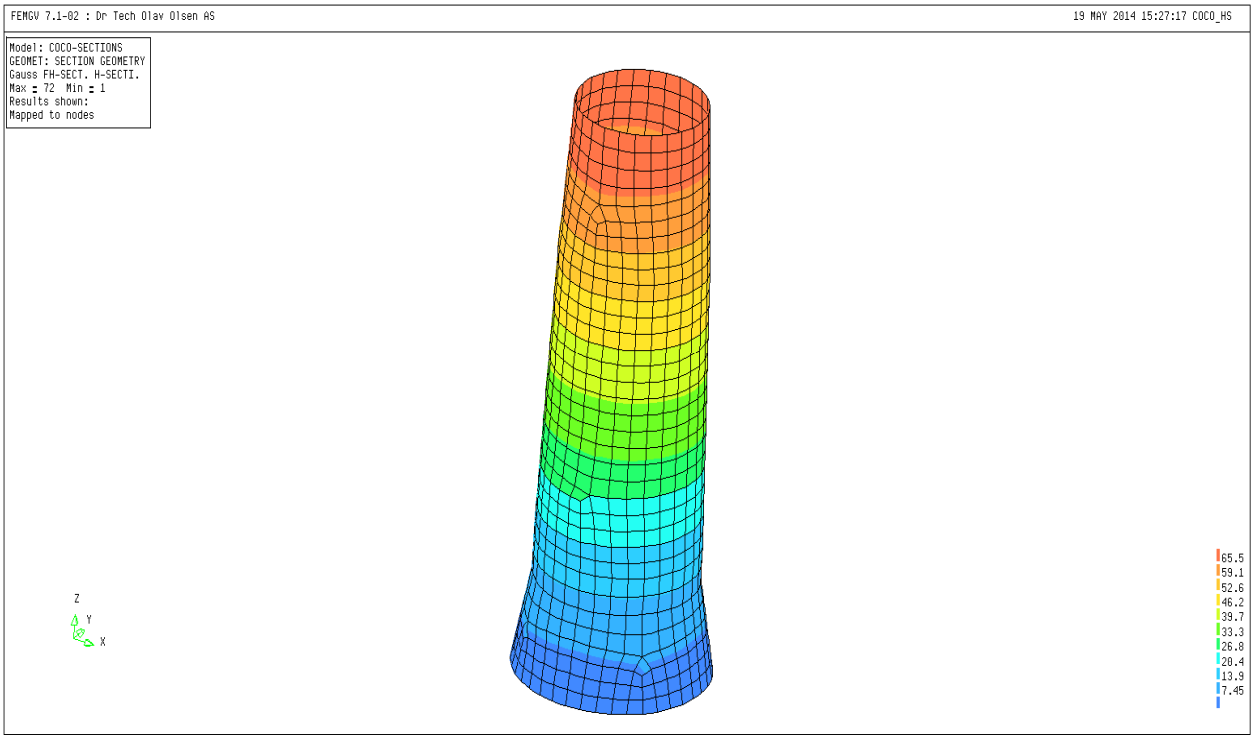

1-AXIS:

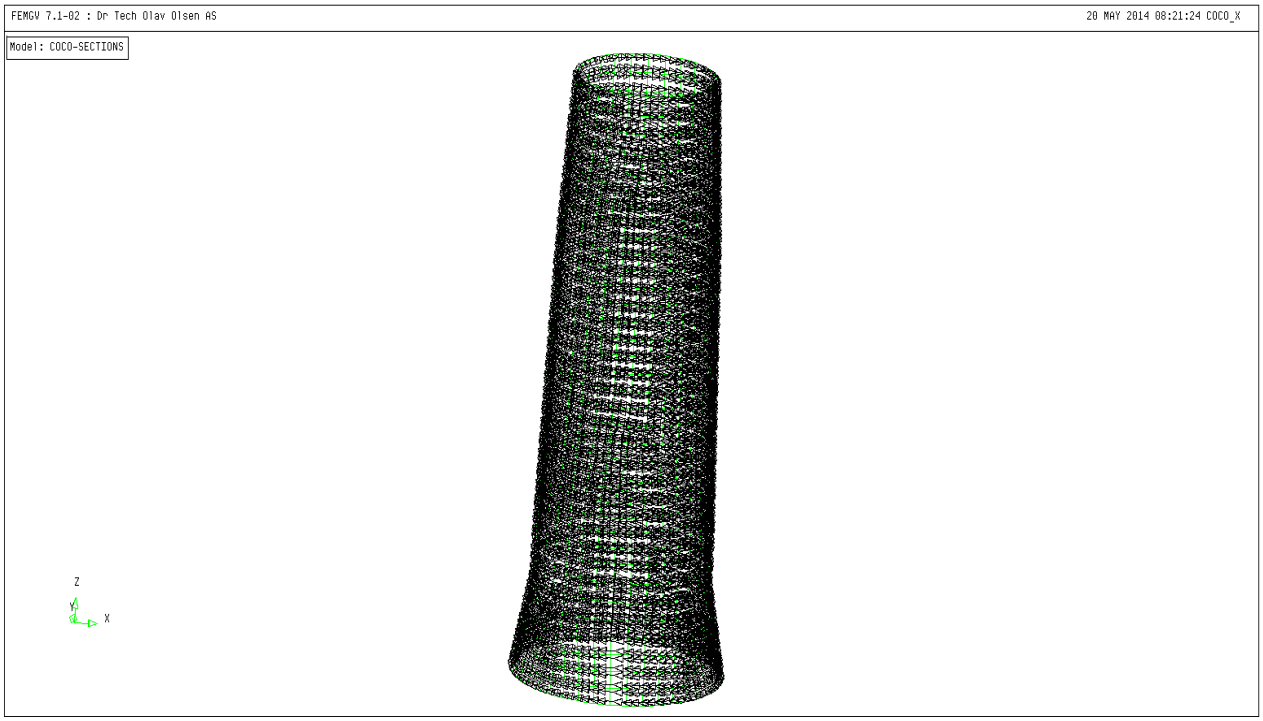
FEMGV 7.1-02 : Dr Tech Olav Olsen AS
20 MAY 2014 08:21:24 COCO_X
Model: COCO-SECTIONS
Z
Y
X

2-AXIS:

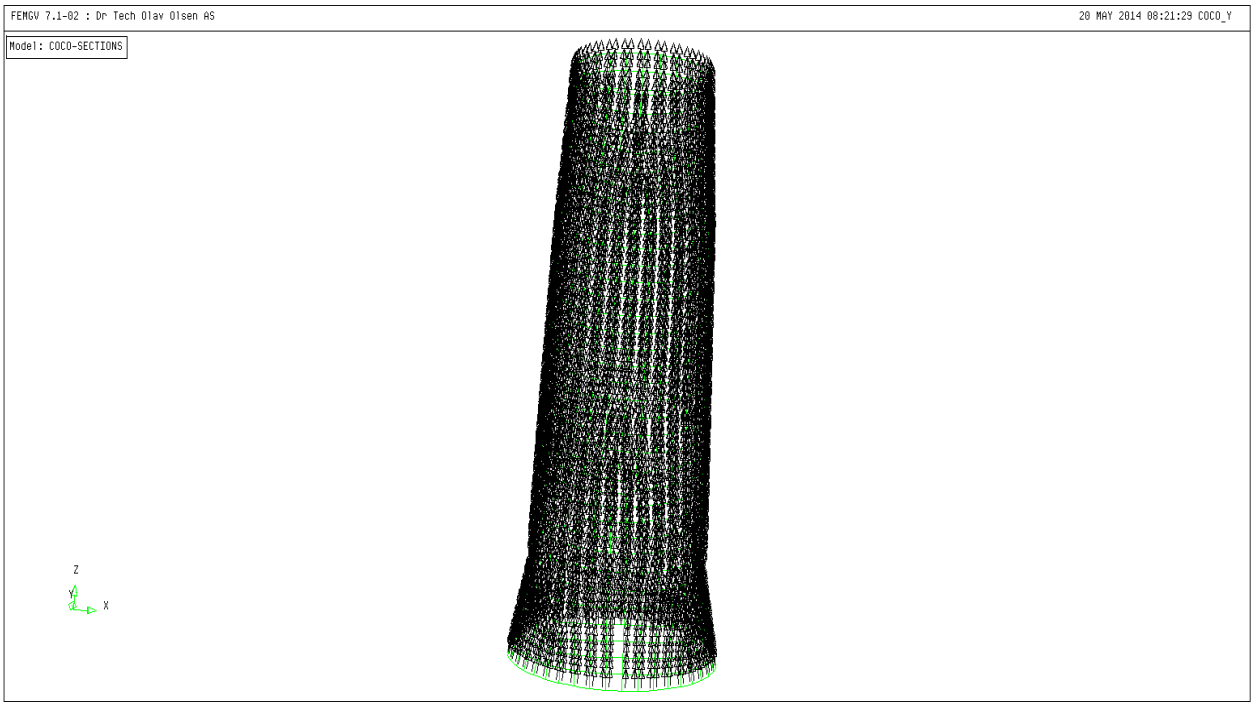
FEMGV 7.1-02 : Dr Tech Olav Olsen AS
20 MAY 2014 08:21:29 COCO_Y
Model: COCO-SECTIONS
Z
Y
X

3-AXIS:

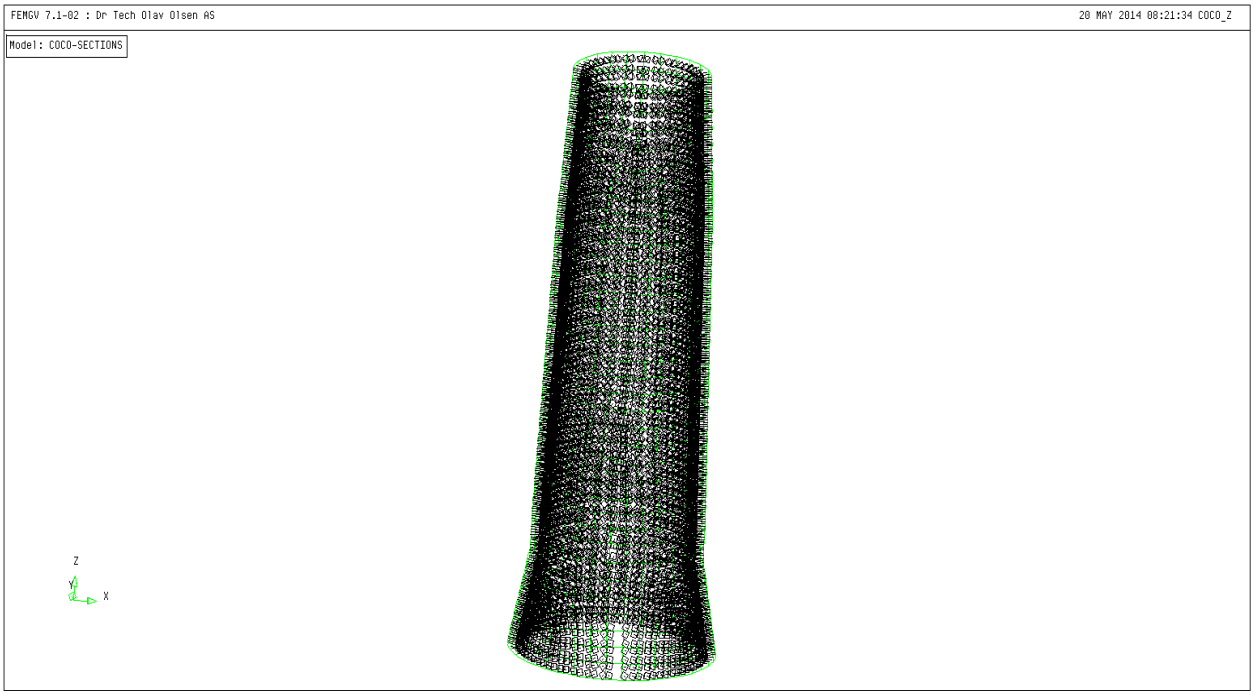
FEMGV 7.1-02 : Dr Tech Olav Olsen AS
20 MAY 2014 08:21:34 COCO_Z
Model: COCO-SECTIONS
Z
Y
X

Central Column CC:

F-SECTION:

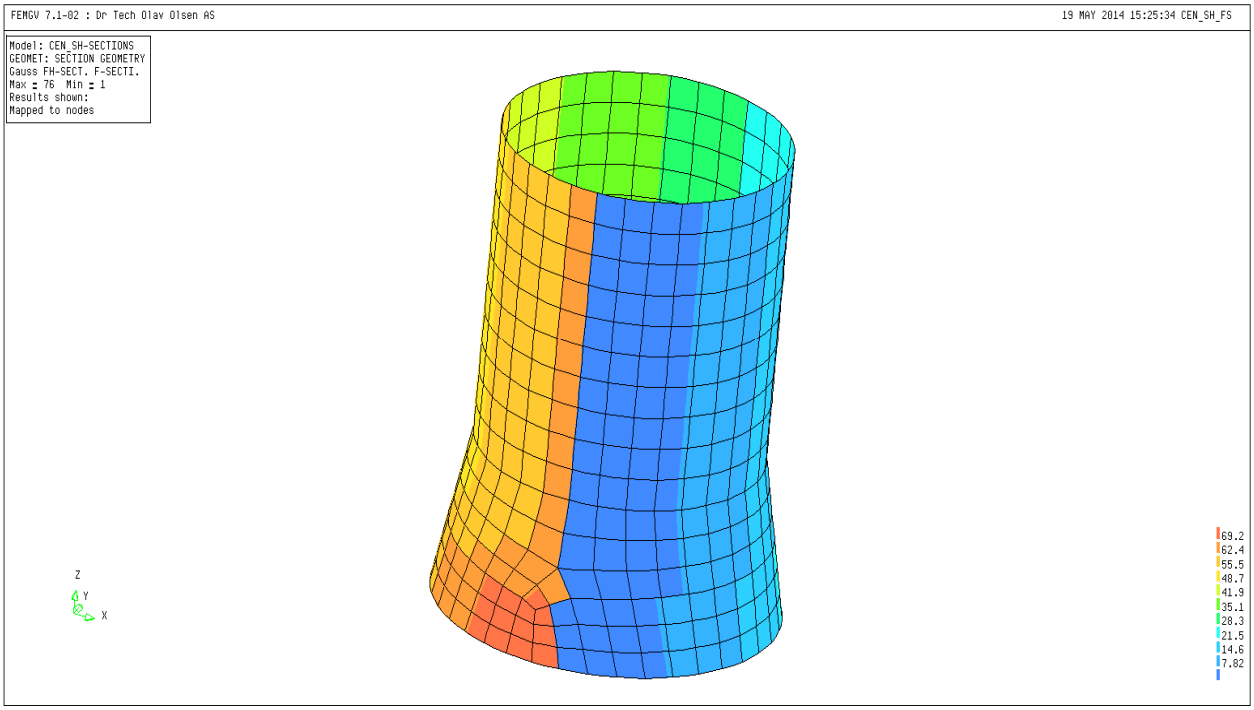

H-SECTION:

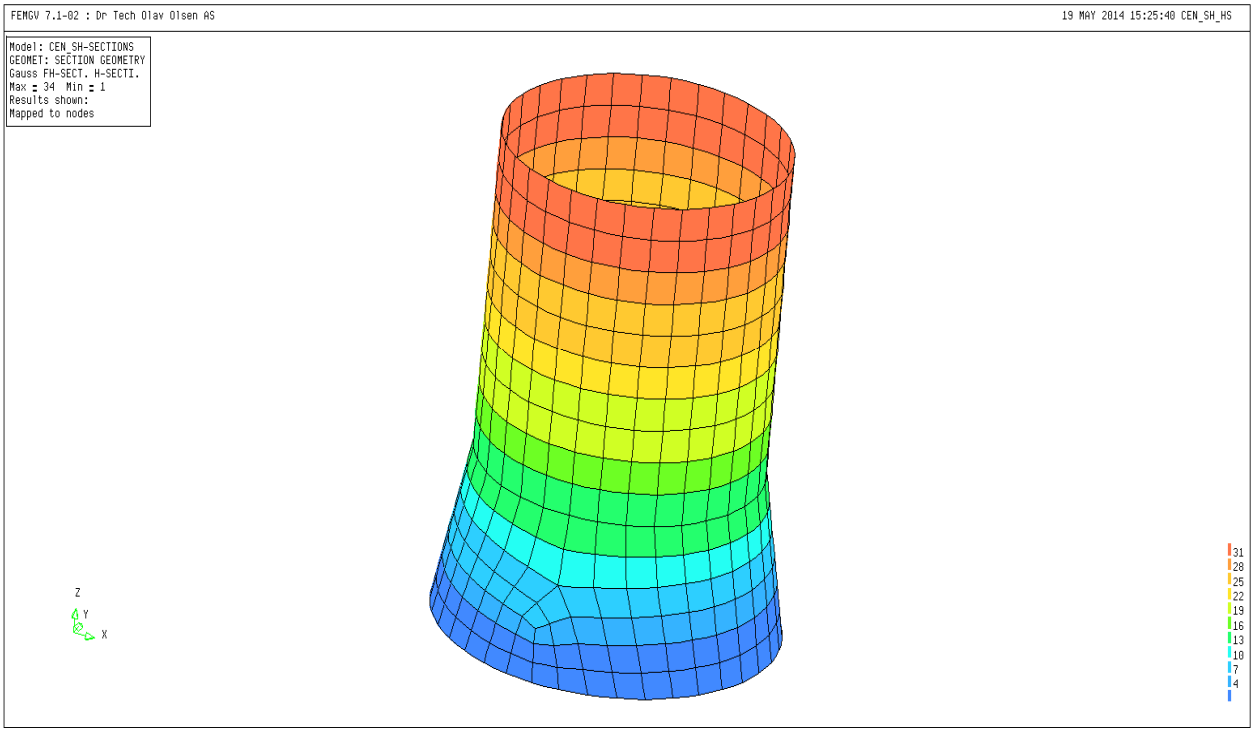

1-AXIS:

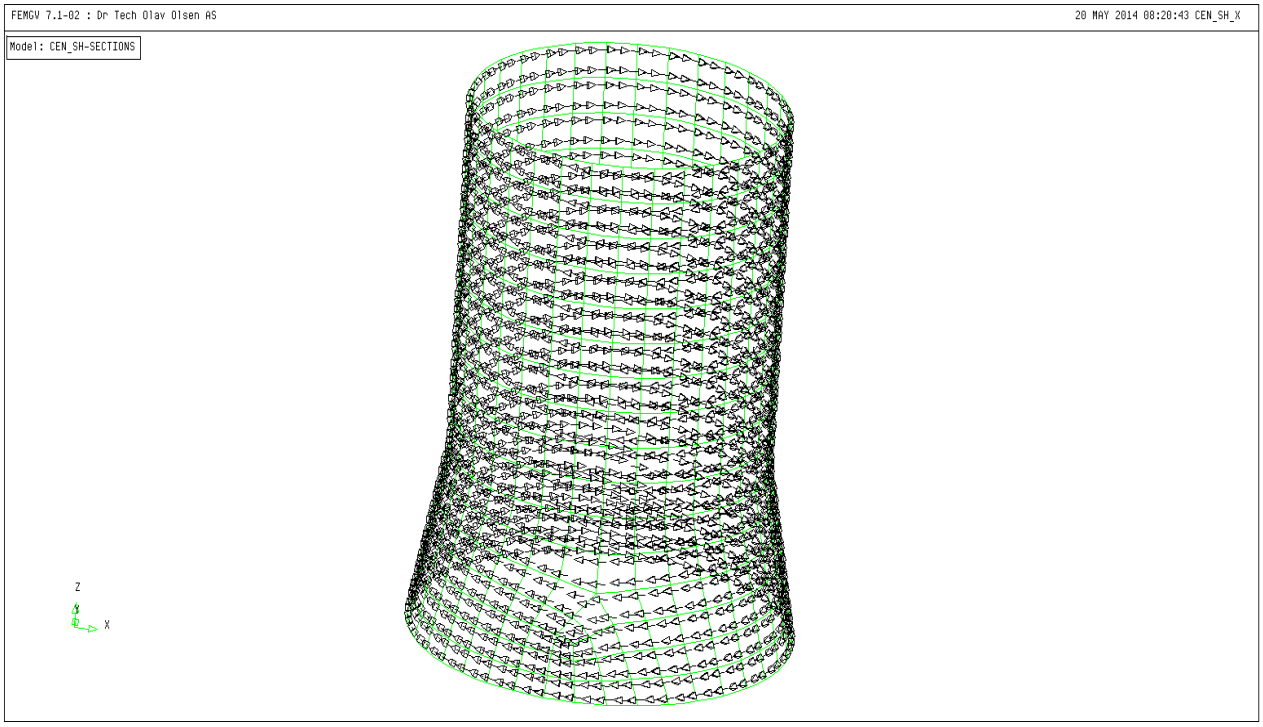
FEMGV 7.1-02 : Dr Tech Olav Olsen AS
20 MAY 2014 08:20:43 CEN_SH_X
Model: CEN_SH-SECTIONS
Z
X

2-AXIS:

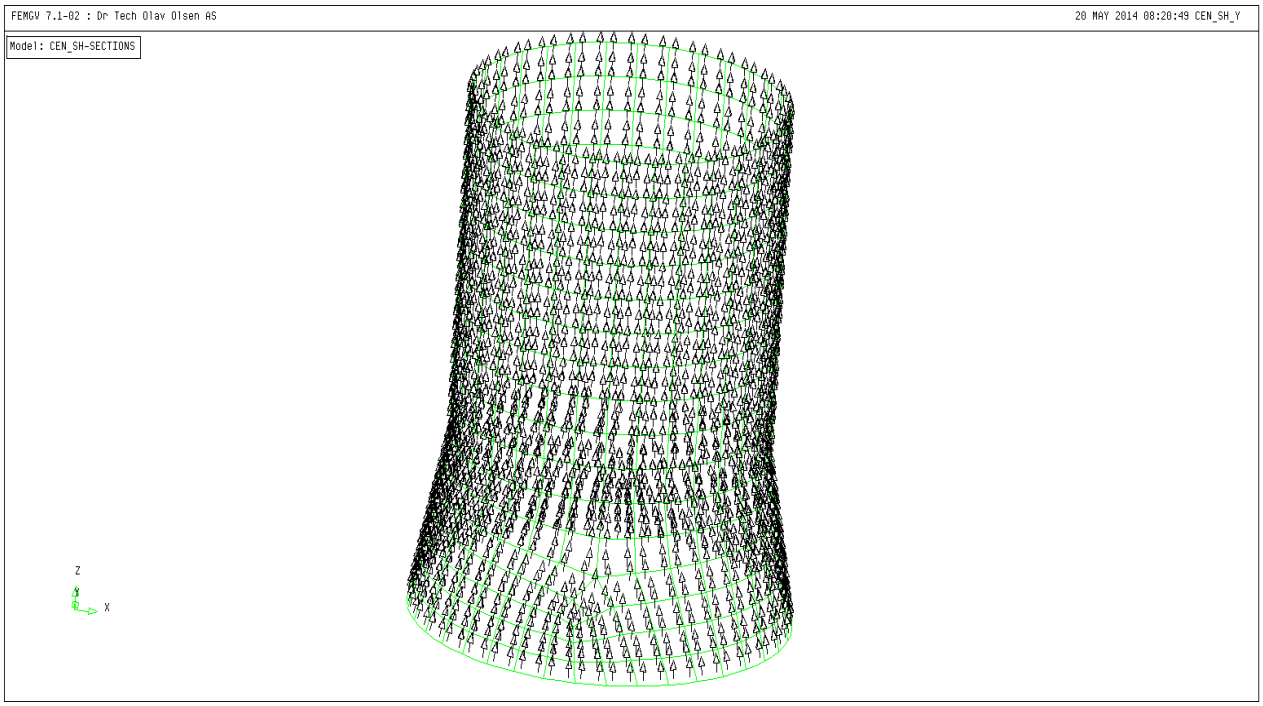
FEMGV 7.1-02 : Dr Tech Olav Olsen AS
20 MAY 2014 08:20:49 CEN_SH_Y
Model: CEN_SH-SECTIONS
Z
X

3-AXIS:

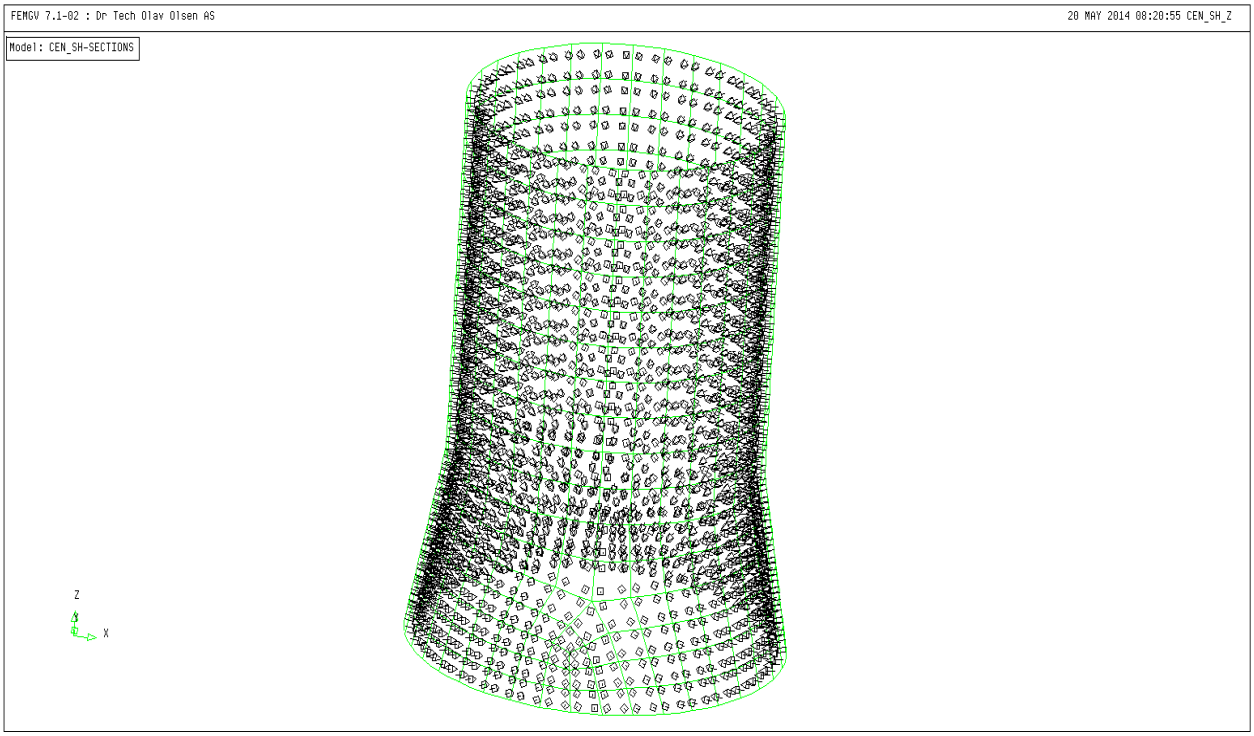
FEMGV 7.1-02 : Dr Tech Olav Olsen AS
20 MAY 2014 08:20:55 CEN_SH_Z
Model: CEN_SH-SECTIONS
Z
X

Angled Wall AW_12:

F-SECTION:

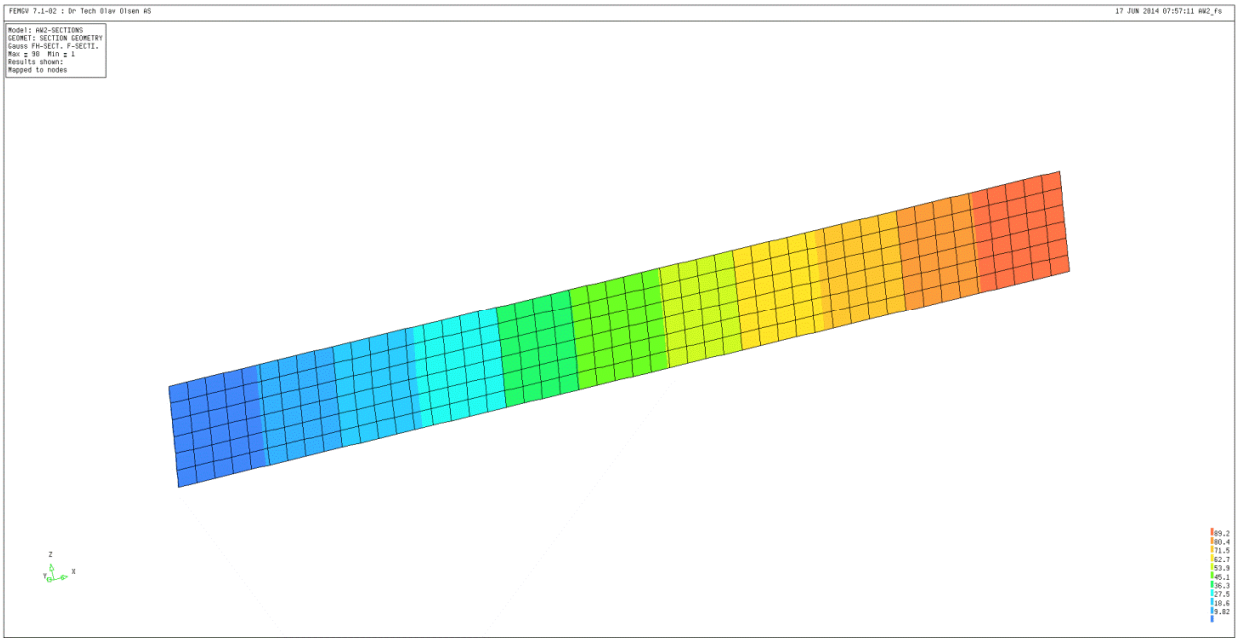

H-SECTION:

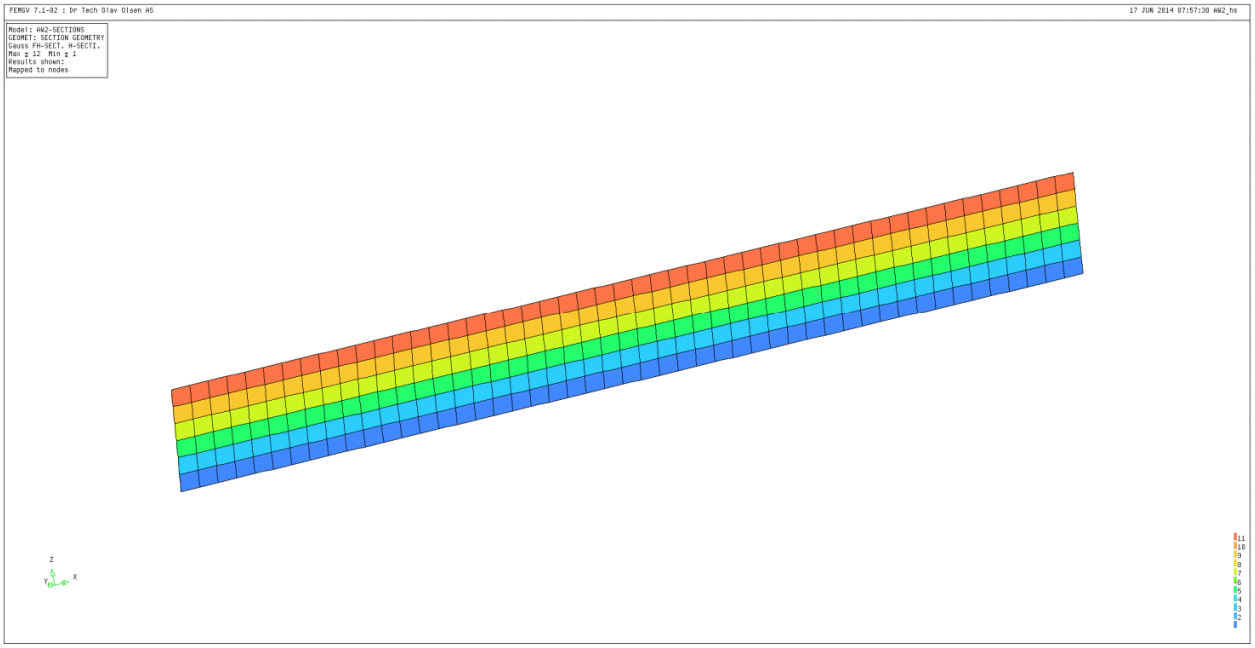

1-AXIS:

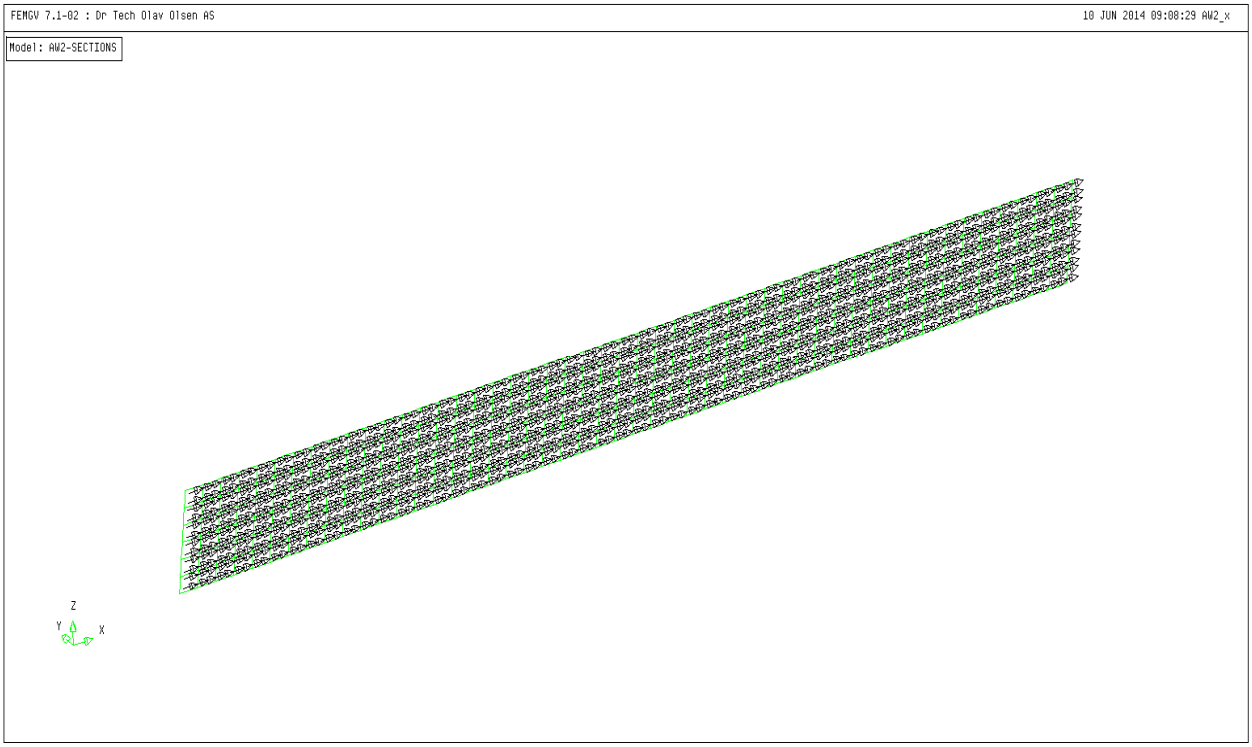
FEMGV 7.1-02 : Dr Tech Olav Olsen AS
10 JUN 2014 09:08:29 AW2_x
Model: AW2-SECTIONS
Z
Y
X

2-AXIS:

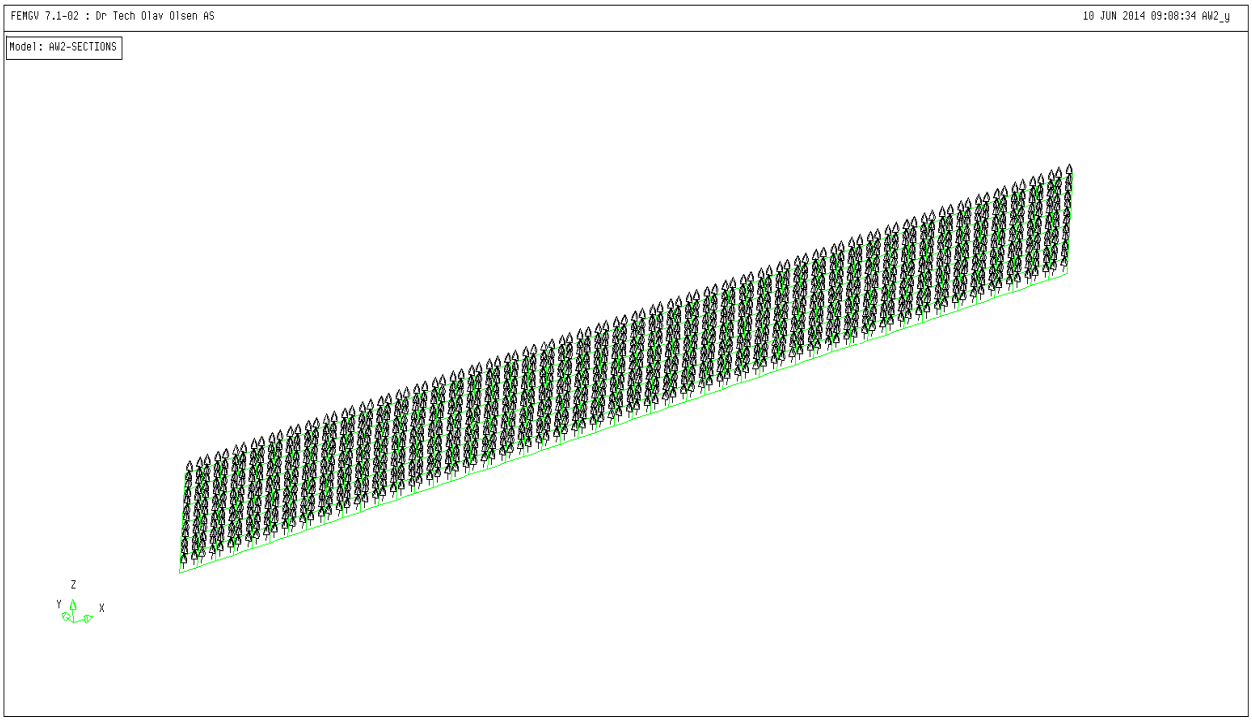
FEMGV 7.1-02 : Dr Tech Olav Olsen AS
10 JUN 2014 09:08:34 AW2_y
Model: AW2-SECTIONS
Z
Y
X

3-AXIS:

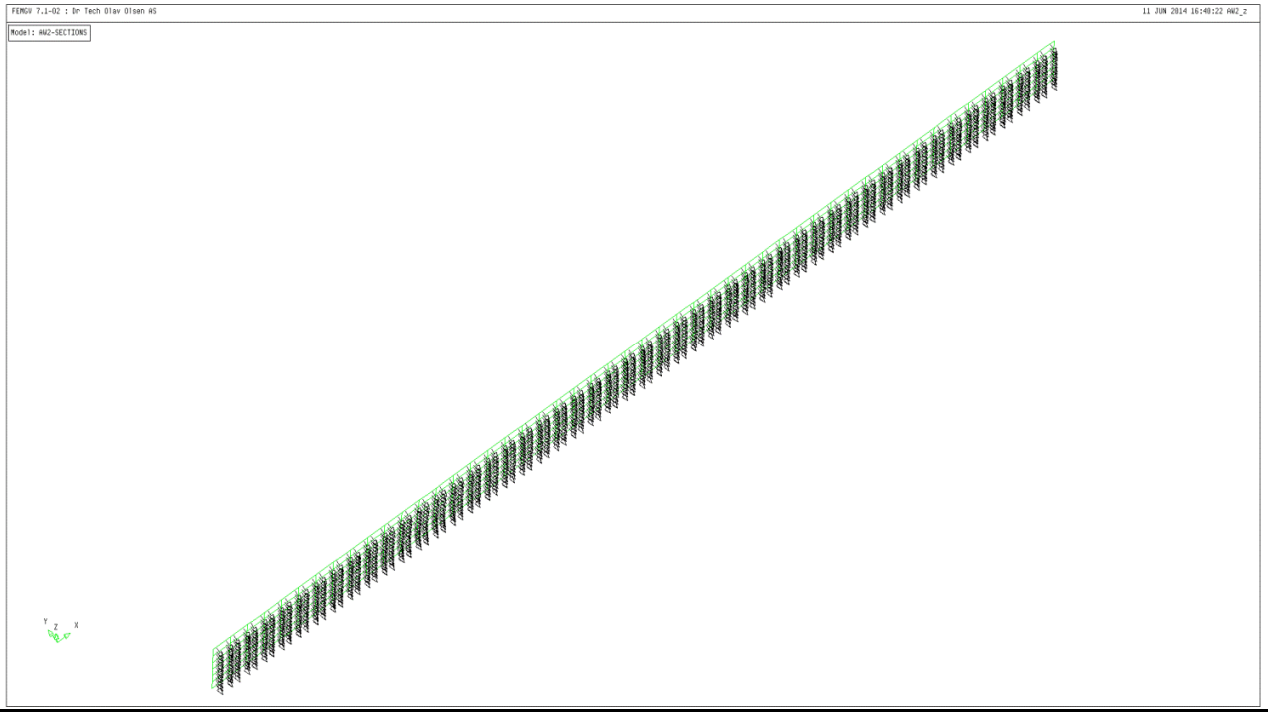
FEMGV 7.1-02 : Dr Tech Olav Olsen AS
11 JUN 2014 16:40:22 AW2_z
Model: AW2-SECTIONS
Y
Z
X

Appendix D

Structural drawings

This appendix contains structural drawing for the concept floater with results based on ULS design checks: top view, side view and pontoon cross section.

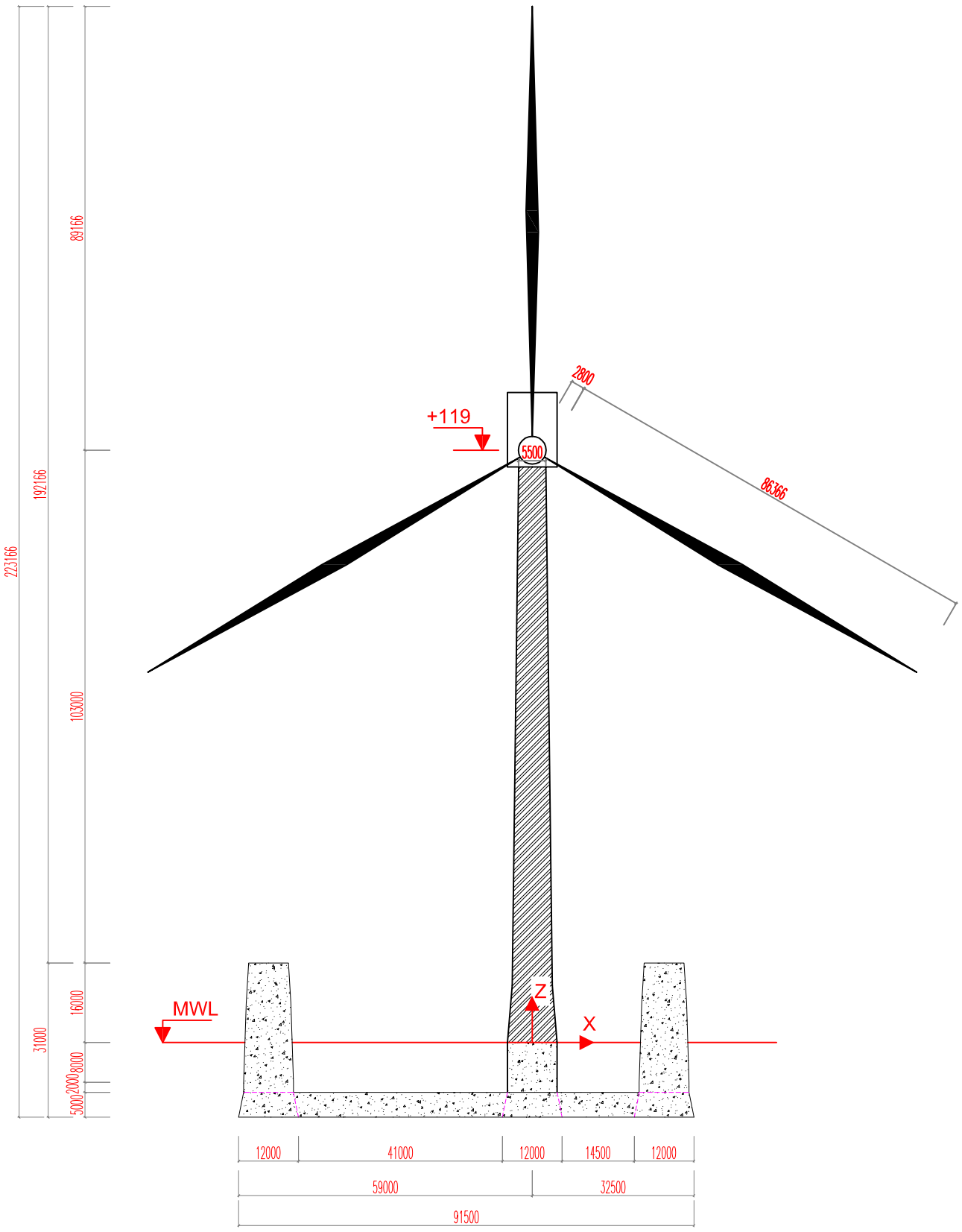

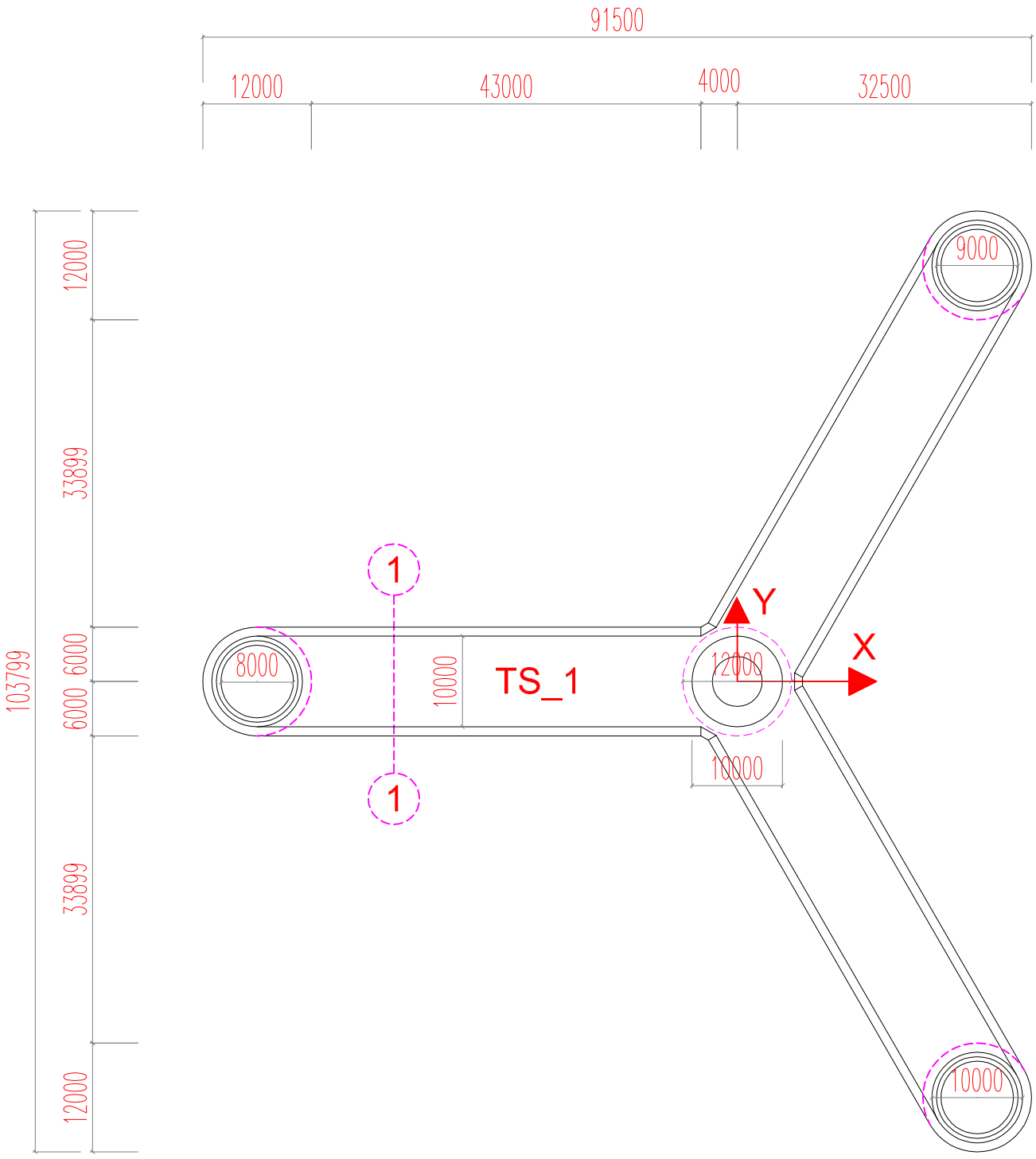

Section 1–1